No 727481 RESERVE
D2.1 v1.0
Definition of Frequency under High Dynamic Conditions

The research leading to these results has received funding from the European Union's Horizon 2020 Research and Innovation Programme, under Grant Agreement no 727481.

Project Name:	RESERVE
Contractual Delivery Date:	30.09.2017
Actual Delivery Date:	30.09.2017
Contributors:	Álvaro Ortega (UCD), Federico Milano (UCD), Aysar Musa (RWTH), Lucian Toma (UPB), Dan Preotescu (CRE)
Workpackage:	WP2 – Frequency Stability by Design
Security:	PU
Nature:	R
Version:	1.0
Total number of pages:	83

Abstract:

This deliverable proposes a general expression to estimate frequency variations during the transient of electric power systems. The proposed expression is derived based on standard assumptions of power system models for transient stability analysis and can be readily implemented in power system software tools for transient stability analysis. The formula is aimed at improving the accuracy of bus frequency estimation in electromechanical power system models. Simulation results based on a variety of case studies using different test networks show that the proposed formula is accurate, numerically robust and computationally efficient.

Keyword list:

Frequency estimation, quasi-static phasor model, dq-frame model, transient stability analysis, center of inertia, washout filter, phase-locked loop, wind energy conversion system, solar photo-voltaic generation, energy storage system, flexible load.

Executive Summary

This Deliverable (D) 2.1 presents the work of Task (T) 2.1 within the wider context of Work Package (WP) 2 and RESERVE. WP2 focuses on solving the challenges of stabilising and automating frequency in the new energy network architecture characterized by 100% renewable energy sources (RESs). With this aim, the following objectives are chased in WP2:

- To extract a monitoring concept that can exploit the existing system information from each generator to define a system level picture in close to real-time.
- To define a strategy for the evaluation of existing networks and attributes.
- To define a strategy for the on-line measurement of the important parameters.
- To define a general dynamic frequency stability criteria for grids with high penetration of renewables and controllable loads.
- To analyse the dynamic requirement for frequency in 100% RES scenario.
- To extend the concept to a virtual inertia to a wider and more flexible Linear Swing Dynamics approach.
- To draft ancillary service definitions and network codes for validation in WP5 and harmonisation and standardisation in WP6.

The frequency of an electric energy system is an indicator of its power unbalance and is thus a fundamental quantity for estimation and control.

In steady-state conditions, the frequency is unique in the whole system, regardless its physical dimensions. However, in the first seconds of a transient following a contingency, each synchronous machine and, hence, each bus of the system, show a different frequency. This information is gathered by the ENTSO-E Commission Regulation (EU) 2016/631 of 14 April 2016 Establishing a Network Code on Requirements for Grid Connection of Generators, which defines *frequency* as follows: *frequency means the electric frequency of the system expressed in hertz that can be measured in all parts of the synchronous area under the assumption of a consistent value for the system in the time frame of seconds, with only minor differences between different measurement locations. Its nominal value is 50Hz*.

This definition of frequency is accurate for current power systems, where synchronous machines still represent a high share of the total system generation. The rationale behind is that power plants based on synchronous machines intrinsically respond to local frequency deviations through their inertia. However, this scenario is rapidly changing with the increasing penetration of Renewable Energy Sources (RESs), since RESs are generally non-synchronous and have no inertia. As a consequence, as the share of RESs increases, the overall system inertia decreases, resulting in larger frequency deviations after a power imbalance. Therefore, the assumption that only minor differences exist between different frequency measurement locations can be incorrect. In this regard, **this deliverable proposes a new definition of *frequency* under high dynamic conditions** in the context of high and/or 100% RES penetration.

To be able to know with accuracy local deviations of the frequency in transient conditions is fundamental to take proper control actions and recover the nominal frequency (and thus, the power balance) as soon as possible. However, how to properly estimate the frequency and which frequency signals are best for the control of non-synchronous generation, storage and flexible loads is still an open question.

This deliverable discusses and compares – through a comprehensive set of simulations considering different case studies, scenarios and devices – different techniques, namely, phase-locked loop (PLL) devices and the concept of center of inertia (COI), to estimate the frequency during electromechanical transients. The deliverable also discusses a technique, namely the *frequency divider* (FD), proposed by the authors to properly estimate local bus frequencies. The relevance and accuracy of the FD formula have been validated by means of electromagnetic transient analysis which considers all fast electromagnetic dynamics, the three-phase, possibly unbalanced models of every dynamic element of the grid, and detailed phasor measurement unit (PMU) models.

Relevant remarks based on simulation results are as follows.

- The FD provides “exact” local bus frequency estimations and can be utilized as an ideal reference for other techniques.
- The standard synchronous reference frame model of the PLL works reasonably well compared to the FD formula.
- PLLs and similar devices that implement a numerical derivative of the bus voltage phase angle can lead to non-physical oscillations and, possibly to instabilities. It is crucial to properly design the PLLs to prevent their coupling with fast dynamics.
- Low pass filters of frequency estimators, while introducing a slight delay in the controlled signal, reduces the operations of the converters and have no impact on the overall dynamic response of the system.
- The COI filters out local frequency variations. This fact may cause poorly-damped frequency oscillations, especially if coupled to devices with a slow response.
- Solar generation, compared to wind power plants, tend to provide a slightly faster and, often, more effective, control. This is due to the fact that in solar generation there are no moving mechanical part.
- The inclusion of energy storage systems (ESSs) in the grid allows reducing, to a large extent, frequency and voltage variations due to severe contingencies such as faults. However, the response of the ESS can be significantly deteriorated if current saturations of the storage device are reached.
- The number of measures required by the exact FD formula are cumbersome for real-world systems. However, the measures required to provide an acceptable estimation of the bus frequencies can be reduced considerably without loss of accuracy.

Simulation results indicate that the modelling and, hence, the technique to estimate the frequency signal make a significant difference in the transient behaviour of a power system with inclusion of frequency controllers other than primary frequency regulators of synchronous machines. The definition of a criterion to estimate the fidelity of such power system models is thus an urgent research topic with relevant impact on system operators, practitioners and industry applications.

Authors

Partner	Name	Phone/Fax/e-mail
UCD		
	Álvaro Ortega Manjavacas	Phone: +353 1 716 1857 e-mail: alvaro.ortegamanjavacas@ucd.ie
	Federico Milano	Phone: +353 1 716 1844 Fax: +353 1 283 0534 e-mail: federico.milano@ucd.ie
RWTH		
	Aysar Musa	Phone: +49 15776940065 e-mail: amusa@eonerc.rwth-aachen.de

Project Internal Reviewers

Partner	Name
POLITO	Francesco Arrigo
POLITO	Tao Huang
CRE	Dan Preotescu
RWTH	Marco Cupelli

Table of Contents

1. Introduction

1.1 Task 2.1

This deliverable is the major output of Task T2.1 in the Work Package WP2. In T2.1, the main goal has been to properly define local bus frequencies during transients. This definition of bus frequency considers the frequency as it is distributed across the network, as opposed to considering it as a global system variable, which is the current status quo in power systems analysis. The definition of the frequency in this paradigm is thus closer to that of real-world devices that measure local frequencies such as phasor measurement units (PMUs), and is based on sampling phase quantities, filtering the noise and defining the time-varying frequency of the fundamental component of the signal. These methods are based on phasor analysis, and the accuracy of results can be compared to those found using electromagnetic transient (EMT) analysis which includes all fast electromagnetic dynamics, the three-phase, possibly unbalanced models of every dynamic element of the grid, and detailed PMU models.

1.2 Objectives and Outline of the Deliverable

D2.1 shows that properly defining the local frequencies is crucial for the proper control and stabilization of the frequency in current and future power systems. To this aim, a comprehensive study based on a large variety of frequency control devices and different approaches to define the frequency is provided. In particular, the frequency measurement and estimation techniques considered in this deliverable are the centre of inertia (COI), the washout filter, the phase-locked loop (PLL), and the frequency divider (FD) formula that is proposed in this work. The accuracy of these techniques have been tested considering several frequency control devices, namely wind energy conversion systems (WECS), solar photo-voltaic generation (SPVG), energy storage systems (ESS) and thermostatically controlled loads (TCL). The results of this deliverable indicate that, depending on the frequency estimation technique applied, different transient responses are to be expected from the frequency control device, and hence, of the overall power system.

1.3 How to Read this Document

This is a stand-alone document that can be read on its own. However, this deliverable can be read together with D2.2 for a better understanding of the relation between frequency estimation and control in transmission systems.

Additional dependencies and links of D2.1 with other deliverables, tasks and work packages from the RESERVE project are summarized below (see Fig. 1.1).

- The case studies presented in Appendix D have been based on the different Scenarios on the Frequency defined in D1.1 (T1.1, WP1).
- Models and results presented in this report will be later used by T2.3 and T2.5 (WP2) to define the Linear Swing Dynamic Operations and their ICT requirements of D2.3, D2.4 and D2.5, respectively.
- T2.6 will also utilize the concepts and results introduced above in the definition of practical recommendations of ancillary services and network codes for the implementation of the frequency control of non-synchronous devices as well as the communication system involved in such a control. These recommendations will be included in D2.6 and D2.7, and will be tested and validated by T5.3 (WP5) in D5.4 and D5.5.

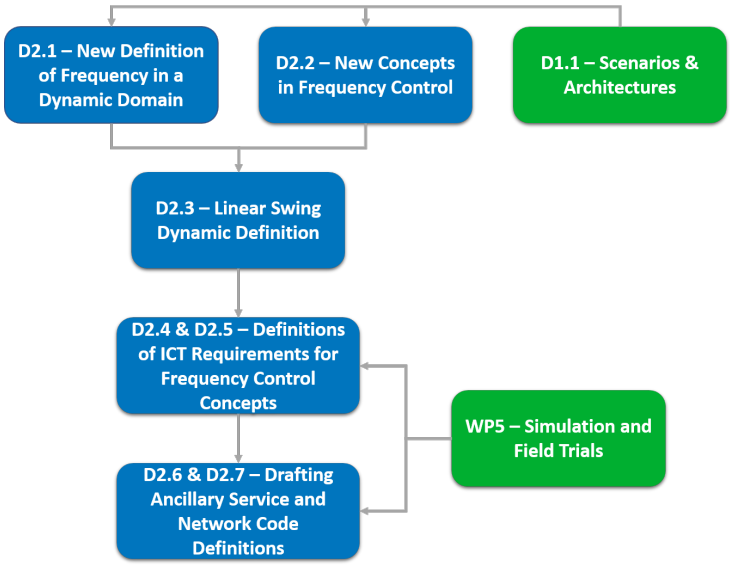

Figure 1.1: Relations between Deliverables in WP2 and other Work Packages.

1.4 Structure of the Deliverable

This deliverable is organized as follows. Chapter 2 provides a background of the concept of *frequency*, and the implications of the presence of frequency variations in power systems, while Chapter 3 presents the rationale behind the need of frequency control in power systems, and highlights the control strategies that are currently applied. Chapter 4 provides the rationale behind the proper definition of the frequency of a power system during transients. A new frequency estimation technique proposed in this deliverable, named *frequency divider* formula, is also described in Chapter 4. The description of the case studies carried out in this chapter is presented in Chapter 5. The case studies consider a large variety of topologies, frequency control devices, and frequency estimation techniques, and simulation results are comprehensively discussed in Chapter 6. Finally, Chapter 7 presents conclusions and draws future work directions.

2. Fundamental Frequency and Frequency Deviations in Power Systems

Any basic module on power systems taught in Engineering programmes sooner or later states that “the frequency in a power system is the same everywhere.” This information is clearly an oversimplification and is actually incorrect. A more accurate definition of *frequency* is provided in [18], as follows: *frequency means the electric frequency of the system expressed in hertz that can be measured in all parts of the synchronous area under the assumption of a consistent value for the system in the time frame of seconds, with only minor differences between different measurement locations. Its nominal value is 50Hz*. An important observation from this definition is that the frequency slightly fluctuates from bus to bus due to local load variations. More importantly, after a contingency such fluctuations can become large and, in some cases, lead to the loss of synchronism of some generator and, even, to the collapse of the whole system.

The study of the loss of synchronism (transient stability analysis) is actually one of the most important dynamic analyses carried out hundreds of times per minute, every minute, by system operators all around the world. Hence, the statement above is an oversimplification of a complex topic. The fundamental concept, however, is that the frequency of an electrical energy system is basically a common “property” of the system itself, at least in an ideal steady-state condition. It is relatively easy to show, in fact, that the only condition for which all machines are in steady-state is when they are synchronous, i.e., when their rotor speeds are equal.

Without digging into the maths (see e.g. [31, 37], and D2.2 for more details), it can be useful to say that the principle with which synchronous machines synchronize is basically the same that leads to the synchronization of pendulum clocks in the famous empirical observation described by Huygens in 1665 (see, for example, [48]).

The following two remarks are relevant:

- The condition for which the machines are synchronous does not actually imply that the frequency is equal to the nominal one, i.e., 50 Hz (or 314.16 rad/s). Surprisingly enough, the machines are most of the time rotating at speeds different than the nominal one as shown in Fig. 2.1. This means that for the vast majority of time, the system is actually in transient conditions and, hence, the frequency is not exactly the same everywhere. It is important to note, however, that large frequency deviations are not allowed (see Table 4.1).
- Satisfying such a condition is an intrinsic property of synchronous machines. In other words, the machines tend to synchronize even without the help of controllers.

The latter remark does not mean that synchronous machines do not need control. In actual power systems, primary machine controllers, namely, turbine governors and automatic voltage regulators are mandatory and fundamental for the operation of the whole system (this point is outlined in next section below and new frequency control techniques are discussed in D2.2). However, it is important to note that the behaviour of synchronous machines is intrinsically stable even without such controllers. Instability arises due to mainly three, often combined, effects:

- High loading conditions;
- Large disturbances, e.g., three-phase faults; and
- Poor tuning of machine controllers.

The next section discusses the effect of primary and secondary frequency control on power systems.

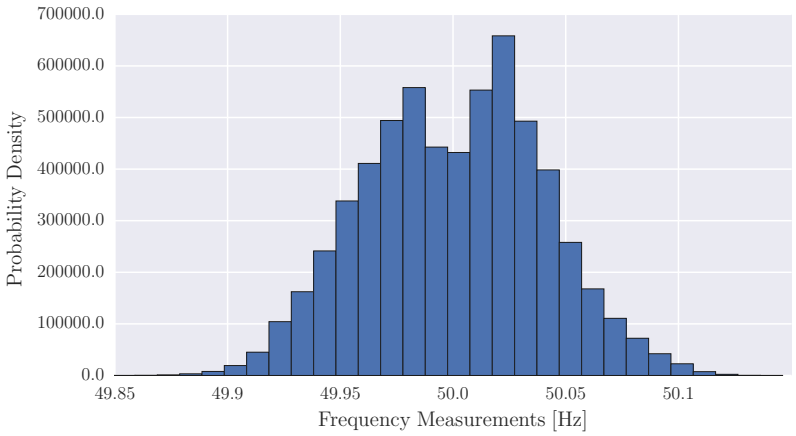

Figure 2.1: Probability density of the frequency of the Irish system measured with a frequency disturbance recorder (FDR) [36] from the 16th to the 22nd of December 2016.

3. Rationale behind Primary and Secondary Frequency Control

This section briefly discusses the rationale behind the need of both primary and secondary frequency control in current mechanical inertia-based power systems. We refer the reader to D2.2 for an in-depth description of both frequency control strategies. Note that, in this scenario, one does not need to estimate or measure any frequency, except for maybe at one pilot bus chosen for the secondary frequency control.

3.1 Primary Frequency Control

The main objective of the frequency regulation of a high-voltage (HV) transmission system is to maintain the balance between the power produced by the generators and the power consumed by the loads at the rated frequency. To avoid large excursions of the system frequency following a disturbance, say ΔP_D, a primary frequency control (PFC) is included in every synchronous machine-based power plant. Roughly speaking, this consists in a transfer function $G_f(s)$ that takes as input the rotor speed error ε_Ω, i.e., the difference between the synchronous speed $\Delta\Omega^{\text{ref}}$ and the instantaneous machine rotor speed $\Delta\Omega$ and imposes to the machine the required mechanical power ΔP_g to reduce such a frequency error (see the top panel of Fig. 3.1).

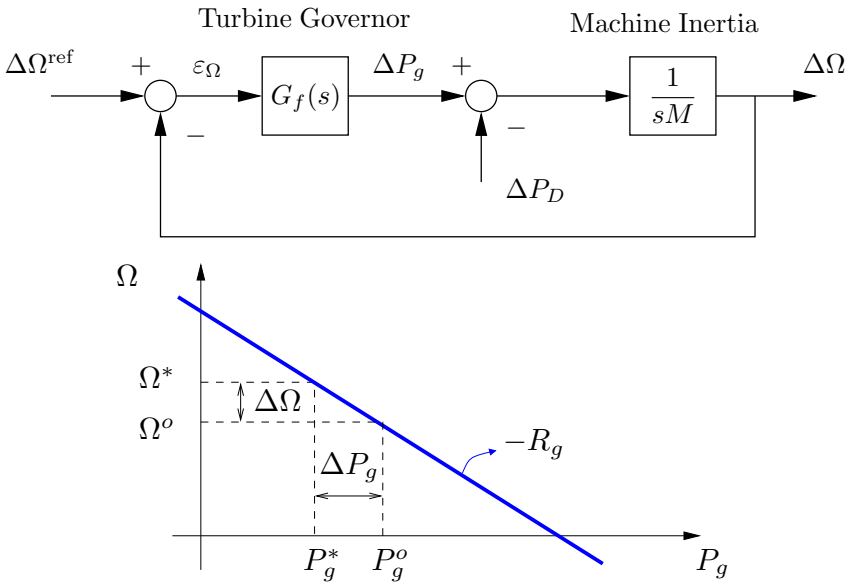

Figure 3.1: Primary frequency control. Top: basic control scheme; Bottom: steady-state characteristic.

Standard turbine governor transfer functions $G_f(s)$ do not perfectly track the frequency and, thus, the error ε_Ω is not null in steady-state. The magnitude of ε_Ω, and thus of the frequency variation $\Delta\Omega$ in steady-state, will depend on a parameter of the turbine governor, generally referred to as the *droop* R_g, and on the variation of the total electrical power demand ΔP_D (see the bottom panel of Fig. 3.1). For grids with several synchronous machines, each machine contributes separately to the regulation of the frequency according to their specific droops. In general, the droops of the machines of a system tend to be very similar to avoid that some machine regulates less or more than the others.

3.2 Secondary Frequency Control

In most large interconnected systems, the secondary frequency control or automatic generation control (AGC), is utilized to remove the frequency steady-state error due to the PFC through an appropriate rescheduling of generating units. To ensure stability, however, the AGC is much slower than the PFC. This leads to the fact that, for a considerable amount of time, the frequency of the system is actually not the synchronous one, i.e., 50 Hz, as illustrated in the example depicted in Fig. 3.2.

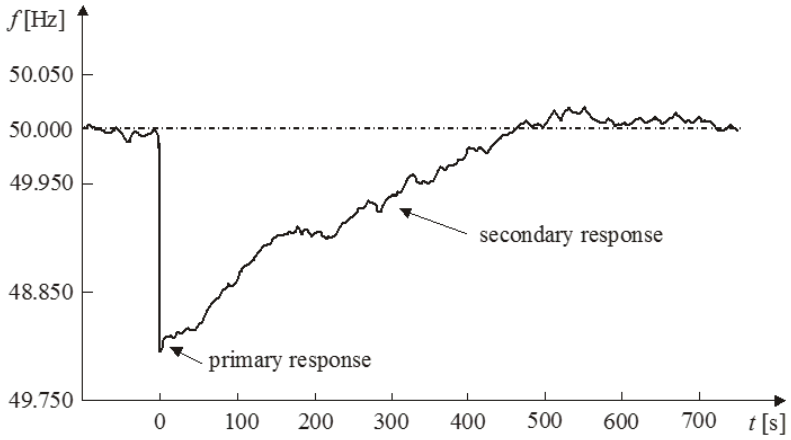

Figure 3.2: Example of automatic frequency control.

Another example is also presented in Chapter 2, where Fig.2.1 shows that the frequency of the Irish power system under normal operating conditions is characterized by a bimodal distribution. Such a distribution is due, in the case of the Irish system, to the dead-band included in the PFC of synchronous machine-based power plants and the absence of the AGC – more details can be found in [36]. Whenever the AGC is included into the system, the frequency variations distribute as a normal distribution, with a mean frequency equal to the synchronous one.

4. Measuring vs. Estimating the Frequency

The frequency of an electrical signal cannot be measured directly. When the penetration of power electronics converters and distributed energy resources was not massive, the estimation of the frequency was basically limited to rotating machines through the measure of the mechanical angular speed of the shaft. This was the case of the primary frequency control of synchronous machines and speed/position control of motor in industrial applications.

The large penetration of power electronics-based devices, such as all voltage sourced converter (VSC)-based and current sourced converter (CSC)-based distributed energy resources (DERs) and the development of phasor measurement units (PMUs), has led to the need to define the phase angle of voltage and/or current phasors. This is typically obtained by means of phase-lock loops (PLLs) [10, 46]. PMUs, apart of PLLs, also include a GPS signal to synchronise angle measurements. A by-product of PLLs is that an intermediate variable of the loop is a good estimation of the frequency deviation (see, for example, Fig. B.2 and the discussion provided in Subsection B.3).

In recent years, there has been a proliferation of devices able to estimate the frequency also at distribution, e.g., micro PMUs (μPMU) [57] and low voltage levels, e.g., FDRs [69, 74],

4.1 Need for Frequency Estimation in Power Systems

The previous section states why the frequency of a power system is close to, but for most of the time not exactly equal to the nominal frequency.

For the correct operation of the power system the frequency cannot deviate too much from the nominal value. Large variations, in fact, cause, in the short term (seconds) the loss of synchronism of synchronous machines and, in the long term (minutes), the malfunctioning of devices and protections, which, ultimately, can trigger system-wide blackouts. An example of this process is the blackout occurred in Italy on 28th October 2003 [8].

Table 4.1 shows frequency quality parameters for the synchronous areas that compose the ENTSO-E, namely, continental Europe area (CE), Great Britain (GB), the all-island Irish system (IRE), and the synchronous inter-Nordic system (NE).[1]

Table 4.1: ENTSO-E Network Code: frequency quality parameters per synchronous area

Quantity	CE	GB	IRE	NE
Standard frequency range	$\pm$ 50 mHz	$\pm$ 200 mHz	$\pm$ 200 mHz	$\pm$ 100 mHz
Max. instantaneous Freq. deviation	800 mHz	800 mHz	1000 mHz	1000 mHz
Max. steady-state Freq. deviation	200 mHz	500 mHz	500 mHz	500 mHz
Time to recover frequency	*not used*	1 min	2 min	*not used*
Time to restore frequency	15 min	10 min	20 min	15 min
Alert state trigger time	5 min	10 min	10 min	5 min

Based on the limits reported in Table 4.1, ENTSO-E defines relevant balancing principles and rules in the Network Code on Load-Frequency Control and Reserves. This network code defines three levels of controls, as follows.

- Frequency Containment (FC): FC shall aim at containing the system frequency deviation after an incident within a pre-defined range which is similar to the traditional primary load-frequency control.
- Frequency Restoration (FR): FR shall aim at restoring the system frequency to its nominal frequency of 50 Hz which is similar to the traditional secondary load-frequency control.

[1] ENTSO-E networks codes are available at `http://annualreport2016.entsoe.eu/network-codes/`.

- Replacement Reserves (RR): RR replace the activated reserves to restore the available reserves in the system or for economic optimization which is similar to the Tertiary Load-Frequency control.

It is important to observe that there are basically two relevant time scales for frequency deviations, namely the one due to the inertia response of synchronous machines and the one related to the primary frequency response of synchronous machines (see Fig. 4.1 and Subsection 4.3.2 of Deliverable D1.1).

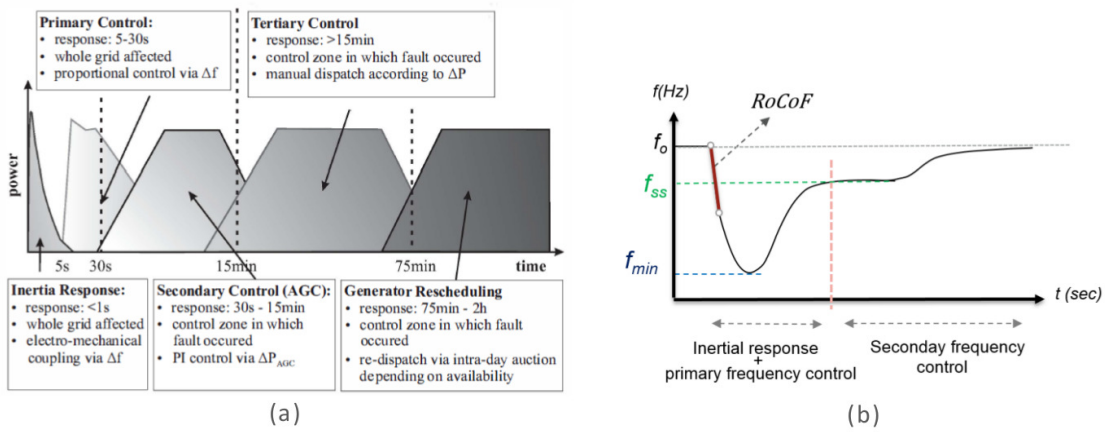

Figure 4.1: Synchronous machine synchronization and frequency regulation: (a) relevant time scales; and (b) typical frequency dynamic following a contingency.

This deliverable discusses transient effects due the inertia response of synchronous machines whereas primary and secondary frequency regulation as well as the impact of the frequency control of renewable energy resources is discussed in Deliverable D2.2.

For the time scale considered in this deliverable, i.e., from few hundreds of milliseconds to few seconds following a contingency, the frequency of each machine cannot be assumed to be the same everywhere and, hence, the location and the accuracy of the frequency estimation is important for the system.

Figure 4.2 shows the separation of the Turkish system occurred after a cascade line tripping phenomenon occurred on 31st March 2015. The East region of the network (with energy surplus) was disconnected from the West part (energy deficit) and finally collapsed. The event led to frequency oscillations visible in the Romanian system, as shown in Fig. 4.3.

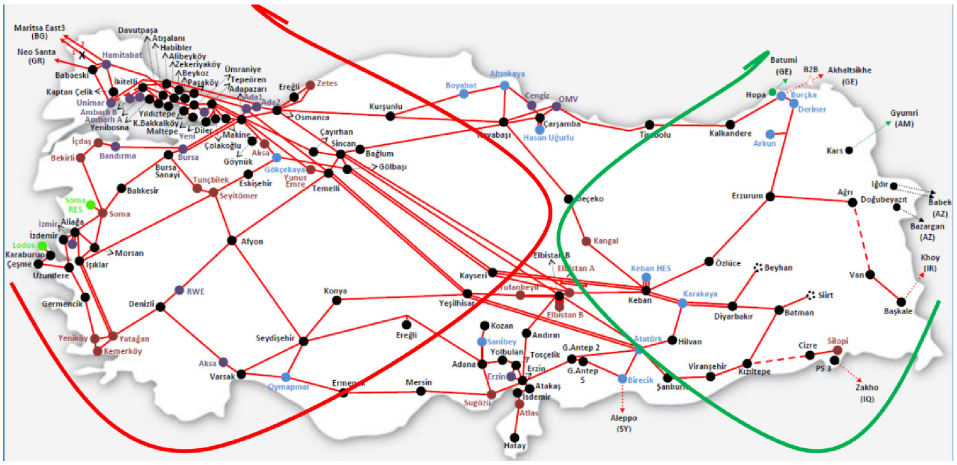

Figure 4.2: Separation of the Turkish transmission grid that led to the collapse of the Western region on 31st March 2015 (data provided by TransElectrica).

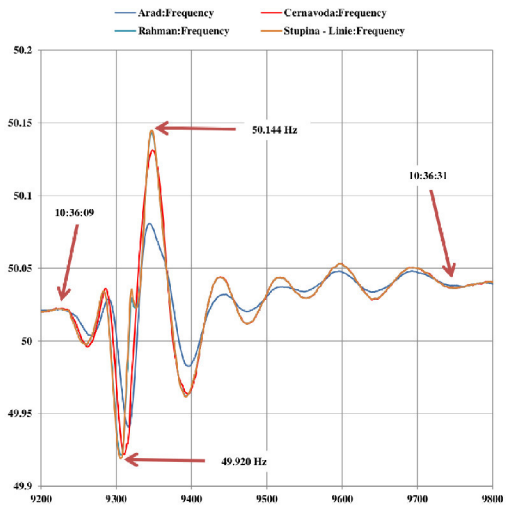

Figure 4.3: PMU measurements of geographically separated nodes in Romania following the event that led to the collapse of the Turkish grid (data provided by TransElectrica).

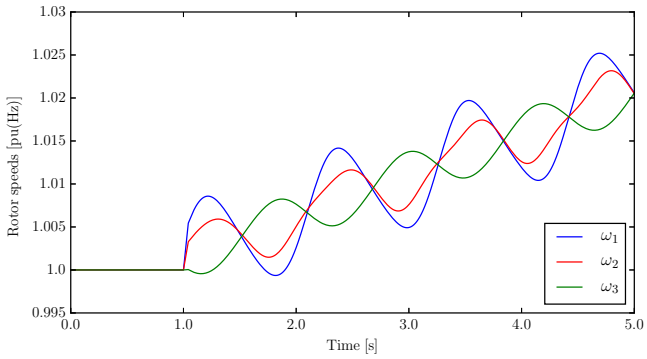

Figure 4.4: Rotor speed dynamics following a three-phase faults for a simple 3-machine test systems.

It is important to note that frequency deviations can be consistently different depending on the location of the fault and the machines. It is thus impossible to predict *a priori* the behaviour of each machine. It is also very important to note that the oscillations of the rotor speed and, hence, of the local frequency, depends on the *modes* of the system and the *clusters* that the synchronous machines form. Each coherent cluster oscillates differently than the others. In particular, at a given time, some clusters locally accelerate and other locally decelerate.

This behaviour can be easily illustrated using an example where the machines form only two clusters. Figure 4.4 shows the transient response of the rotor speed for the 3-machine WSCC test system (see Figure C.1 in Appendix C), which is largely used in the literature for transient stability analysis [59, 5]. The transient is originated by a three-phase fault. This leads the machines to oscillate and, as it can be clearly seen in Figure 4.4, the rotor speeds of machines 1 and 2 are coherent (cluster 1) and oscillate in counter-phase with respect to machine 3 (cluster 2). In a more complex systems, with several machines, there will be more clusters and more oscillating modes, but for each mode, there will one or more clusters oscillating *against* the others.

Therefore, from observing Figs. 4.3 and 4.4, the definition by [18] of *frequency* provided in Chapter 2 is not applicable during the first instants after a large disturbance. Moreover, it is to be expected that, as the penetration of non-synchronous generation increases, so will the local frequency deviations. Therefore, a new definition of *frequency* is required for high dynamic conditions that will characterize the power systems with 100% RES penetration.

From observing Figure 4.4, one can understand why it is important to measure the right (preferably, *local*) frequency signal. Whether the frequency is increasing or decreasing, in fact, is not a global property of the system, but depends on the cluster where the measure is taken. Hence, a controller aimed at regulating the frequency has to be fed with the proper frequency signal. In the past, when only the synchronous machines of large power plants were providing frequency control, the local frequency was always available and there was no doubt on which was the signal to be used (i.e., rotor speed deviations). However, it is not so clear which is the most appropriate frequency signal to use for distributed energy resources or loads equipped with frequency control. It is possible that the local frequency measured through a PMU or a PLL is actually not the best signal and that a remote measure or a signal obtained as the combination of more than one measure leads to better performances. The remainder of this deliverable duly investigates the effect of different strategies to measure and control the frequency.

4.2 Techniques to Estimate the Frequency

When dealing with power system dynamic analysis and control, we necessarily rely on computer-based simulations. There is no other meaningful way to define the behaviour of complex systems with hundreds of synchronous machines and thousands of state variables. This is quite to be expected but leads to an important and not-so-obvious caveat that has to be always kept in mind.

In a simulated model, all quantities are available, these are the variables that, along with the set of differential algebraic equations (DAEs), define the mathematical model to be simulated. Clearly, during the simulation, all these variables are available and can be known instantaneously with the required precision. Measured quantities are a small subset of the variables of the DAEs.

With regards to the topic of this deliverable, it is thus important to distinguish clearly between actual measured quantities, e.g., the output of PLL devices and rotor speed deviations (that are certainly available to local controller of DERs and synchronous machines, respectively) and simulated quantities, which can be computed during the simulation but are not available everywhere in the network at a given time, e.g., the speed of the center of inertia.

Then, from the simulation point of view, we have an additional complication, since frequency deviations are not actually taken into account in the model of the network. This is a counter-intuitive, although well-accepted simplification that leads to the definition of high-voltage transmission system models. The rationale behind this assumption has its roots in the models of the grid as it was before the large penetration of DERs and the smart-grid era.

The main idea is that, in real-world systems, frequency deviations are rather small (again, we refer the reader to Table 4.1). Moreover, if the only device that can provide frequency regulation is the synchronous machine, there is no need to carry on a detailed information of the frequency deviations in transmission lines, transformers and loads. Hence, the standard power system model that is implemented in the totality of commercial software tools for transient stability analysis is as follows (see Appendix 11 for details):

- Park (dq-axis) model of synchronous machines. This model retains transient and sub-transient dynamics, as well as the rotor speed and angle dynamics.
- Time-domain and/or dq-axis models for the controllers of synchronous machines other devices.
- Lumped, single-phase equivalent, quasi-steady-state models for transmission lines and transformers.

The latter assumption implies that the voltages at all buses of the system are phasors, whose frequency is assumed to be equal to the nominal frequency (e.g., 50 Hz) of the system. While this assumption can appear inadequate to study the dynamic response of a transmission system, it is actually quite accurate (see for example the discussion in [37]), provided that one does not need to estimate frequency deviations at buses.

Standard power system models and simulations are thus unable to determine how the frequency vary in the transmission system and, in particular, at the buses of non-synchronous DERs and loads. This fact leads to the conclusion that with standard power system models, we can estimate frequency deviations (through, for example, approximated models of PLLs and PMUs) but we do not know the *exact* value of such deviations. This makes particularly complicate to understand whether a frequency controller is ineffective because of an inaccurate estimation strategy or because the signal, even if measured perfectly, is not adequate.

To cope with this issue, we have developed the concept of *frequency divider* (FD), whose mathematical background is extensively discussed in Section B.4 of Appendix B. The FD formula, under some approximations and assumptions, provides the information that is missing from standard power system models, namely, the *exact* frequency deviations at every bus of the grid. The interested reader can find in Appendix C a thorough study aimed at validating the proposed FD formula by means of fully-fledged real-time digital simulations and hardware-in-the-loop PMU devices. The results of this comparison are promising and indicate that the hypothesis and approximations assumed to derive the expression of the FD formula are quite reasonable and lead to accurate estimations of the frequency at the network buses.

An argument against the utilization of the FD and standard power system model for transient stability analysis could be that one can use accurate fully-fledged electromagnetic models and real-time digital simulators. While this is certainly possible, it would be still too time consuming and too costly to set up the model of a large real-world transmission system on a real-time digital simulator. More importantly, even if this was possible, the frequency at network bus should be still be estimated using PLLs or equivalent devices, and, in turn, there would not be any significant advantage with respect to a simulation based on a standard power system model for transient stability analysis.

Using the FD, standard synchronous machine models and adequate models of PLLs and washout filters, we are able, in the same simulation, to have the following signals:

- Exact rotor speed deviations of synchronous machines;
- Ideal centre of inertia signal;
- Ideal frequency deviations at network buses; and
- Estimations of frequency deviations at network buses.

The latter are the signals that are utilized in the actual controllers of DERs and flexible loads. These signals are also potentially affected by numerical issues (e.g., spikes due to the numerical derivative of a step variation of the bus voltage) and physical issues (e.g., delays and noise). A detailed description of the frequency estimation techniques considered in this document are given in Appendix B.

With the signals above it is thus possible to study the following:

1. Determine which frequency signals are best to control the frequency through DERs and other non-synchronous devices.
2. Identify the PLL implementations that minimize the effects of numerical issues;
3. Identify the PLL implementations that minimize the effects of physical issues; and
4. Define the minimum requirements that the devices that estimate the frequency have to satisfy to be adequate to be used for the frequency control of non-synchronous devices.

This deliverable addresses points 1 and 2 above. We will address remaining points while completing the work for Task 2.1.

5. Impact of Frequency Estimation on Frequency Control

It is relevant to study the effect of the provision of primary frequency control by non-synchronous power system devices. With this aim, Wind Energy Conversions Systems (WECSs), Solar Photo-Voltaic Generation (SPVG), Energy Storage Systems (ESSs), and Thermostatically Controlled Loads (TCLs) are analysed in Sections D.1, D.2, D.3 and D.4, respectively, of Appendix D. This appendix also provides a comparison of the performance of the frequency controllers of these devices when their input signals are generated by each of the frequency estimation techniques presented in Appendix B.

The tests carried out in Appendix D cover a variety of aspects, as described below.

5.1 Topology of the System

Several test systems with different characteristics, loading levels and "weaknesses" are considered. These are:

- *WSCC 9-bus, 3-machine system*. This network is highly symmetrical (loads and generation are evenly distributed in the network) and has been largely utilised in the literature for transient stability and frequency control and stability analyses, e.g., [59, 5]. This network is utilised in Chapter C and Sections D.1.1 and D.2.1.
- *IEEE 14-bus system*. This network shows two main regions, one with generation and voltage support (through synchronous compensators and shunt capacitors) and a region with loads. It is particularly adequate to carry out small-signal stability and voltage stability analyses, e.g., [37]. This network is utilised in Sections D.3.1 and D.4.1.
- *New England 39-bus, 10 machine system*. This is the largest test system considered in this report. It is largely used in the literature to test inter-area controllers, carry out transient stability, small-signal stability and voltage stability analyses. This network is utilised in Section D.4.2.

5.2 Frequency Control Devices

A variety of non-synchronous devices that are expected to play an important role in the near future to control the frequency are considered in the report. These are:

- *Wind energy conversion systems (WECSs)*. Currently, WECS with variable-speed control include a maximum power point tracking (MPPT) device that measures the current rotor speed of the turbine and imposes the optimal output power by changing the currents in the power electronic converter connected to the generator. Frequency control can be obtained by modifying the output of the MPPT and imposing an active power reference that takes into account frequency deviations (see Figure D.1). Clearly, it is always possible to decrease the optimal active power reference given by the MPPT. To increase such a reference, one should impose that the wind turbine is not operating at its optimal value, i.e., it provides a reserve. Several control schemes have been proposed in the literature, the most common ones being those that imposes a rate of change of frequency (RoCoF) control in parallel with the MPPT [55, 35, 43, 33]. WECS are discussed in Section D.1 of Appendix D.
- *Solar photo-voltaic generation (SPVG)*. Similarly to WECS, SPVG systems include a MPPT device that adjust the voltage at the terminal bus of PV cells to maximize the power generated by the cell itself. In principle, the optimal voltage can be defined based on the measures of the solar radiance and temperature of the cell but, most MPPTs are based on a simple trial-&-error technique. Since the control of SPVGs only involve electrical quantities, the MPPT can be modelled as an active power set-point for short-term simulations [65]. Frequency controllers modify such a set-point. As for WECS, increasing the active power set-point is possible only if one assumes that the SPVG provide active power reserve. SPVGs are discussed in Section D.2 of Appendix D.

- *Energy storage systems* (ESSs). These devices have been object of intense research in the last decade. While their cost is still preventing the installation of large ESSs in transmission systems, this situation may changing in the near future [51]. ESSs can be installed alone or as part of virtual power plants, i.e., combined with WECS and/or SPVGs. Depending on the technology used for the ESS (battery, flywheel, superconducting coils, etc.), the time response and capacity can vary considerably and so does the expected impact on frequency control [52]. ESSs are discussed in Section D.3 of Appendix D.

- *Thermostatically controlled loads (TCLs)*. Load demand response and load flexibility is an emerging research topic, which has attracted considerable attention in recent years (see, for example, IEEE Power & Energy magazine, Vol. 15, No. 1, January/February 2017, which is almost entirely dedicated to energy system flexibility). The idea behind load flexibility is relatively simple: some loads, such as heating systems, air conditioning, refrigerators, can shift or vary their power consumption without significantly impacting on their performance. However, if a large portion of the load can be regulated, the impact of the grid can be huge. Frequency control can be particularly efficient in all those cases were the time constant of the load (e.g., thermodynamic time constants can be several minutes or hours) is much larger than the time constant of the frequency control (seconds to minutes). In this deliverable we focus on aggregated models of TCLs, thus assuming that a certain percentage of the load can provide frequency control. Thermostatically controlled loads are discussed in Section D.4 of Appendix D.

5.3 Frequency Estimation

- *No frequency control*. This scenario is relevant to compare the effect of non-synchronous devices controlling the frequency and can be assumed to be the dynamic response of current power systems where only synchronous machines of large power plants provide inertia and primary and secondary frequency regulation.

- *Centre of inertia (COI)*. The COI is an *ideal* signal that weight rotor speeds with the inertia of synchronous generators. The main features of this signal are that local frequency oscillations and noise are generally filtered out and topological information is lost. Another relevant characteristic is that the COI signal does not show “jumps” or numerical spikes, because it is computed based on machine rotor speeds which are state variables, i.e., are continuous. The COI is widely used in the literature to define the effect of primary and secondary frequency regulation, but due to the difficulty of communicating and collecting the measures of the rotor speeds, it is seldom computed by system operators. In recent years, due to the deregulation of power systems, such measurements are also often confidential. Hence, control centres often use, instead of the COI, the frequency estimated at a “pilot bus” of the system (typically a bus with high short-circuit ratio). The analytical definition of the frequency of the COI is given in Section B.1.

- *Washout filter and PLL-based frequency estimation*. These are the actual devices commonly utilised to determine the local frequency. PLLs, in particular, are key components of all power electronic converters and PMU devices [67]. The main features are: (i) ability to determine the local frequency of a time-varying ac voltage measure; (ii) the accuracy of the resulting signal is greatly affected by the control scheme, noise, delays, etc. Since voltages have very fast dynamics, the estimated frequency can show numerical issues, such as jumps and spikes. A way to reduce such spikes is to include appropriate filtering. However, filters tend to introduce a delay in the measure, which, as discussed in Appendix D, can impact on the frequency control. It is thus necessary to define a trade-off between accuracy and delay of the estimated frequency. A description of the basic functioning and control schemes of washout filters and basic PLL devices are given in Sections B.2 and B.3, respectively.

- *Frequency divider formula*. The FD formula is a recent development [39] based on standard assumptions of power system models for transient stability analysis. Assuming that we can measure a set of frequencies at the border buses of a given region of the

power system and at the buses where the frequency is imposed (typically, synchronous machine buses), the frequency of all remaining buses can be estimated knowing the topology and the admittance matrix of the network. If the known frequencies are all synchronous machine rotor speeds, then the FD formula returns the *exact* frequency deviations at all buses. The formula has the advantage that can be used also in combination with or using exclusively PMU measurements, thus appearing as a practical tool for system operators. When PMU measurements are utilised, however, numerical issues can affect the results. The theory leading to the FD formula is presented in Section B.4 while a discussion on its practical implementation is given in Appendix E.

5.4 Links with Scenarios on the Frequency

The test systems considered in Appendix D, while being considerably different from the Romanian system that will be studied at the final stage of the project, they have been carefully set up and tuned in order to resemble, as accurately as possible, the different frequency scenarios presented in D1.1. Note that the purpose of Appendix D is to study the contribution of each frequency regulation device, separately, i.e., scenarios that combine different RESs such as wind and solar generation are not considered.

In particular, the following links between the scenarios described in D1.1 and the ones considered in this report are present:

- **Section D.1 and Scenarios Sf_A1 and Sf_A2**. The share of wind-based generation considered in Section D.1 is $\sim$30%. Results of the case studies presented in this section are thus relevant for later studies that will consider Scenarios Sf_A1 (26.5%) and Sf_A2 (49.0%).[1]
- **Section D.2 and Scenarios Sf_A1 and Sf_A3**. Similarly to the wind generation scenario, the penetration of SPVG in Section D.2 is also $\sim$30%, i.e., intermediate to scenarios Sf_A1 (11.0%) and Sf_A3 (40.3%).[1]
- **Section D.3 and Scenario Sf_B5**. The capacity of ESSs installed in Section D.3 is $\sim$11% of the total active power generated, and $\sim$20% of wind power generation is also considered in this scenario. This makes Section D.3 an useful test-bed to provide preliminary results of Scenario Sf_B5, where wind, solar and storage will be added to hydro and pumped-hydro power plants.
- **Section D.4 and Scenario Sf_B4**. In Section D.4, the contribution of flexible loads such as TCLs to the frequency regulation is studied. Therefore, results presented in this section can be of particular relevance for scenario Sf_B4 where no inertia is present in the system, thus frequency regulation from both generation and demand sides is required.

[1] For the time scales and scenarios considered in Appendix D, similar results and conclusions can be obtained for both nuclear/fossil fuel and hydro power plants.

6. Discussion of Results

Based on the simulation results on WECSs, SPVGs, ESSs and TCLs, presented in Appendix D, the following general remarks are relevant.

1. Results obtained using the FD are, in general always better in terms of frequency regulation than the other signals. This result is a consequence of the fact that the FD formula is the *exact* value of local frequency deviations. The FD can thus be utilized as a reference for testing the quality of the frequency estimated by the PLL and other estimation approaches.

2. When using standard power system electromechanical models, the standard synchronous reference frame model of the PLL compares reasonably well compared to the FD formula. Noise and numerical spikes do not deteriorate significantly the quality of the control, provided that WECSs include a proper low pass filter within their primary frequency controllers.

3. The numerical derivative of the bus voltage phase angle of the washout filter and PLLs can lead to non-physical oscillations and, possibly to numerical instabilities. In simulations, the effect of numerical issues due to washout filters and PLLs can be hidden if a reduced order model of synchronous machines and other dynamic devices is used. However, the dynamic coupling of flux dynamics and PLLs, can lead to unexpected (even unstable) dynamic response. It is interesting to note that, when using FD signal, undamped oscillations due to the coupling with fast dynamics disappear. It is thus crucial to properly design the PLLs to prevent its coupling with fast dynamics especially with devices with slow response (e.g., TCLs).

4. All frequency controllers include a low pass filter that, while introducing a slight delay in the controlled signal, reduces the operations of the converters and have no impact on the overall dynamic response of the system. The low-pass filter also allows reducing the impact of the noise and numerical issues present when the PLL is used to estimate the frequency.

5. The COI signal is inadequate to simulate, in some cases (e.g., WECSs), the behaviour of frequency controllers, although its average nature often leads to an overall smoother frequency response. This consideration could be further developed in the future considering coordinated area controllers sharing an average value of the frequency signal rather than utilizing a local one. Moreover, the average rotor speed provided by the COI filters local frequency variations. This fact may cause poorly-damped frequency oscillations, especially if coupled to devices with a slow response, such as TCLs.

6. SPVG devices, compared to WECS, tend to provide a slightly faster and, often, more effective, control. This is because in SPVG device there is no moving mechanical part.

7. The inclusion of ESSs in the system allows reducing, to a large extent, frequency and voltage variations due to severe contingencies such as faults, and to the stochastic nature of RESs such as wind power plants, thanks to the capability of ESSs to inject/absorb both active and reactive power simultaneously. However, the response of the ESS can be significantly deteriorated if current saturations of the storage device are reached. It is thus desirable that the converters included in the ESSs are over-designed to reduced current saturations.

8. The number of measures required by the exact *frequency divider* formula are cumbersome for real-world systems. However, the measures required to provide an acceptable estimation of the bus frequencies can be reduced considerably without loss of accuracy utilising the technique proposed in Appendix E. The results provided in this appendix prove the intuition that, in real-world transmission systems, only a very reduced number of synchronous machines are required to estimate the frequency of a certain bus of the network.

From the remarks above, it is concluded that a proper modelling of the control signals can make a significant difference in the transient stability analysis of a power system with inclusion of frequency controllers other than primary frequency regulators of synchronous machines. The definition of a criterion to estimate the fidelity of such power system models is thus as an interesting and urgent research topic.

7. Conclusion and Future Work

7.1 Conclusion

In this document, we have demonstrated that the current definition of *frequency* provided in [18] needs to be updated in order to take into account the high dynamic conditions that will characterize the upcoming power systems with very high or 100% RES penetration. In this regard, we propose in this deliverable a modification of such definition, as follows:

Frequency means the electric frequency of the system expressed in hertz that can be measured in all parts of the synchronous area under the assumption of a consistent value for the system, with only minor differences between different measurement locations in quasi steady-state conditions. Its nominal value is 50Hz.

In the definition above, two concepts have been modified with respect to the one provided in [18]. First, the definition of frequency, and thus the assumptions therein, should be valid for any time frame, not only for *the time frame of seconds*. Second, we have shown in this deliverable that, during transients, frequency variations between different measurement locations can be substantial, and must be taken into account for a proper operation and security of the network. Therefore, the assumption that *only minor differences* exist is applicable only in quasi steady-state conditions.

An important remark of the definition above is that quasi steady-state conditions are not affected by small disturbances such as noises. However, large disturbances and contingencies such as faults, loss of generating units and/or loads, and stiff RES active power variations, can lead, during a certain amount of time not known a priori, to high dynamic conditions in the system during which the frequency experiences local variations that can be large and fast. In such conditions, the definition of *frequency* above does not apply, and thus a new, complementary definition of *Rate of Change of Frequency* during high dynamic conditions becomes apparent. This new definition will be one of the outputs of Task T2.6.

This deliverable also shows the need to properly estimate local bus frequencies during electromechanical transients of high-voltage transmission system.

The document proposes and discusses a mathematical tool, namely the frequency divider, that is able to provide a precise estimation of local bus frequencies, based on the knowledge of synchronous machine rotor speeds and/or the frequencies at interconnection buses.

The frequency divider approach is utilized in the simulations as a mean to obtain the exact value of bus frequency variations. These signals are compared with actual physical devices, such as PLLs. Results show that the actual behaviour of PLLs can deviate from the expected (ideal) value due to fast flux transients, numerical derivation, latency and noise.

Based on simulation results obtained with both Dome software (developed at UCD by the authors) as well as RTDS and HiL (at the RWTH laboratory), we conclude that the frequency divider is a valuable tool to validate the dynamic behaviour and calibrate the parameters of the physical devices that are utilized to estimate local bus frequencies. The study carried out with the help of RWTH and based on a RTDS and HiL satisfies the objective of Milestone D2.1.

We also compare the impact on frequency control of local bus frequencies and a global signal, namely, the frequency of the COI. We conclude that local bus frequencies are to be preferred when dealing with short-term electromechanical transients.

A comprehensive study of the effect of different frequency signals on a variety of devices is carried out in the document. We considered WECS, SPVG, TCL and ESS devices. The conclusion is that devices fully decoupled from the ac grid through power electronics converters, namely, SPVG and ESS, are faster and, hence, more effective in short term transients than ac-coupled devices (WECS based on DFIGs and TCL). This indicates that VSC-connected devices can be

particularly effective for RoCoF (e.g., inertial) control. Again, due to the short time frame of the involved dynamic phenomena, accurate and precise estimation of the local frequency is crucial.

A quantitative appraisal of the matrix involved in the proposed frequency divider formula, which is obtained from the algebraic manipulation of the well-known network admittance matrix, also allows defining the participation factor of each generator and interconnection bus to each bus frequency. This is a valuable result with relevant consequences in the implementation of the frequency state estimation and associated communication systems.

Finally, new provisions on network codes have to be written to provide guidelines on the required frequency estimation, control and stability margins in the future energy systems.

7.2 Future Work

Based on the work presented in this deliverable, the following research concepts will be developed in future stages of WP2.

- *RoCoF control provided by ESSs.* In power systems with high shares of mechanical inertia-based generation, RoCoF control is inherently provided by the synchronous machines due to their instantaneous response to any power imbalance. However, as the share of non-synchronous generation increases, so does the need of additional RoCoF control devices. In this regard, ESSs are expected to play an important role in the RoCoF regulation of 100% RES systems, thanks to their ability to supply/absorb relatively large amounts of active power in very short time periods. In this regard, the goal of the study is to compare, for a 100% RES scenario considering the Romanian transmission system, the contribution of a variety of ESS technologies such as batteries, flywheels and supercapacitors, on the RoCoF reduction of a power system subject to a variety of uncertainties and contingencies. The aim is to determine the best ESS configuration that optimizes the RoCoF regulation, based on the different power ratings and time responses that characterizes each ESS technology. Once the best ESS configuration is defined, the effect on the performance of the ESS RoCoF control of the different frequency estimation techniques presented in this deliverable will be studied in detail. This study will complement the work on the provision of primary and secondary frequency control by ESSs presented in D2.2, and that will be further developed in WP2.

- *Frequency takers and frequency makers.* An assumption on which the definition of the FD formula is based is the fact that non-synchronous generation and loads do not impose the frequency at their point of connection with the grid. These devices are thus *frequency takers*, as opposed to synchronous generators of conventional power plants, which do impose the frequency at their point of connection and are thus *frequency makers*. This assumption is reasonable as long as non-synchronous devices do not regulate the frequency or, if they do, have small capacity. The increasing penetration of DERs and flexible loads, however, will lead to a situation where non-synchronous devices significantly impact on the local frequency deviations. For scenarios with very high or 100% penetration of RESs, most of which are non-synchronous, the distinction between frequency makers and frequency takers is thus not straightforward. From the point of view of the frequency control and the definition of the FD formula, the fact that non-synchronous generation or even load buses can become frequency makers would change the set of frequency measures to be considered and, hence, would impact on the design of the communication system. Another foreseeable issue is that, due to the stochastic nature of some DERs, a node can switch from frequency taker to frequency maker depending on the availability of renewable energy resources. It is thus important to define a quantitative criterion to distinguish between frequency takers and frequency makers to ensure that the estimated local frequencies are reliable.

- *Frequency state estimation for on-line stability analysis.* The FD formula can be interpreted as a conventional linear state estimation problem [20]. Such an optimization problem appears as a promising approach to estimate synchronous machine rotor speeds and, in general, any unknown frequency of a transmission grid, based on PMU

and/or PLL measurements. A proper formulation of the state estimation problem may allow reducing the number of required PMU measurements or, if measurements at all buses are available, it can provide a robust estimation of synchronous machine rotor speeds. This can have relevant applications in on-line transient and frequency stability analyses and consequently in the implementation of proper corrective control strategies. However, due to the short time scales involved, especially when dealing with transient instability, such an estimation would be useful only if PMU measurements are properly collected and transmitted to control centres. It is thus crucial to define the requirements that the communication system has to satisfy to make possible the implementation of such a state estimation for corrective control.

- *Impact of noise and delays of communication systems on the frequency control of non-synchronous devices.* Any practical implementation of the FD formula, requires the definition of the acceptable levels of noise and delays of the communication system to allow for an appropriate control. With this aim, it is important to define the stability margins of the combined effect of delays and noise of the frequency signals. The objective is to provide a quantitative criterion to decide whether a given communication network is feasible for frequency regulation.

8. References

[1] Electrical Energy Storage. white paper, Dec. 2011.

[2] AKHIL, A. A., HUFF, G., CURRIER, A. B., KAUN, B. C., RASTLER, D. M., CHEN, S. B., COTTER, A. L., BRADSHAW, D. T., AND GAUNTLET, W. D. *DOE/EPRI Electricity Storage Handbook in Collaboration with NRECA*. Feb 2015.

[3] ANAYA-LARA, O., HUGHES, F., JENKINS, N., AND STRBAC, G. Contribution of DFIG-based Wind Farms to Power System Short-term Frequency Regulation. *IEE Proceedings on Generation, Transmission and Distribution 153*, 2 (March 2006), 164–170.

[4] ANDERSON, P. M. *Analysis of Faulted Power Systems*. Wiley-IEEE Press, New York, NY, 1995.

[5] ANDERSON, P. M., AND FOUAD, A. A. *Power System Control and Stability*, second ed. Wiley-IEEE Press, New York, NY, 2002.

[6] BEAUDIN, M., ZAREIPOUR, H., SCHELLENBERGLABE, A., AND ROSEHART, W. Energy storage for mitigating the variability of renewable electricity sources: An updated review. *Energy for Sustainable Development 14* (2010), 302–313.

[7] BERG, G. L. Power System Load Representation. *Proceedings of the IEEE 120*, 3 (1973), 344–348.

[8] BERIZZI, A. The Italian 2003 blackout. In *IEEE Power Engineering Society General Meeting, 2004.* (June 2004), pp. 1673–1679 Vol.2.

[9] BEVRANI, H., GHOSH, A., AND LEDWICH, G. Renewable Energy Sources and Frequency Regulation: Survey and New Perspectives. *IET Renewable Power Generation, IET 4*, 5 (Sept 2010), 438–457.

[10] BLAABJERG, F., TEODORESCU, R., LISERRE, M., AND TIMBUS, A. V. Overview of control and grid synchronization for distributed power generation systems. *IEEE Trans. on Industrial Electronics 53*, 5 (Oct 2006), 1398–1409.

[11] CASTRO, L., AND ACHA, E. On the Provision of Frequency Regulation in Low Inertia AC Grids Using HVDC Systems. *IEEE Transactions on Smart Grid PP*, 99 (2015), 1–11.

[12] CHAUHAN, A., AND SAINI, R. Statistical Analysis of Wind Speed Data Using Weibull Distribution Parameters. In *1st International Conference on Non Conventional Energy (ICONCE 2014)* (Kalyani, India, Jan. 2014), pp. 160–163.

[13] DASSIOS, I. K., CUFFE, P., AND KEANE, A. Visualizing voltage relationships using the unity row summation and real valued properties of the flg matrix. *Electric Power Systems Research 140* (2016), 611 – 618.

[14] DIGSILENT. *PowerFactory Technical Reference Ver. 15*. Gomaringen, Germany, 2015.

[15] DUESTERHOEFT, W. C., SCHULZ, M. W., AND CLARKE, E. Determination of Instantaneous Currents and Voltages by Means of Alpha, Beta, and Zero Components. *Transactions of the American Institute of Electrical Engineers 70*, 2 (July 1951), 1248–1255.

[16] EKANAYAKE, J., AND JENKINS, N. Comparison of the Response of Doubly Fed and Fixed-Speed Induction Generator Wind Turbines to Changes in Network Frequency. *IEEE Trans. on Energy Conversion 19*, 4 (Dec. 2004), 800–802.

[17] EL-HAWARY, M. E. *Electrical Energy Systems*, second ed. CRC Press, Boca Raton, FL, 2000.

[18] EUROPEAN NETWORK OF TRANSMISSION SYSTEM OPERATORS FOR ELECTRICITY (ENTSO-E). Commission Regulation (EU) 2016/631 of 14 April 2016 establishing a network code on requirements for grid connection of generators, 2016.

[19] FERNANDEZ-BERNAL, F., ROUCO, L., CENTENO, P., GONZALEZ, M., AND ALONSO, M. Modelling of Photovoltaic Plants for Power System Dynamic Studies. In *2002 Fifth International Conference on Power System Management and Control Conf. Publ. No. 488)* (April 2002), pp. 341–346.

[20] GÓMEZ-EXPÓSITO, A., CONEJO, A. J., AND CAÑIZARES, C. A. *Electric Energy Systems: Analysis and Operation*. CRC Press, Boca Raton, FL, 2009.

[21] GROSS, C. A. *Power System Analysis*, second ed. John Wiley & Sons, New York, NY, 1986.

[22] HIRSCH, P. *Extended Transient-Midterm Stability Program (ETMSP), Ver.3.1 User's Manual*. EPRI, 1994.

[23] HSU, C.-S., CHEN, M.-S., AND LEE, W. Approach for Bus Frequency Estimating in Power System Simulations. *IEE Proceedings-Generation, Transmission and Distribution 145*, 4 (Jul 1998), 431–435.

[24] IEEE TASK FORCE ON LOAD REPRESENTATION FOR DYNAMIC PERFORMANCE. Load Representation for Dynamic Performance Analysis [of Power Systems]. *IEEE Transactions on Power Systems 8*, 2 (May 1993), 472–482.

[25] ILLINOIS CENTER FOR A SMARTER ELECTRIC GRID (ICSEG). IEEE 39-Bus System. URL: http://publish.illinois.edu/smartergrid/ieee-39-bus-system/.

[26] KARIMI, H., KARIMI-GHARTEMANI, M., AND IRAVANI, M. R. Estimation of frequency and its rate of change for applications in power systems. *IEEE Trans. on Power Delivery 19*, 2 (April 2004), 472–480.

[27] KO, H. S., YOON, G. G., AND HONG, W. P. Active Use of DFIG-Based Variable-Speed Wind-Turbine for Voltage Regulation at a Remote Location. *IEEE Transactions on Power Systems 22*, 4 (Nov 2007), 1916–1925.

[28] KODSI, S. K. M., AND CAÑIZARES, C. A. Modeling and Simulation of IEEE 14-bus System with FACTS Controllers. Tech. Rep. 2003-3, University of Waterloo, Waterloo, Mar. 2003.

[29] KRAUSE, P. C., WASYNCZUK, O., AND SUDHOFF, S. D. *Analysis of Electric Machinery and Drive Systems*, second ed. Wiley-IEEE Press, 2002.

[30] KUNDU, S., SINITSYN, N., HISKENS, I., AND BACKHAUS, S. Modeling and Control of Thermostatically Controlled Loads. In *17th Power Systems Computation Conference 2011, (PSCC 2011 STOCKHOLM)* (2011), pp. 969–975.

[31] KUNDUR, P. *Power System Stability and Control*. McGraw-Hill, New York, 1994.

[32] LU MIAO, JINYU WEN, HAILIAN XIE, CHENGYAN YUE, AND WEI-JEN LEE. Coordinated Control Strategy of Wind Turbine Generator and Energy Storage Equipment for Frequency Support. *IEEE Transactions on Industry Applications 51*, 4 (July 2015), 2732–2742.

[33] MARGARIS, I. D., PAPATHANASSIOU, S. A., HATZIARGYRIOU, N. D., HANSEN, A. D., AND SORENSEN, P. Frequency control in autonomous power systems with high wind power penetration. *IEEE Trans. on Sustainable Energy 3*, 2 (April 2012), 189–199.

[34] MATHIEU, J. L., KOCH, S., AND CALLAWAY, D. S. State Estimation and Control of Electric Loads to Manage Real-Time Energy Imbalance. *IEEE Transactions on Power Systems 28*, 1 (2013), 430–440.

[35] MAURICIO, J. M., MARANO, A., GÓMEZ-EXPÓSITO, A., AND RAMOS, J. L. M. Frequency Regulation Contribution Through Variable-Speed Wind Energy Conversion Systems. *IEEE Transactions on Power Systems 24*, 1 (Feb 2009), 173–180.

[36] MELE, F. M., ORTEGA, Á., ZÁRATE-MIÑANO, R., AND MILANO, F. Impact of variability, uncertainty and frequency regulation on power system frequency distribution. In *2016 Power Systems Computation Conference (PSCC)* (June 2016), pp. 1–8.

[37] MILANO, F. *Power System Modelling and Scripting*. Springer, London, 2010.

[38] MILANO, F. A Python-based Software Tool for Power System Analysis. In *Procs. of the IEEE PES General Meeting* (Vancouver, BC, July 2013).

[39] MILANO, F., AND ORTEGA, Á. Frequency Divider. *IEEE Transactions on Power Systems* (2016). (in press).

[40] MILANO, F., AND ZÁRATE-MIÑANO, R. Study of the Interaction between Wind Power Plants and SMES Systems. In *12th Wind Integration Workshop* (London, UK, Oct. 2013).

[41] MILANO, F., AND ZÁRATE-MIÑANO, R. A systematic method to model power systems as stochastic differential algebraic equations. *IEEE Trans. on Power Systems 28*, 4 (Nov 2013), 4537–4544.

[42] MINYUAN GUAN, WULUE PAN, JING ZHANG, QUANRUI HAO, JINGZHOU CHENG, AND XIANG ZHENG. Synchronous Generator Emulation Control Strategy for Voltage Source Converter (VSC) Stations. *IEEE Transactions on Power Systems 30*, 6 (Nov 2015), 3093–3101.

[43] MORREN, J., DE HAAN, S. W. H., KLING, W. L., AND FERREIRA, J. A. Wind turbines emulating inertia and supporting primary frequency control. *IEEE Transactions on Power Systems 21*, 1 (Feb 2006), 433–434.

[44] MORREN, J., PIERIK, J., AND DE HAAN, S. W. H. Inertial response of variable speed wind turbines. *Electric Power Systems Research 76*, 11 (2006), 980–987.

[45] MOUTIS, P., VASSILAKIS, A., SAMPANI, A., AND HATZIARGYRIOU, N. DC Switch Driven Active Power Output Control of Photovoltaic Inverters for the Provision of Frequency Regulation. *IEEE Transactions on Sustainable Energy 6*, 4 (Oct 2015), 1485–1493.

[46] NICASTRI, A., AND NAGLIERO, A. Comparison and evaluation of the PLL techniques for the design of the grid-connected inverter systems. In *2010 IEEE International Symposium on Industrial Electronics* (July 2010), pp. 3865–3870.

[47] NUTARO, J., AND PROTOPOPESCU, V. Calculating Frequency at Loads in Simulations of Electro-Mechanical Transients. *IEEE Transactions on Smart Grid 3*, 1 (March 2012), 233–240.

[48] OLIVEIRA, H. M., AND MELO, L. V. Huygens Synchronization of Two Clocks. *Scientific Reports 5* (2015). Available at: www.nature.com/articles/srep11548.

[49] ORTEGA, Á., AND MILANO, F. Design of a Control Limiter to Improve the Dynamic Response of Energy Storage Systems. In *Power Engineering Society General Meeting, IEEE* (Denver, Colorado, USA, July 2015).

[50] ORTEGA, Á., AND MILANO, F. Comparison of Bus Frequency Estimators for Power System Transient Stability Analysis. In *International Conference on Power System Technology (POWERCON)* (Wollongong, Australia, Sept. 2016).

[51] ORTEGA, Á., AND MILANO, F. Generalized Model of VSC-Based Energy Storage Systems for Transient Stability Analysis. *IEEE Transactions on Power Systems 31*, 5 (Sept 2016), 3369–3380.

[52] ORTEGA, Á., AND MILANO, F. Modeling, simulation, and comparison of control techniques for energy storage systems. *IEEE Transactions on Power Systems 32*, 3 (May 2017), 2445–2454.

[53] PALIZBAN, O., AND KAUHANIEMI, K. Energy Storage Systems in Modern Grids - Matrix of Technologies and Applications. *ELSEVIER Journal of Energy Storage 6* (2016), 248–259.

[54] PAVELLA, M., ERNST, D., AND RUIZ-VEGA, D. *Transient Stability of Power Systems – A Unified approach to Assessment and Control*. Kluwer Academic Publishers, Boston, 2000.

[55] RAMTHARAN, G., EKANAYAKE, J. B., AND JENKINS, N. Frequency support from doubly fed induction generator wind turbines. *IET Renewable Power Generation 1*, 1 (March 2007), 3–9.

[56] RIBEIRO, P. F., JOHNSON, B. K., CROW, M. L., ARSOY, A., AND LIU, Y. Energy Storage Systems for Advanced Power Applications. *Proceedings of the IEEE 89*, 12 (Dec. 2001), 1774–1756.

[57] ROBERTS, C., STEWART, E. M., AND MILANO, F. Validation of the ornstein-uhlenbeck process for load modeling based on μpmu measurements. In *19th Power System Computation Conference (PSCC)* (Genoa, Italy, June 2016).

[58] SAMARAKOON, K., EKANAYAKE, J., AND JENKINS, N. Investigation of Domestic Load Control to Provide Primary Frequency Response Using Smart Meters. *IEEE Transactions on Smart Grid 3*, 1 (March 2012), 282–292.

[59] SAUER, P. W., AND PAI, M. A. *Power System Dynamics and Stability*. Prentice Hall, Upper Saddle River, NJ, 1998.

[60] SINGH, M., AND SANTOSO, S. Dynamic models for wind turbines and wind power plants. Tech. rep., NREL, Oct 2011.

[61] SLOOTWEG, J. G., POLINDER, H., AND KLING, W. L. Dynamic modelling of a wind turbine with doubly fed induction generator. In *IEEE PES Summer Meeting* (July 2001), vol. 1, pp. 644–649 vol.1.

[62] SOUDJANI, S. E. Z., AND ABATE, A. Aggregation of Thermostatically Controlled Loads by Formal Abstractions. In *Control Conference (ECC), 2013 European* (2013), pp. 4232–4237.

[63] STEVENSON, W. D. *Elements of Power System Analysis*, third ed. McGraw-Hill, New York, NY, 1975.

[64] SWIERCZYNSKI, M., STROE, D., STAN, A.-I., TEODORESCU, R., AND SAUER, D. Selection and Performance-Degradation Modeling of $LiMO_2$/Li_4 Ti_5 O_{12} and $LiFePO_4$/C Battery Cells as Suitable Energy Storage Systems for Grid Integration With Wind Power Plants: An Example for the Primary Frequency Regulation Service. *IEEE Transactions on Sustainable Energy 5*, 1 (Jan 2014), 90–101.

[65] TAMIMI, B., CAÑIZARES, C., AND BHATTACHARYA, K. Modeling and Performance Analysis of Large Solar Photo-Voltaic Generation on Voltage Stability and Inter-area Oscillations. In *2011 IEEE Power and Energy Society General Meeting* (July 2011), pp. 1–6.

[66] TAYLOR, C., AND LEFEBVRE, S. HVDC Controls for System Dynamic Performance. *IEEE Transactions on Power Systems 6*, 2 (May 1991), 743–752.

[67] TEODORESCU, R., LISERRE, M., AND RODRÍGUEZ, P. *Grid Converters for Photovoltaic and Wind Power Systems*. Wiley, Chichester, UK, 2011.

[68] TILLER, M. M. *Introduction to Physical Modeling with Modelica*. Kluwer Academic Publishers, Boston, 2001.

[69] WANG, L., BURGETT, J., ZUO, J., XU, C. C., BILLIAN, B. J., CONNERS, R. W., AND LIU, Y. Frequency disturbance recorder design and developments. In *2007 IEEE Power Engineering Society General Meeting* (June 2007), pp. 1–7.

[70] WANG, L., AND ET AL. Frequency Disturbance Recorder Design and Developments. *IEEE PES General Meeting* (2007), 1–7.

[71] WINKELMAN, J., CHOW, J., BOWLER, B., AVRAMOVIC, B., AND KOKOTOVIC, P. An Analysis of Interarea Dynamics of Multi-Machine Systems. *IEEE Transactions on Power Apparatus and Systems PAS-100*, 2 (Feb 1981), 754–763.

[72] XIE, L., CARVALHO, P. M. S., FERREIRA, L. A. F. M., LIU, J., KROGH, B. H., POPLI, N., AND ILIC, M. D. Wind integration in power systems: Operational challenges and possible solutions. *Proceedings of the IEEE 99*, 1 (Jan 2011), 214–232.

[73] YANG, K., AND WALID, A. Outage-Storage Tradeoff in Frequency Regulation for Smart Grid With Renewables. *IEEE Transactions on Smart Grid 4*, 1 (March 2013), 245–252.

[74] ZHAN, L., LIU, Y., CULLISS, J., ZHAO, J., AND LIU, Y. Dynamic single-phase synchronized phase and frequency estimation at the distribution level. *IEEE Transactions on Smart Grid 6*, 4 (July 2015), 2013–2022.

9. List of Abbreviations

AGC	Automatic Generation Control
AVR	Automatic Voltage Regulator
BES	Battery Energy Storage
CAES	Compressed Air Energy Storage
COI	Centre of Inertia
CSC	Current Sourced Converter
DAE	Differential Algebraic Equation
DER	Distributed Energy Resource
DFIG	Doubly-Fed Induction Generator
EMF	Electromotive Force
EMT	Electromagnetic Transient
ENTSO-E	European Network of Transmission System Operators for Electricity
ESS	Energy Storage Systems
FACTS	Flexible AC Transmission System
FC	Frequency Containment
FD	Frequency Divider
FDR	Frequency Disturbance Recorder
FCES	Fuel Cell Energy Storage
FES	Flywheel Energy Storage
FR	Frequency Restoration
GPS	Global Positioning System
HV	High-Voltage
HVDC	High-Voltage Direct Current
IEEE	Institute of Electrical and Electronics Engineers
LF	Loop Filter
MPPT	Maximum Power Point Tracking
PD	Phase Detector
PDC	Phasor data concentrator
PFC	Primary Frequency Control
PHES	Pumped Hydro Energy Storage
PLL	Phase-Locked Loop
PMU	Phasor Measurement Unit
PV	Photo-Voltaic
RES	Renewable Energy Sources
RoCoF	Rate of Change of Frequency
RR	Replacement Reserves
RTDS	Real Time Digital Simulators
SCES	Super Capacitor Energy Storage
SIL	Storage Input Limiter
SMES	Superconducting Magnetic Energy Storage
SPVG	Solar Photo-Voltaic Generation
TCL	Thermostatically Controlled Loads
TG	Turbine Governor
VOC	Voltage Oscillator Control
VSC	Voltage Sourced Converter
WECS	Wind Energy Conversions Systems
WF	Washout Filter
WP	Work Package
WSCC	Western Systems Coordinating Council

10. List of Figures

11. List of Tables

Annex

A. Definition of Time and Frequency Domains

Power systems are characterized by a wide range of time constants, which can span from microseconds to several days/months (see Fig. A.1). For transient and frequency stability analysis, which are the ones of interest in this report, the time frames of relevance usually span from few milliseconds to several minutes. In this time window, some of the fastest dynamics are those of the magnetic and electrical fields of the electrical machines such as the synchronous machines. These *electromagnetic* transients (EMT) usually span few tens of milliseconds. Dynamics of power system controllers are also often contained in this time frame. The slowest dynamics of major interest on power system transient and frequency stability analysis are due to the mechanical and electrical energies stored in the rotating machines and in the network, respectively. These *electromechanical* transients can span several seconds. A number of power system controllers and devices also have *slow* time constants (e.g., primary and secondary frequency regulation, tie-line regulation). Faster (e.g., lightning over-voltages) and slower (e.g., daily load following) dynamics are also present in power system analysis, and depending on the requirements and purposes of the studies, they can also be considered.

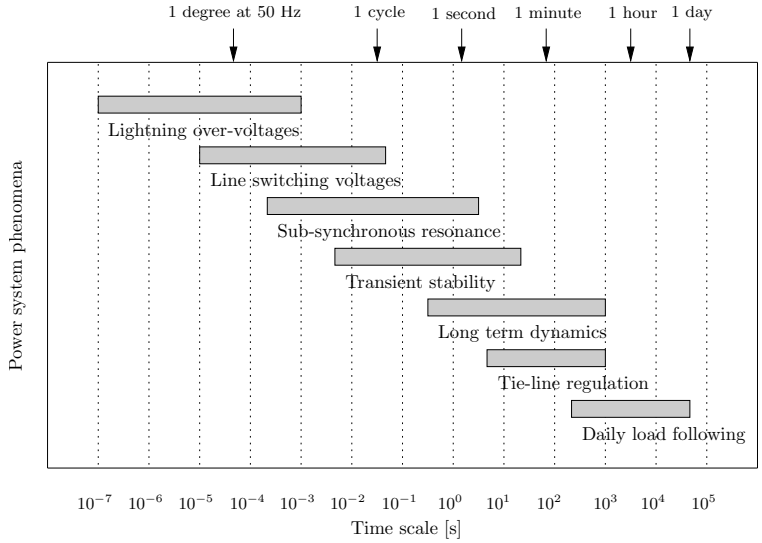

Figure A.1: Time scales of relevant power system dynamics.

The broad spectrum of time constants that are contained in a power system, makes the simulation of the behaviour of such systems a challenging task. On one hand, one can simulate the power system using a EMT model for a highly accurate simulation. EMT models usually are formulated usually in the three-phase (abc) representation. The main drawback of this approach is the computational power required, specially for large power systems. Therefore, simulations performed with the EMT model usually focus on dynamics that span up to few seconds.

To overcome the problem of EMT models complexity, a widely accepted solution is to neglect the electromagnetic transients of power system components. This is based on the assumption that the focus of most power system studies is on their electromechanical behaviour. In these studies, electrical quantities such as currents and voltages are described by their steady-state, fundamental frequency values. Moreover, there exist other commonly used transformations and approximations that lead to a simplified and efficient representation of power system models, such as the $dq0$ and the phasor representations.

This appendix provides an overview of the most common representations of power system components. With this aim, the abc, $dq0$ and phasor representations are described in Sections A.1, A.2 and A.3, respectively. Finally, the model of the overall power system is highlighted in Section A.4.

A.1 Time Domain – The abc Representation

The most general model that can be used for representing power systems is the following set of *hybrid differential equations*:

$$\dot{\boldsymbol{\xi}} = \boldsymbol{\varphi}(\boldsymbol{\xi}, \boldsymbol{u}, t) \tag{A.1}$$

where $\boldsymbol{\xi}$ ($\boldsymbol{\xi} \in \mathbb{R}^{n_\xi}$) is the vector of state variables, $\boldsymbol{u}$ ($\boldsymbol{u} \in \mathbb{R}^{n_u}$) the vector of discrete variables, t ($t \in \mathbb{R}^+$) the time, and $\boldsymbol{\varphi}$ ($\boldsymbol{\varphi} : \mathbb{R}^{n_\xi} \times \mathbb{R}^{n_u} \times \mathbb{R}^+ \mapsto \mathbb{R}^{n_\xi}$) the vector of differential equations.

Since considering every time scale present in power system analysis is not practical from the simulation point of view, a common solution is to divide the vector of general state variables $\boldsymbol{\xi}$ into three sub-vectors:

- State variables $\boldsymbol{\xi}_s$ characterized by slow dynamics (i.e., *large* time constants);
- State variables $\boldsymbol{\xi}_i$ whose dynamics are of interest;
- State variables $\boldsymbol{\xi}_f$ characterized by fast dynamics (i.e., *small* time constants).

In mathematical terms, one has:

$$\begin{cases} \dot{\boldsymbol{\xi}}_s = \boldsymbol{\varphi}_s(\boldsymbol{\xi}_s, \boldsymbol{\xi}_i, \boldsymbol{\xi}_f, \boldsymbol{u}, t) \\ \dot{\boldsymbol{\xi}}_i = \boldsymbol{\varphi}_i(\boldsymbol{\xi}_s, \boldsymbol{\xi}_i, \boldsymbol{\xi}_f, \boldsymbol{u}, t) \\ \dot{\boldsymbol{\xi}}_f = \boldsymbol{\varphi}_f(\boldsymbol{\xi}_s, \boldsymbol{\xi}_i, \boldsymbol{\xi}_f, \boldsymbol{u}, t) \end{cases} \tag{A.2}$$

where $\boldsymbol{\xi} = [\boldsymbol{\xi}_s^{\mathrm{T}}, \boldsymbol{\xi}_i^{\mathrm{T}}, \boldsymbol{\xi}_f^{\mathrm{T}}]^{\mathrm{T}}$.

In (A.2), the time evolution of $\boldsymbol{\xi}_s$ can be considered so slow that their variations can be neglected (e.g., $\boldsymbol{\xi}_s$ are *frozen* at a given value). On the other hand, the dynamics of $\boldsymbol{\xi}_f$ can be considered so fast that their variations can be considered instantaneous.

Finally, the resulting model is thereby a set of nonlinear differential algebraic equations (DAEs) with discrete variables, as follows:

$$\begin{cases} \dot{\boldsymbol{x}} = \boldsymbol{f}(\boldsymbol{x}, \boldsymbol{y}, \boldsymbol{\eta}, \boldsymbol{u}, t) \\ \boldsymbol{0} = \boldsymbol{g}(\boldsymbol{x}, \boldsymbol{y}, \boldsymbol{\eta}, \boldsymbol{u}, t) \end{cases} \tag{A.3}$$

where $\boldsymbol{x}$ ($\boldsymbol{x} \in \mathbb{R}^{n_x}$) indicates the vector state variables, $\boldsymbol{y}$ ($\boldsymbol{y} \in \mathbb{R}^{n_y}$) are the algebraic variables, $\boldsymbol{\eta}$ ($\boldsymbol{\eta} \in \mathbb{R}^{n_\eta}$) are the controllable parameters, $\boldsymbol{f}$ ($\boldsymbol{\varphi} : \mathbb{R}^{n_x} \times \mathbb{R}^{n_y} \times \mathbb{R}^{n_\eta} \times \mathbb{R}^{n_u} \times \mathbb{R}^+ \mapsto \mathbb{R}^{n_x}$) are the differential equations, and $\boldsymbol{g}$ ($\boldsymbol{\varphi} : \mathbb{R}^{n_x} \times \mathbb{R}^{n_y} \times \mathbb{R}^{n_\eta} \times \mathbb{R}^{n_u} \times \mathbb{R}^+ \mapsto \mathbb{R}^{n_y}$). Comparing (A.3) with (A.2), the following correspondences hold:

$$\boldsymbol{\eta} \equiv \boldsymbol{\xi}_s, \quad \boldsymbol{x} \equiv \boldsymbol{\xi}_i, \quad \boldsymbol{y} \equiv \boldsymbol{\xi}_f, \quad \boldsymbol{f} \equiv \boldsymbol{\varphi}_i, \quad \boldsymbol{g} \equiv \boldsymbol{\varphi}_f \tag{A.4}$$

Note that the DAE system (A.3) can be defined for any time scale. The terms *slow* and *fast* do not mean anything unless the reference time scale is defined. For example, the time scale that concerns transient and frequency stability analysis ranges from 0.01 s to 10 s or, which is the same, from 0.1 Hz to 100 Hz. This is the time scale range of interest in this document.

The first step towards the modelling of power systems in the time domain is the representation of the variables of the model as time varying quantities. With regard to ac grids, electrical quantities are sinusoids with certain amplitude and frequency. A common way to represent a generic three-phase (3ϕ), steady-state, ac current $\boldsymbol{i}(t)$ is as follows:

$$\boldsymbol{i}(t) = \begin{bmatrix} i_a(t) \\ i_b(t) \\ i_c(t) \end{bmatrix} = \begin{bmatrix} I_a \cos(\omega t + \phi_a) \\ I_b \cos(\omega t + \phi_b) \\ I_c \cos(\omega t + \phi_c) \end{bmatrix} \tag{A.5}$$

where I_a, I_b and I_c are the amplitudes of each phase, and ϕ_a, ϕ_b and ϕ_c are phase offsets.

This way to formulate electrical quantities in ac grids is the so-called $\boldsymbol{abc}$ **representation**, and is commonly used by Real Time Digital Simulators (RTDSs), which generally use the EMT power system model.

During normal operation, electrical quantities are in balanced conditions, i.e., the three components of $\boldsymbol{i}(t)$ have the same amplitude I and frequency ω, and their angles are 120 degrees in phase (positive sequence). Therefore, (A.5) can be written as:

$$\boldsymbol{i}(t) = \begin{bmatrix} i_a(t) \\ i_b(t) \\ i_c(t) \end{bmatrix} = \begin{bmatrix} I\cos(\omega t + \phi_i) \\ I\cos(\omega t + \phi_i - \frac{2\pi}{3}) \\ I\cos(\omega t + \phi_i + \frac{2\pi}{3}) \end{bmatrix} \tag{A.6}$$

Similarly, the expression of a balanced, 3ϕ ac voltage in time domain is given by:

$$\boldsymbol{v}(t) = \begin{bmatrix} v_a(t) \\ v_b(t) \\ v_c(t) \end{bmatrix} = \begin{bmatrix} V\cos(\omega t + \phi_v) \\ V\cos(\omega t + \phi_v - \frac{2\pi}{3}) \\ V\cos(\omega t + \phi_v + \frac{2\pi}{3}) \end{bmatrix} \tag{A.7}$$

From (A.6) and (A.7), it can be seen that the computational burden of the simulations of a large system is substantial when using the abc representation, since the three phases of all electrical quantities will vary with the system frequency, even during steady state conditions.

A.1.1 Example: 3ϕ RL Circuit

To illustrate the abc representation, the symmetrical 3ϕ RL circuit, depicted in Fig. A.2, is considered.

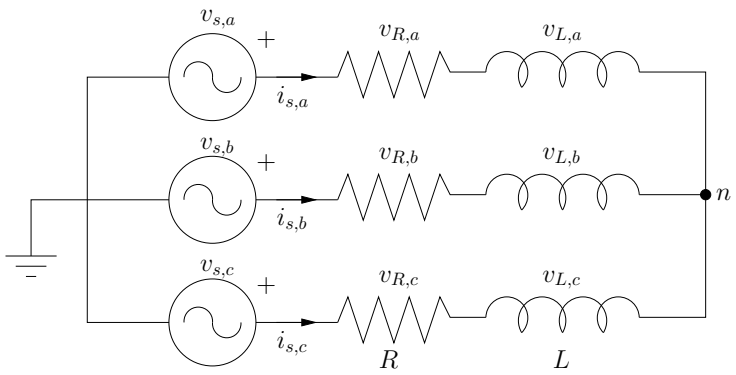

Figure A.2: Scheme of a 3ϕ series RL circuit.

The voltages of the sources can be computed as follows:

$$\boldsymbol{v}_{s,abc}(t) = \begin{bmatrix} v_{s,a}(t) \\ v_{s,b}(t) \\ v_{s,c}(t) \end{bmatrix} = \begin{bmatrix} v_{R,a}(t) + v_{L,a}(t) \\ v_{R,b}(t) + v_{L,b}(t) \\ v_{R,c}(t) + v_{L,c}(t) \end{bmatrix} \tag{A.8}$$

Knowing that the voltage at the resistor and the inductor of phase i are $v_{R,i}(t) = Ri_{s,i}(t)$, and $v_{L,i}(t) = L\frac{di_{s,i}(t)}{dt}$, respectively, (A.8) becomes:

$$\begin{cases} v_{s,a}(t) = Ri_{s,a}(t) + L\dfrac{di_{s,a}(t)}{dt} \\ v_{s,b}(t) = Ri_{s,b}(t) + L\dfrac{di_{s,b}(t)}{dt} \\ v_{s,c}(t) = Ri_{s,c}(t) + L\dfrac{di_{s,c}(t)}{dt} \end{cases} \tag{A.9}$$

Equations (A.9) can be rewritten as a set of differential equations similar to (A.3):

$$\begin{cases} \dfrac{di_{s,a}(t)}{dt} = \dot{i}_{s,a}(t) = \dfrac{1}{L}(v_{s,a}(t) - Ri_{s,a}(t)) \\ \dfrac{di_{s,b}(t)}{dt} = \dot{i}_{s,b}(t) = \dfrac{1}{L}(v_{s,b}(t) - Ri_{s,b}(t)) \\ \dfrac{di_{s,c}(t)}{dt} = \dot{i}_{s,c}(t) = \dfrac{1}{L}(v_{s,c}(t) - Ri_{s,c}(t)) \end{cases} \tag{A.10}$$

A.2 Park Transformation – The $dq0$ Representation

The $dq0$ representation is another common way to formulate the model of power system devices, specially for rotating electrical machines (e.g., the synchronous machine). This representation, which is derived from a variable transformation of the abc one (known as the **Park Transformation** [31, 5]), simplifies the formulation and simulation of systems that include such electrical machines. The rationale behind the Park transformation is the removal of the dependency of the stator and rotor inductances on the angle $\theta(t)$ by which the phase a of the stator current is lead by the direct (d) axis of the rotor (field winding), by using a rotating reference frame with the same angular speed as the machine rotor. Therefore, while using the abc representation the inductances vary with $\theta(t)$, which in turn vary with time, using the Park transformation such inductances are constant in time.

To illustrate the Park transformation, the balanced 3ϕ current expressed in (A.6) is used. Three new variables are needed in the transformation, one per component of $i(t)$. The first two variables are related to the new rotating reference frame by means of the direct and quadrature (d and q) rotor axis. These two variables are as follows:[1]

$$\begin{cases} i_d = \ K_d \left[i_a \cos(\theta) + i_b \cos\left(\theta - \dfrac{2\pi}{3}\right) + i_c \cos\left(\theta + \dfrac{2\pi}{3}\right) \right] \\ i_q = -K_q \left[i_a \sin(\theta) + i_b \sin\left(\theta - \dfrac{2\pi}{3}\right) + i_c \sin\left(\theta + \dfrac{2\pi}{3}\right) \right] \end{cases} \tag{A.11}$$

where K_d and K_q are arbitrary constants.

Substituting (A.6) in (A.11), and assuming $\phi_i = 0$, one has for the direct component:

$$i_d = K_d \left[I\cos(\omega t)\cos(\theta) + I\cos\left(\omega t - \frac{2\pi}{3}\right)\cos\left(\theta - \frac{2\pi}{3}\right) + I\cos\left(\omega t + \frac{2\pi}{3}\right)\cos\left(\theta + \frac{2\pi}{3}\right) \right] \tag{A.12}$$

After some calculations, (A.12) results in:

$$i_d = K_d \frac{3}{2} I\cos(\omega t - \theta) \tag{A.13}$$

After a similar procedure, the expression of i_q becomes:

$$i_q = -K_q \frac{3}{2} I\sin(\omega t - \theta) \tag{A.14}$$

Common values for both K_d and K_q constants are $2/3$, for which the peak values of i_d and i_q are the same as those of the phases of $i(t)$ and equal to I; and $\sqrt{2/3}$, for which the transformation matrix becomes orthogonal, i.e., its inverse is equal to its transpose.

i_d and i_q together have the property of producing an identical field to that of the original phase currents. Therefore, the third and last variable to be defined must not be associated to any space

[1] The q-axis leads by 90 degrees the d-axis.

field in the air-gap between stator and rotor. A common solution is to use the zero sequence current, i_0:

$$i_0 = \frac{1}{3}(i_a + i_b + i_c) \tag{A.15}$$

Under balanced conditions $i_a + i_b + i_c = i_0 = 0$.

From (A.11) and (A.15), and assuming $K_d = K_q = \frac{2}{3}$, the matrix form of the transformation matrix from abc to $dq0$ representations is given by:

$$\mathbf{P} = \frac{2}{3}\begin{bmatrix} \cos\theta & \cos\left(\theta - \frac{2\pi}{3}\right) & \cos\left(\theta + \frac{2\pi}{3}\right) \\ -\sin\theta & -\sin\left(\theta - \frac{2\pi}{3}\right) & -\sin\left(\theta + \frac{2\pi}{3}\right) \\ \frac{1}{2} & \frac{1}{2} & \frac{1}{2} \end{bmatrix} \tag{A.16}$$

Therefore:

$$\begin{bmatrix} i_d \\ i_q \\ i_0 \end{bmatrix} = \mathbf{P}\begin{bmatrix} i_a \\ i_b \\ i_c \end{bmatrix} \tag{A.17}$$

The inverse transformation, i.e., from the $dq0$ to the abc representation is thus:

$$\begin{bmatrix} i_a \\ i_b \\ i_c \end{bmatrix} = \mathbf{P}^{-1}\begin{bmatrix} i_d \\ i_q \\ i_0 \end{bmatrix} \tag{A.18}$$

Note that when $K_d = K_q = \frac{2}{3} \Rightarrow \mathbf{P}^{-1} \neq \mathbf{P}^{\mathrm{T}}$. This property of orthogonality is achieved when $K_d = K_q = \sqrt{\frac{2}{3}}$. Thus:

$$\hat{\mathbf{P}} = \sqrt{\frac{2}{3}}\begin{bmatrix} \cos\theta & \cos\left(\theta - \frac{2\pi}{3}\right) & \cos\left(\theta + \frac{2\pi}{3}\right) \\ -\sin\theta & -\sin\left(\theta - \frac{2\pi}{3}\right) & -\sin\left(\theta + \frac{2\pi}{3}\right) \\ \frac{1}{\sqrt{2}} & \frac{1}{\sqrt{2}} & \frac{1}{\sqrt{2}} \end{bmatrix} \tag{A.19}$$

Another common representation used to model power system devices is the $\alpha\beta\gamma$-frame, which is derived from the abc representation by means of the **Clarke Transformation**. In this representation, electrical quantities are referred to a stationary reference frame, i.e., $\omega_{\alpha\beta\gamma} = 0$, where the component α is in phase with the component a. The interested reader can find a detailed description of this transformation and its applications in [15].

A.2.1 Example: 3ϕ RL Circuit

Apart of removing the dependence on time of the inductances of the rotor and the stator of a rotating machine, other advantages are present when using the $dq0$ representation to model power system devices. One of the most relevant is the order reduction of the model if certain conditions are satisfied. To illustrate this, the 3ϕ RL circuit of Fig. A.2 is again considered.

The first step is to define the time derivative of the transformed variables:

$$\mathbf{P}\frac{d}{dt}\boldsymbol{f}_{abc}(t) = \mathbf{P}\frac{d}{dt}\left\{\mathbf{P}^{-1}\boldsymbol{f}_{dq0}(t)\right\} = \left\{\mathbf{P}\frac{d}{dt}\mathbf{P}^{-1}\right\}\boldsymbol{f}_{dq0}(t) + \mathbf{P}\mathbf{P}^{-1}\frac{d}{dt}\boldsymbol{f}_{dq0}(t) \tag{A.20}$$

where $\mathbf{P}\mathbf{P}^{-1} = \boldsymbol{I}_3$ and $\mathbf{P}\frac{d}{dt}\mathbf{P}^{-1} =$

$$
\begin{aligned}
&= \frac{2}{3}\begin{bmatrix} \cos\theta & \cos\left(\theta-\frac{2\pi}{3}\right) & \cos\left(\theta+\frac{2\pi}{3}\right) \\ -\sin\theta & -\sin\left(\theta-\frac{2\pi}{3}\right) & -\sin\left(\theta+\frac{2\pi}{3}\right) \\ \frac{1}{2} & \frac{1}{2} & \frac{1}{2} \end{bmatrix} \omega_r \begin{bmatrix} -\sin\theta & -\cos\theta & 0 \\ -\sin\left(\theta-\frac{2\pi}{3}\right) & -\cos\left(\theta-\frac{2\pi}{3}\right) & 0 \\ -\sin\left(\theta+\frac{2\pi}{3}\right) & -\cos\left(\theta+\frac{2\pi}{3}\right) & 0 \end{bmatrix} = \\
&= \frac{2}{3}\omega_r \begin{bmatrix} 0 & \frac{3}{2} & 0 \\ -\frac{3}{2} & 0 & 0 \\ 0 & 0 & 0 \end{bmatrix} = \omega_r \begin{bmatrix} 0 & 1 & 0 \\ -1 & 0 & 0 \\ 0 & 0 & 0 \end{bmatrix} = \omega_r \mathbf{P}_\omega
\end{aligned} \tag{A.21}
$$

where $\omega_r(t) = \dfrac{d\theta(t)}{dt}$ is the rotational speed of the dq reference frame.[2] Therefore:

$$
\mathbf{P}\frac{d}{dt}\boldsymbol{f}_{abc}(t) = \frac{d}{dt}\boldsymbol{f}_{dq0}(t) + \omega_r \mathbf{P}_\omega \boldsymbol{f}_{dq0}(t) \tag{A.22}
$$

Expanding (A.22), one has:

$$
\begin{cases}
\dot{f}_d(t) = \dfrac{d}{dt}f_d(t) + \omega_r f_q(t) \\
\dot{f}_q(t) = \dfrac{d}{dt}f_q(t) - \omega_r(t) f_d(t) \\
\dot{f}_0(t) = \dfrac{d}{dt}f_0(t)
\end{cases} \tag{A.23}
$$

Note that $\theta(t)$ and $\omega_r(t)$ can be any function of time, and thus not necessarily constant.

Then, the voltage $\boldsymbol{v}_{s,abc}$ in (A.8) can be written in the $dq0$ representation applying the Park transformation:

$$
\boldsymbol{v}_{s,dq0}(t) = \mathbf{P}\boldsymbol{v}_{s,abc}(t) = \mathbf{P}\left(R\boldsymbol{i}_{s,abc}(t) + L\frac{d}{dt}\boldsymbol{i}_{s,abc}(t)\right) = R\mathbf{P}\boldsymbol{i}_{s,abc}(t) + L\mathbf{P}\frac{d}{dt}\boldsymbol{i}_{s,abc}(t) \tag{A.24}
$$

where, from (A.17), $\mathbf{P}\boldsymbol{i}_{s,abc}(t) = \boldsymbol{i}_{s,dq0}(t)$, and from (A.22), $\mathbf{P}\frac{d}{dt}\boldsymbol{i}_{s,abc}(t) = \frac{d}{dt}\boldsymbol{i}_{s,dq0}(t) + \omega_r \mathbf{P}_\omega \boldsymbol{i}_{s,dq0}(t)$. Therefore:

$$
\begin{aligned}
\boldsymbol{v}_{s,dq0}(t) = \begin{bmatrix} v_{s,d}(t) \\ v_{s,q}(t) \\ v_{s,0}(t) \end{bmatrix} &= R\begin{bmatrix} i_{s,d}(t) \\ i_{s,q}(t) \\ i_{s,0}(t) \end{bmatrix} + L\frac{d}{dt}\begin{bmatrix} i_{s,d}(t) \\ i_{s,q}(t) \\ i_{s,0}(t) \end{bmatrix} + L\omega_r \begin{bmatrix} 0 & 1 & 0 \\ -1 & 0 & 0 \\ 0 & 0 & 0 \end{bmatrix}\begin{bmatrix} i_{s,d}(t) \\ i_{s,q}(t) \\ i_{s,0}(t) \end{bmatrix} \\
&= \begin{bmatrix} Ri_{s,d}(t) + L\dfrac{di_{s,d}(t)}{dt} + L\omega_r i_{s,q}(t) \\ Ri_{s,q}(t) + L\dfrac{di_{s,q}(t)}{dt} - L\omega_r i_{s,d}(t) \\ Ri_{s,0}(t) + L\dfrac{di_{s,0}(t)}{dt} \end{bmatrix}
\end{aligned} \tag{A.25}
$$

Note that, from (A.15), under steady-state and balanced conditions, $v_{s,0}(t) = i_{s,0}(t) = 0$, and thus $\frac{di_{s,0}(t)}{dt} = 0$. Therefore, the set of differential equations that represents the behaviour of a symmetrical and balanced series 3ϕ RL circuit is as follows:

$$
\begin{cases}
L\dfrac{di_{s,d}(t)}{dt} = v_{s,d}(t) - Ri_{s,d}(t) - L\omega_r i_{s,q}(t) \\
L\dfrac{di_{s,q}(t)}{dt} = v_{s,q}(t) - Ri_{s,q}(t) + L\omega_r i_{s,d}(t)
\end{cases} \tag{A.26}
$$

[2] Note that the dependence on time of $\theta(t)$ and $\omega_r(t)$ is omitted in (A.21).

Or, in compact form using *Park's vectors*:

$$\vec{v}_{s,dq}(t) = R\vec{i}_{s,dq}(t) + \mathrm{p}L\vec{i}_{s,dq}(t) \tag{A.27}$$

with $\mathrm{p} = \left(\frac{d}{dt} - j\omega_r\right)$; $\vec{v}_{s,dq}(t) = v_{s,d}(t) + jv_{s,q}(t)$; and $\vec{i}_{s,dq}(t) = i_{s,d}(t) + ji_{s,q}(t)$.

Comparing (A.10) with (A.26) and (A.27), it can be seen that using the $dq0$ representation the order of the set of DAEs is reduced, thus lessening the complexity of the system and improving the computational efficiency.

A.3 Frequency Domain – The Phasor Representation

In both abc and $dq0$ representations, electrical quantities such as voltages and currents are time variant. However, a significant simplification in the formulation can be achieved if it is considered that the frequency of the sinusoidal signals, ω, is constant and equal to the system frequency, ω_s, and that the system operates under balanced conditions. With this premises, it is possible to formulate such electrical quantities in the frequency domain, rather than in the time domain. In the frequency domain, electrical quantities are expressed by means of *phasors*.

The concept of phasor is based on the Euler's identity:

$$e^{\pm j\varphi} = \cos(\varphi) \pm j\sin(\varphi) \tag{A.28}$$

which allows the definition of the cosine and sine of the angle φ as the real and imaginary parts of the exponential function, respectively:

$$\begin{cases} \cos(\varphi) = \Re\{e^{j\varphi}\} \\ \sin(\varphi) = \Im\{e^{j\varphi}\} \end{cases} \tag{A.29}$$

Therefore, a sinusoidal ac voltage of the form $v(t) = V_M\cos(\omega t + \theta_v)$ can be written in the phasor representation as follows:

$$v(t) = \Re\{V_M e^{j(\omega t+\theta_v)}\} = \Re\{\sqrt{2}V_{\mathrm{rms}}e^{j(\theta_v)}e^{j(\omega t)}\} = \Re\{\sqrt{2}\bar{V}e^{j(\omega t)}\} \tag{A.30}$$

where V_{rms} is the root-mean-square value, or effective value, of the voltage.

The term $\bar{V} = V_{\mathrm{rms}}e^{j(\theta_v)}$ in (A.30) is the phasor representation of the voltage $v(t)$ in exponential form. This phasor can be represented in rectangular and polar forms, as follows:

$$\bar{V} = V_{\mathrm{rms}}e^{j(\theta_v)} = V_{\mathrm{rms}}\cos\theta_v + jV_{\mathrm{rms}}\sin\theta_v = V_{\mathrm{rms}}\angle\theta_v \tag{A.31}$$

Phasors can also represent three-phase quantities. Applying the $dq0$ transformation to the balanced, three-phase current in (A.6), one has:[3]

$$i(t) = \begin{bmatrix} i_d(t) \\ i_q(t) \\ i_0(t) \end{bmatrix} = \begin{bmatrix} I_{\mathrm{rms}}\cos(\omega t + \phi_i - \theta) \\ I_{\mathrm{rms}}\sin(\omega t + \phi_i - \theta) \\ 0 \end{bmatrix} \tag{A.32}$$

where $\theta = \omega_r t + \theta_0$ is the angle by which the d axis leads the phase a of the current, and θ_0 is the value of the angle at $t = 0$. Note that $K_d = K_q = \frac{2}{3\sqrt{2}}$ so that the peak values of i_d and i_q are equal to the effective value of $i(t)$.

[3] The d-axis leads 90 degrees the q-axis.

If $\omega_r = \omega$, then the direct and quadrature components of the current become:

$$\begin{cases} i_d = I_{\text{rms}} \cos(\phi_i - \theta_0) \\ i_q = I_{\text{rms}} \sin(\phi_i - \theta_0) \end{cases} \tag{A.33}$$

where both components are scalar quantities.

Relating (A.33) with the rectangular form of a phasor in (A.31), then it is simple to write the phasor representation of the three-phase current $i(t)$:

$$\bar{I} = i_d + j i_q \tag{A.34}$$

Finally, Fig. A.3 depicts the graphical representation of the phasor $\bar{I}$.

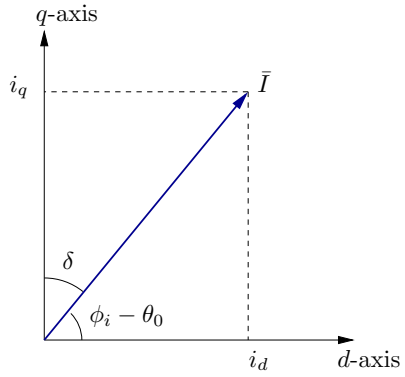

Figure A.3: Graphical representation of the phasor of a three-phase current.

A.3.1 Example: 3ϕ RL Circuit

For the sake of illustration, the model of the balanced, symmetrical 3ϕ RL series circuit of Fig. A.2 is formulated in the phasor representation. Assuming steady-state conditions, and that the dq reference frame rotates at the same speed as the frequency of the system, i.e., $\omega_r = \omega$, then the phasors of the 3ϕ voltage, $\bar{V}_s$, and current, $\bar{I}_s$, of the circuit can be obtained. Thus, the equation that represents the circuit is given by:

$$\bar{V}_s = R\bar{I}_s + j\omega L\bar{I}_s \tag{A.35}$$

where the term $j\omega L$ represents an ideal inductor in the phasor domain.

Comparing (A.10) and (A.35), it is clear that the phasor representation highly simplifies the model, passing from three differential equations to one with complex variables.

Note that, under balanced conditions, and if the rotational reference frame of the Park transformation, ω_r, rotates with constant angular speed and equal to the system frequency, ω, then the Park's vector expression of (A.27) coincides with the phasor representation (A.35).

A.4 Electromechanical Transient Model of Power Systems

A commonly-used and well-accepted power system model for frequency and transient stability studies, like the ones carried out in this document, is a combination of the three representations described above. From the simplicity, efficiency and accuracy points of view, it is convenient to model different groups of power system devices using different representations, leading to the peculiar mix of time and frequency domains seen in power system modelling. To illustrate this concept, the models of a variety of power system devices for transient and frequency stability studies are provided in the remainder of this section.

A.4.1 Time Domain-based Models of Power System Devices

The main group of devices that are modelled in the time domain are the controllers that are present in power systems. These include primary and secondary frequency and voltage regulators of synchronous machines, wind turbines and FACTS controllers, among others.

For the sake of example, the system of DAEs of a Turbine Governor (TG) Type I (see Fig. A.4) is defined below.

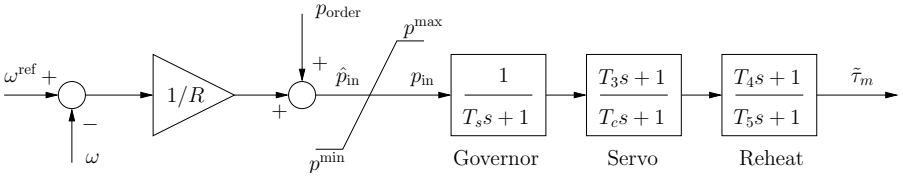

Figure A.4: Turbine governor Type I control diagram.

$$\begin{cases} \hat{p}_{\text{in}} = p_{\text{order}} + \dfrac{1}{R}(\omega^{\text{ref}} - \omega) \\ p_{\text{in}} = \begin{cases} \hat{p}_{\text{in}} & \text{if} \quad p^{\min} \leq \hat{p}_{\text{in}} \leq p^{\max} \\ p^{\max} & \text{if} \quad \hat{p}_{\text{in}} > p^{\max} \\ p^{\min} & \text{if} \quad \hat{p}_{\text{in}} < p^{\min} \end{cases} \\ \dot{x}_{g1} = \dfrac{(p_{\text{in}} - x_{g1})}{T_s} \\ \dot{x}_{g2} = \dfrac{\left(\left(1 - \frac{T_3}{T_c} x_{g1}\right) - x_{g2}\right)}{T_c} \\ \dot{x}_{g3} = \dfrac{\left(\left(1 - \frac{T_4}{T_5}\right)\left(x_{g2} + \frac{T_3}{T_c} x_{g1}\right) - x_{g3}\right)}{T_5} \\ \tilde{\tau}_m = x_{g3} + \dfrac{T_4}{T_5}\left(x_{g2} + \dfrac{T_3}{T_c} x_{g1}\right) \end{cases} \tag{A.36}$$

where ω and ω^{ref} are the actual and reference rotor speeds of the synchronous machine, respectively, R is the regulator droop, p^{order} is a signal provided by the Automatic Generation Control (AGC) that coordinates the regulation of the machines in the system, $p^{\min}$ and $p^{\max}$ are the minimum and maximum turbine power outputs, $\tilde{\tau}_m$ is the input mechanical torque of the machine, and T_c, T_s, T_3, T_4, T_5 are time constants.

A.4.2 The Synchronous Machine in the $dq0$ Representation

Nowadays, the most important power system device from both the transient and the frequency stability points of view is the synchronous machine. As seen in Section A.2, the most common representation of the model of rotating electrical machines is the $dq0$. A large variety of models of the synchronous machine can be found in the literature [31, 5]. Among them, a commonly-used model for stability studies is the 4^{th} order, one d- and one q-axis model, which is described below. In this model, sub-transient dynamics are neglected.

The mechanical equations, that represent the dynamics of the angle, δ, and angular speed, ω, of the rotor are as follows:

$$\begin{cases} \dot{\delta} = \omega_n(\omega - \omega_s) \\ \dot{\omega} = \dfrac{1}{2H}(\tau_m - \tau_e - D(\omega - \omega_s)) \end{cases} \tag{A.37}$$

where ω_s and ω_n are the synchronous frequency and its base, respectively; τ_m and τ_e are the mechanical and electrical torques of the machine, respectively; H is the machine inertia constant; and D is the damping coefficient.

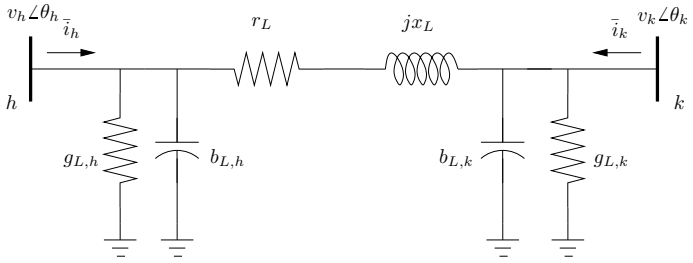

Figure A.5: Transmission line lumped π-circuit.

The electrical equations are:

$$\begin{cases} \dot{e}'_q = \dfrac{-e'_q - (x_d - x'_d)i_d + v_f}{T'_{d0}} \\ \dot{e}'_d = \dfrac{-e'_d + (x_q - x'_q)i_q}{T'_{q0}} \\ 0 = v_q + r_a i_q - e'_q + x'_d i_d \\ 0 = v_d + r_a i_d - e'_d - x'_q i_q \end{cases} \tag{A.38}$$

where the subscripts d- and q refer to the direct and quadrature components of the variable, respectively; e' is the transient stator voltage; v and i are the stator voltage and current, respectively; v_f is the field voltage; T'_0 is the transient time constant; x and x' are the synchronous and transient reactances, respectively; and r_a is the armature resistance.

A.4.3 The Transmission Line in the Phasor Representation

Several power system books provide a rigorous description of the determination of transmission line parameters [17, 21, 63]. In this section, it is assumed that a short line can be represented as π lumped model as shown in Figure A.5. *Short* means that

$$\ell \ll \lambda \tag{A.39}$$

where ℓ is the line length and λ is the wave length defined as:

$$\lambda = \frac{1}{f_n \sqrt{L_\ell C_\ell}} \tag{A.40}$$

where f_n is the rated frequency of the ac system, and L_ℓ and C_ℓ are the per-unit length inductance and capacity respectively, of the transmission line. Assuming typical values of L_ℓ and C_ℓ (that depend on the line geometry) and considering $f_n = 50$ Hz, high voltage overhead transmission lines are characterized by $\lambda \approx 6000$ km, while cables by $\lambda \in (2000, 2800)$ km. In practice, the transmission line length is never $\ell > \lambda/4$ and the vast majority satisfies the condition $\ell < \lambda/8$ (e.g., ≈ 750 km at 50 Hz). For $\ell \leq \lambda/30$, the error introduced using lumped parameters is $\leq 1\%$. At 50 Hz, this condition leads to $\ell \leq 200$ km. The hypothesis of short line is assumed for the remainder of this report.

The equivalent circuit of Figure A.5 includes a series resistance, a series reactance and four shunt elements, namely sending-end conductance and susceptance and receiving-end conductance and susceptance. The complex powers injected at each node are:

$$\begin{cases} \bar{s}_h = \bar{v}_h \bar{i}_h^* \\ \bar{s}_k = \bar{v}_k \bar{i}_k^* \end{cases} \tag{A.41}$$

Table A.1: Transmission line parameters.

Variable	Description	Unit
$b_{L,h}, b_{L,k}$	Shunt susceptances	pu
C_ℓ	Per-unit length line capacity	F/km
$g_{L,h}, g_{L,k}$	Shunt conductances	pu
L_ℓ	Per-unit length line inductance	H/km
ℓ_t	Total line length	km
R_ℓ	Per-unit length line resistance	Ω/km
r_L	Resistance	pu
x_L	Reactance	pu

According to the π model of Figure A.5, the injected currents $\bar{i}_h$ and $\bar{i}_k$ can be written as:

$$\begin{bmatrix} \bar{i}_h \\ \bar{i}_k \end{bmatrix} = \begin{bmatrix} \bar{y}_L + \bar{y}_{L,h} & -\bar{y}_L \\ -\bar{y}_L & \bar{y}_L + \bar{y}_{L,k} \end{bmatrix} \begin{bmatrix} \bar{v}_h \\ \bar{v}_k \end{bmatrix} \tag{A.42}$$

where

$$\begin{cases} \bar{y}_L = g_L + jb_L = (r_L + jx_L)^{-1} \\ \bar{y}_{L,h} = g_{L,h} + jb_{L,h} \\ \bar{y}_{L,k} = g_{L,k} + jb_{L,k} \end{cases} \tag{A.43}$$

Hence, (A.41) can be rewritten as:

$$\begin{cases} p_h = v_h^2(g_L + g_{L,h}) - v_h v_k(g_L \cos\theta_{hk} + b_L \sin\theta_{hk}) \\ q_h = -v_h^2(b_L + b_{L,h}) - v_h v_k(g_L \sin\theta_{hk} - b_L \cos\theta_{hk}) \\ p_k = v_k^2(g_L + g_{L,k}) - v_h v_k(g_L \cos\theta_{hk} - b_L \sin\theta_{hk}) \\ q_k = -v_k^2(b_L + b_{L,k}) + v_h v_k(g_L \sin\theta_{hk} + b_L \cos\theta_{hk}) \end{cases} \tag{A.44}$$

where $\theta_{hk} = \theta_h - \theta_k$.

For short lines, $g_{L,h} \approx g_{L,k} \approx 0$. This assumption also derives from the difficulty of evaluating shunt parasite conductances, which are generally neglected. The lumped series resistance and reactance can be computed as:

$$\begin{cases} r_L = R_\ell \ell_t / Z_b \\ x_L \approx \omega_s L_\ell \ell_t / Z_b \end{cases} \tag{A.45}$$

where $\omega_s = 2\pi f_n$ is the synchronous pulsation in rad/s, Z_b is the base impedance in Ω and other parameters are defined in Table A.1. The per-unit length resistance R_ℓ depends on the temperature, on the section and on resistivity of the conductor. The lumped shunt susceptances $b_{L,h}$ and $b_{L,k}$ can be approximated as:

$$b_{L,h} \approx b_{L,k} \approx \frac{1}{2}\omega_s C_\ell \ell_t Z_b \tag{A.46}$$

Even though for standard transmission lines $b_{L,h} \approx b_{L,k}$, it is better to maintain separated these parameters for the sake of generality. In this way, line sectioning as well as transformers can share the same programming code as transmission lines.

B. Frequency Estimation Techniques

The conventional power system model for transient stability analysis is based on the assumption of quasi-steady-state phasors for voltages and currents. The crucial hypothesis on which such a model is defined is that the frequency required to define all phasors and system parameters is constant and equal to its nominal value. This model is appropriate as long as only the rotor speed variations of synchronous machines is needed to regulate the system frequency through standard primary and secondary frequency regulators. In recent years, however, an increasing number of devices other than synchronous machines are expected to provide frequency regulation. These include, among others, distributed energy resources such as wind and solar generation [3, 55, 35, 9, 45]; flexible loads providing load demand response [58, 34]; High-Voltage Direct Current (HVDC) transmission systems [66, 42, 11]; and energy storage systems [73, 64, 32]. However, these devices do not generally impose the frequency at their connection point with the grid. There is thus, from a modelling point of view, the need to define with accuracy the local frequency at every bus of the network.

From the simulation point of view, these devices pose the problem of properly defining the frequency signal to be used as input of the regulators. In fact, conventional electromechanical models for transient stability analysis structurally neglect frequency variations in transmission lines and loads. On the other hand, fully-fledged electromagnetic models, which would easily allow determining the frequency at any point of the system, are too computationally demanding as the time scales of interest when dealing with frequency regulations are in the order of minutes, not milliseconds.

The most common way to estimate the system frequency in transient stability analysis is the evaluation of the Centre of Inertia (COI), which is an arithmetic mean of rotor speeds of synchronous machines weighted through their inertia constants. The frequency of the COI is well-accepted and widely used in the literature on transient and frequency stability analysis [71, 54]. While the COI is particularly useful to define the frequency of clusters of coherent machines, it cannot capture local oscillations and is thus not adequate to implement and simulate the frequency controllers discussed above.

Another common approach consists in defining the numerical derivative of the phase angle of bus voltage phasors through some sort of filtering, e.g., a Washout Filter (WF). This approach was first discussed in [24] along with the COI model, and is commonly used in proprietary software tools for power system simulation, e.g., [14].

The issues of the numerical differentiation of voltage angles are well known. The literature on this subject has mainly focused on the definition of analytical expressions, e.g., [47], or more accurate numerical methods, e.g., [23], to define the derivative of bus voltage angles. The common starting point of the two references above is the expression that links bus voltage phasors and current injections at buses through the network admittance matrix. This work proposes an analytical expression which is not model-dependent as that given in [47] and is considerably simpler, but consistent with standard approximations used in power system models for transient stability analysis [39]. This accurate yet simple and computationally inexpensive expression, which is based on the well-known *voltage divider formula*, is used to estimate the frequency at all buses of the system.

The remainder of this appendix is organized as follows. Sections B.1–B.4 describe the mathematical formulations of the frequency estimators studied in this work, namely the COI, the WF, and the proposed Frequency Divider (FD) formula, as well as a frequency measurement technique based on Phase-Locked Loop (PLL) devices. Section B.5 illustrates, through a simple example, the validity of the FD and tests it considering different scenarios and load models. Finally, Section B.6 draws conclusions.

B.1 Center of Inertia

The frequency of the COI, ω_{COI}, is a weighted arithmetic average of the rotor speeds of synchronous machines that are connected to a transmission system. Assuming a set $\mathcal{G}$ of synchronous generators, the expression to compute the COI is:

$$\omega_{\mathrm{COI}} = \frac{\sum_{j\in\mathcal{G}} H_j \omega_j}{\sum_{j\in\mathcal{G}} H_j} \tag{B.1}$$

where ω_j are rotor speeds and H_j are inertia constants.

The inertia-weighted nature of the COI makes this quantity particularly suited to study inter-area oscillations among machine clusters. However, local variations of the machines, especially those characterized by a small inertia, are lost. One can thus expect that the COI is not fully adequate to simulate local frequency controllers. This fact is duly discussed in the case studies of presented in this document, and in [50]. Moreover, from the modelling point of view, it is unrealistic to assume that distributed generators, microgrids and consumers will receive the instantaneous signal of the COI frequency from the system operator. The frequency is actually very likely measured locally, using well-assessed techniques based on the sampling of ac quantities (see, for example, [70]). Thus, it is important to capture local variations of the frequency to properly model the response of such devices.

B.2 Washout Filter

The numerical derivative of the bus voltage phase angles is another well-known approach to estimate the frequency of ac transmission systems [24, 47, 23]. As opposed to the COI, this technique can properly capture local oscillation modes but is prone to numerical issues. Figure B.1 shows a typical implementation of the numerical derivative, i.e., a washout filter (WF) and a low pass filter.

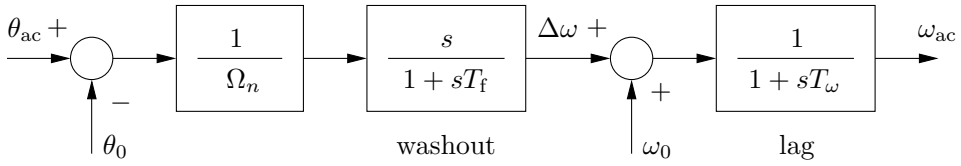

Figure B.1: Numerical derivative of the bus voltage phase angle composed of a washout and a low pass filters. θ_0 is the initial value of the bus voltage phase angle in radians and ω_0 is the synchronous frequency in pu.

Differential equations of the WF are as follows:

$$\begin{cases} \dot{x}_\theta = \dfrac{1}{T_{\mathrm{f}}}\left(\dfrac{1}{\Omega_n}(\theta_{\mathrm{ac}} - \theta_0) - x_\theta\right) \\ \dot{\omega}_{\mathrm{ac}} = \dfrac{1}{T_\omega}(\omega_0 + \Delta\omega - \omega_{\mathrm{ac}}) \end{cases} \tag{B.2}$$

where θ_0 is the initial bus voltage phase angle (e.g., the phase angle as obtained with the power flow analysis); Ω_n is the system nominal frequency in rad/s; ω_0 is the synchronous frequency in pu (typically, $\omega_0 = 1$ pu); T_{f} and T_ω are the time constants of the washout and of the low-pass filters, respectively; x_θ is the state variable of the washout filter; and $\Delta\omega = \dot{x}_\theta$.

In case of rectangular coordinates, to compute the frequency variation $\Delta\omega$, the bus voltage phase angle θ_{ac} has to be defined first. Instead of computing directly θ_{ac}, which might lead to numerical issues, one can define two fictitious state variables, namely $\sin\theta_{\mathrm{ac}}$ and $\cos\theta_{\mathrm{ac}}$, whose

dynamics are defined as follows [14]:

$$\begin{cases} \dfrac{d}{dt}(\cos\theta_{\rm ac}) = \dfrac{1}{T_{\rm f}}(v_{{\rm ac},d}/v_{\rm ac} - \cos\theta_{\rm ac}) \\ \dfrac{d}{dt}(\sin\theta_{\rm ac}) = \dfrac{1}{T_{\rm f}}(v_{{\rm ac},q}/v_{\rm ac} - \sin\theta_{\rm ac}) \end{cases} \tag{B.3}$$

where $v_{\rm ac} = \sqrt{v_{{\rm ac},d}^2 + v_{{\rm ac},q}^2}$. Then, $\Delta\omega$ is obtained as:

$$\Delta\omega = \begin{cases} \frac{d/dt(\sin\theta_{\rm ac})}{\Omega_n \cos\theta_{\rm ac}} , & \text{if } |\cos\theta_{\rm ac}| > |\sin\theta_{\rm ac}| , \\ -\frac{d/dt(\cos\theta_{\rm ac})}{\Omega_n \sin\theta_{\rm ac}} , & \text{otherwise.} \end{cases} \tag{B.4}$$

The interested reader can find in [14] a similar version of (B.3) but for voltages expressed in rectangular coordinates.

The washout filter block is necessary as the input quantity, i.e., the bus voltage phase angle $\theta_{\rm ac}$, is an algebraic variable and thus can *jump* as a consequence of discrete events, such as faults and line outages. The discontinuity of the derivative of $\theta_{\rm ac}$ is the main issue of the WF approach. The low pass filter mitigates numerical issues but also introduces a delay that can be detrimental for the performance of local frequency controllers. A commonly accepted trade-off between accuracy and numerical efficiency is obtained with $T_{\rm f} = 3/\Omega_n$ s and $T_\omega = 0.05$ s, where Ω_n is the nominal frequency of the system in rad/s. These are the values used in the simulations of this document.

B.3 Phase-Locked Loop

In practice, the frequency regulated by power converter-based devices such as Renewable Energy Sources (RESs) is measured locally through PLL devices. Such electronic devices are crucial for the proper synchronization and regulation of the power converter. PLLs are electronic circuits that consist of three main parts: (i) a phase detector (PD); (ii) a loop filter (LF); and (iii) a voltage oscillator control (VOC). The PD measures abc voltages and convert them into $\alpha\beta\gamma$- and $dq0$-reference frames (See Appendix A.2) while the VOC imposes that the v_q component is zero. There are many different implementations of the loop filter (see, for example, [46, 26, 10]) but, most commonly, it consists of a PI controller. An interesting by-product of any PLL is that the output of the LF is an estimation of the frequency deviation at the bus of connection.

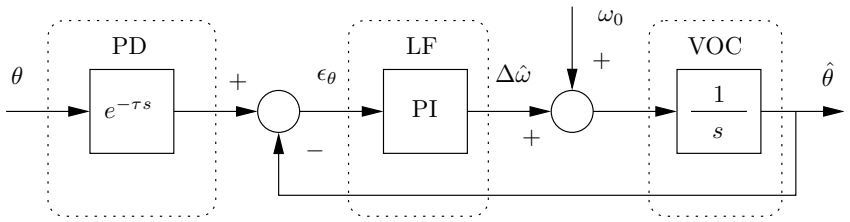

Figure B.2: Scheme of a synchronous reference frame PLL suitable for transient stability analysis.

A fundamental-frequency model of the PLL is depicted in Fig. B.2. This implements a typical synchronous reference frame PLL where the PD is modeled as a pure delay; the LF is a PI controller; and the VOC is implemented as an integrator. The delay τ accounts for the time needed to: (i) retrieve the measures of the three-phase quantities from the grid; (ii) process the measures in order to obtain their $dq0$-components; and (iii) compute the bus voltage phase angles and later the bus frequency signal.

The input of the PLL is the phase angle θ of the bus voltage phasor at which the PLL is connected and the output is the estimated phase angle $\hat{\theta}$. This representation is adequate if the

voltage phasors are expressed in polar coordinates and are equivalent to tracking the v_q voltage component in rectangular coordinates. In fact, one has that $v_q = v \sin\theta$ and, thus, $v_q = 0$ implies $\theta = 0$.

Figure B.2 also shows that the output of the PI controller is an estimation of the frequency deviations $\Delta\hat{\omega}$. The bus frequency estimation is thus given by $\omega_0 + \Delta\hat{\omega}$, where ω_0 is the synchronous speed. Since the input quantity θ is an algebraic variable in the standard transient stability model, the PLL can show numerical issues and provide a frequency estimation affected by jumps and discontinuities following discrete events in the system such as faults or line outages.

B.4 Frequency Divider

The COI and the WF are two well-accepted techniques to estimate the frequency of ac transmission systems. However, as discussed above, they show relevant technical, theoretical and/or numerical drawbacks. An alternative approach is proposed in this section, namely the Frequency Divider (FD) formula, based on the augmented admittances matrix of the system and on the assumption that the frequency along the impedances of transmission lines varies as in a *continuum matter* where synchronous machine rotor speeds define boundary conditions [39].

The very starting point in the development of the FD formula is the augmented admittance matrix, with inclusion of synchronous machine internal impedances as it is commonly defined for short-circuit analysis [4]. System currents and voltages are linked as follows:

$$\begin{bmatrix} \bar{\boldsymbol{i}}_G \\ \bar{\boldsymbol{i}}_B \end{bmatrix} = \begin{bmatrix} \bar{\mathbf{Y}}_{GG} & \bar{\mathbf{Y}}_{GB} \\ \bar{\mathbf{Y}}_{BG} & \bar{\mathbf{Y}}_{BB} + \bar{\mathbf{Y}}_{G0} \end{bmatrix} \begin{bmatrix} \bar{\boldsymbol{e}}_G \\ \bar{\boldsymbol{v}}_B \end{bmatrix} \tag{B.5}$$

where $\bar{\boldsymbol{v}}_B$ and $\bar{\boldsymbol{i}}_B$ are bus voltages and current injections, respectively, at network buses; $\bar{\boldsymbol{i}}_G$ are generator current injections; $\bar{\boldsymbol{e}}_G$ are generator electromotive forces (EMFs) behind the internal generator impedance; $\bar{\mathbf{Y}}_{BB}$ is the standard network admittance matrix; $\bar{\mathbf{Y}}_{GG}$, $\bar{\mathbf{Y}}_{GB}$ and $\bar{\mathbf{Y}}_{BG}$ are admittance matrices obtained using the internal impedances of the synchronous machines; and $\bar{\mathbf{Y}}_{G0}$ is a diagonal matrix that accounts for the internal impedances of the synchronous machines at generator buses. All quantities in (B.5) depend on the frequency. However, the dependency of the admittance matrices above on the frequency is neglected.

Let us assume that load current injections $\bar{\boldsymbol{i}}_B$ can be expressed as a linear function of the bus voltages $\bar{\boldsymbol{v}}_B$:

$$\bar{\boldsymbol{i}}_B = -\bar{\mathbf{Y}}_{B0}\bar{\boldsymbol{v}}_B \tag{B.6}$$

which leads to rewrite (B.5) as follows:

$$\begin{bmatrix} \bar{\boldsymbol{i}}_G \\ \mathbf{0} \end{bmatrix} = \begin{bmatrix} \bar{\mathbf{Y}}_{GG} & \bar{\mathbf{Y}}_{GB} \\ \bar{\mathbf{Y}}_{BG} & \bar{\mathbf{Y}}_{BB} + \bar{\mathbf{Y}}_{G0} + \bar{\mathbf{Y}}_{B0} \end{bmatrix} \begin{bmatrix} \bar{\boldsymbol{e}}_G \\ \bar{\boldsymbol{v}}_B \end{bmatrix} \tag{B.7}$$

Bus voltages $\bar{\boldsymbol{v}}_B$ are thus a function of generator EMFs and can be computed explicitly:

$$\begin{aligned} \bar{\boldsymbol{v}}_B &= -[\bar{\mathbf{Y}}_{BB} + \bar{\mathbf{Y}}_{G0} + \bar{\mathbf{Y}}_{B0}]^{-1}\bar{\mathbf{Y}}_{BG}\bar{\boldsymbol{e}}_G \\ &= \bar{\mathbf{D}}\,\bar{\boldsymbol{e}}_G \end{aligned} \tag{B.8}$$

At this point, the main assumption that is made in [39] is applied, i.e., that the variations of the frequency are “slow”, at least when considering electromechanical transient stability models. Hence:

$$\mathrm{p}\,\bar{v}_h \approx j\,\omega_h\,\bar{v}_h \tag{B.9}$$

where $\omega_h = \omega_0 + \Delta\omega_h$ is the frequency at bus h. Expressions similar to (B.9) hold for all other ac quantities in the systems, i.e., generator EMFs $\bar{e}$ and currents. For example:

$$\mathrm{p}\,\bar{e}_i \approx j\,\omega_i\,\bar{e}_i \tag{B.10}$$

where ω_i is the rotor speed of generator i.

The approximated time derivatives (B.9) and (B.10) are used along with network constraints (B.8) to determine the FD. In particular, differentiating (B.8) with respect to time leads to:

$$\mathrm{p}\bar{\boldsymbol{v}}_B = \mathrm{p}[\bar{\mathbf{D}} \cdot \bar{\boldsymbol{e}}_G] = \mathrm{p}\bar{\mathbf{D}} \cdot \bar{\boldsymbol{e}}_G + \bar{\mathbf{D}} \cdot \mathrm{p}\bar{\boldsymbol{e}}_G \tag{B.11}$$

$$\Rightarrow \quad \mathrm{p}\bar{\boldsymbol{v}}_B \approx \bar{\mathbf{D}} \cdot \mathrm{p}\bar{\boldsymbol{e}}_G \tag{B.12}$$

$$\Rightarrow \quad \frac{d}{dt}\bar{\boldsymbol{v}}_B + j\omega_0\bar{\boldsymbol{v}}_B \approx \bar{\mathbf{D}} \cdot \frac{d}{dt}\bar{\boldsymbol{e}}_G + j\omega_0\bar{\mathbf{D}} \cdot \bar{\boldsymbol{e}}_G \tag{B.13}$$

$$\Rightarrow \quad j\,\mathrm{diag}(\Delta\boldsymbol{\omega}_B)\,\bar{\boldsymbol{v}}_B \approx j\,\bar{\mathbf{D}} \cdot \mathrm{diag}(\Delta\boldsymbol{\omega}_G)\,\bar{\boldsymbol{e}}_G \tag{B.14}$$

where, in (B.11), it is assumed that $\mathrm{p}\bar{\mathbf{D}} \approx \mathbf{0}$, i.e., constant transmission system, load and generator parameters; in (B.13), (B.8) is used to remove the equal terms $j\omega_0\bar{\boldsymbol{v}}_B$ and $j\omega_0\bar{\mathbf{D}} \cdot \bar{\boldsymbol{e}}_G$; $\mathrm{diag}(\cdot)$ is a matrix where diagonal elements are the elements of its argument vector; and $\Delta\boldsymbol{\omega}_B$ and $\Delta\boldsymbol{\omega}_G$ are defined as:

$$\begin{cases} \Delta\boldsymbol{\omega}_B = \boldsymbol{\omega}_B - \omega_0 \cdot \mathbf{1} \\ \Delta\boldsymbol{\omega}_G = \boldsymbol{\omega}_G - \omega_0 \cdot \mathbf{1} \end{cases} \tag{B.15}$$

The set of equations (B.14) and (B.15) allows determining the bus voltage frequencies $\boldsymbol{\omega}_B$. In fact, $\bar{\mathbf{D}}$ are parameters and $\boldsymbol{\omega}_G$, $\bar{\boldsymbol{v}}_B$ and $\bar{\boldsymbol{e}}_G$ are variables determined by integrating the set of Differential Algebraic Equations (DAEs) describing the power system. Equation (B.14) can be significantly simplified without a relevant loss of accuracy. The following approximations and assumptions are applied:

- $\bar{\boldsymbol{v}}_B \approx \mathbf{1}$ pu and $\bar{\boldsymbol{e}}_G \approx \mathbf{1}$ pu;
- The conductances of the elements of all admittance matrices utilized to compute $\bar{\mathbf{D}}$ are negligible, e.g., $\bar{\mathbf{Y}}_{BB} \approx j\mathbf{B}_{BB}$;
- Load admittances are negligible with respect to transmission system ones, hence, $|\bar{\mathbf{Y}}_{B0}| \ll \mathrm{diag}(|\bar{\mathbf{Y}}_{BB}|)$.

Moreover, the condition $\omega_0 = 1$ pu usually holds. All simplifications above are motivated by usual assumptions and typical parameters of transmission systems. Substituting frequency deviations with the expressions in (B.15), (B.14) becomes:

$$\boldsymbol{\omega}_B = \mathbf{1} + \mathbf{D}(\boldsymbol{\omega}_G - \mathbf{1}) \tag{B.16}$$

where

$$\mathbf{D} = -(\mathbf{B}_{BB} + \mathbf{B}_{G0})^{-1}\mathbf{B}_{BG} \tag{B.17}$$

Equation (B.16) is the sought FD expression.

A final important remark is the following. From the computational point of view, (B.16) might not be the most adequate expression to implement in practice. In fact, while $\mathbf{B}_{BB}$, $\mathbf{B}_{G0}$ and $\mathbf{B}_{BG}$ tend to be extremely sparse matrices, $\mathbf{D}$ is not, thus its computational burden can be unacceptable for large systems. For these reasons, the use of (B.16) is impractical for a computer-based implementation of the FD and may cause memory errors on common workstations. Hence, an *acausal* expression was implemented as follows:

$$\mathbf{0} = (\mathbf{B}_{BB} + \mathbf{B}_{G0}) \cdot (\boldsymbol{\omega}_B - \mathbf{1}) + \mathbf{B}_{BG} \cdot (\boldsymbol{\omega}_G - \mathbf{1}) \tag{B.18}$$

The interested reader can find in [68] an extensive discussion on causality and its implications on the modelling of physical systems.

B.4.1 Inclusion of Frequency Measurements

For completeness, we discuss here how the FD formula (B.16) can be modified to include frequency measurements as provided, for example, by Phasor Measurement Unit (PMU) devices, as follows. Let us assume that, apart from synchronous machine rotor speeds, also the bus voltage phasors $\bar{\boldsymbol{v}}_M$ and hence bus frequencies $\boldsymbol{\omega}_M$ are known at a given set of network buses. Such frequencies can be used to compute the remaining unknown bus frequencies. Say that $\boldsymbol{\omega}_B = [\boldsymbol{\omega}_M, \boldsymbol{\omega}_U]$, where $\boldsymbol{\omega}_U$ are the remaining unknown bus frequencies. Then, using same notation as for (B.5), one has:

$$\begin{bmatrix} \bar{\boldsymbol{i}}_G \\ \bar{\boldsymbol{i}}_M \\ \bar{\boldsymbol{i}}_U \end{bmatrix} = \begin{bmatrix} \bar{\mathbf{Y}}_{GG} & \bar{\mathbf{Y}}_{GM} & \bar{\mathbf{Y}}_{GU} \\ \bar{\mathbf{Y}}_{MG} & \bar{\mathbf{Y}}_{MM} + \bar{\mathbf{Y}}_{M0} & \bar{\mathbf{Y}}_{MU} \\ \bar{\mathbf{Y}}_{UG} & \bar{\mathbf{Y}}_{UM} & \bar{\mathbf{Y}}_{UU} + \bar{\mathbf{Y}}_{U0} \end{bmatrix} \begin{bmatrix} \bar{\boldsymbol{e}}_G \\ \bar{\boldsymbol{v}}_M \\ \bar{\boldsymbol{v}}_U \end{bmatrix} \tag{B.19}$$

and, following the same derivations discussed in the previous section, the FD formula (B.16) becomes:

$$\boldsymbol{\omega}_U = \mathbf{1} - (\mathbf{B}_{UU} + \mathbf{B}_{U0})^{-1} \begin{bmatrix} \mathbf{B}_{UG} & \mathbf{B}_{UM} \end{bmatrix} \begin{bmatrix} \boldsymbol{\omega}_G - \mathbf{1} \\ \boldsymbol{\omega}_M - \mathbf{1} \end{bmatrix} \tag{B.20}$$

thus, the acausal expression B.18 can be rewritten as:

$$\mathbf{0} = (\mathbf{B}_{UU} + \mathbf{B}_{U0}) \cdot (\boldsymbol{\omega}_U - \mathbf{1}) + \mathbf{B}_{UG} \cdot (\boldsymbol{\omega}_G - \mathbf{1}) + \mathbf{B}_{UM} \cdot (\boldsymbol{\omega}_M - \mathbf{1}) \tag{B.21}$$

The expression above can be used in two ways. In simulations, one can model PMU devices and use their measures to obtain a better estimation of the frequencies at remaining buses. This is particularly relevant to define the impact of noise and measurement corruptions of the PMU measure, as noise can be easily included in (B.20). In state-estimation, using real-world frequency measures obtained from the system to estimate frequency variations at remaining system buses, and/or rotor speed of synchronous machines that can not be measured/retrieved in any other manner.

B.5 Illustrative Examples

In this section, the FD formula (B.16) derived in Section B.4 is illustrated through a simple example. Such an example will serve to justify why (B.16) is called *frequency divider* and to compare the dynamic behaviour of (B.16) with respect to conventional WFs as well as discuss its conceptual difference with respect to the ω_{COI}.

Let us consider the simple radial system shown in Fig. B.3. The lossless connection, with total reactance $x_{hk} = x_{hi} + x_{ik}$, represents the series of the internal reactances of the machines, and series reactances of the step-up transformers and the transmission line. Hence, the frequencies at buses h and k, say ω_h and ω_k, respectively, are the rotor speeds of the synchronous generators.

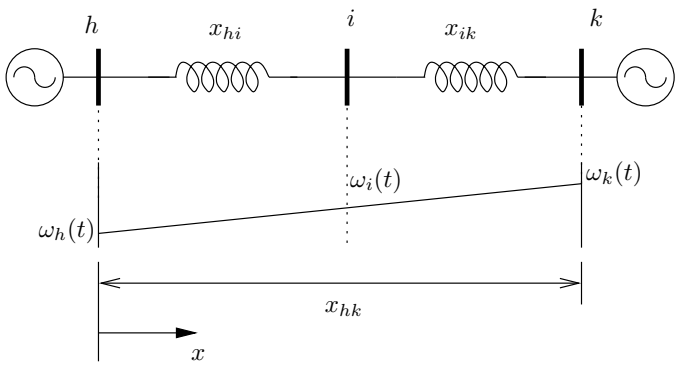

Figure B.3: Two-machine radial system.

Applying the FD formula (B.16):

$$\begin{aligned}\omega_i(t) &= 1 + \boldsymbol{D} \cdot \begin{bmatrix}\omega_h(t)-1\\ \omega_k(t)-1\end{bmatrix} = 1 - (\boldsymbol{B}_{BB}+\boldsymbol{B}_{G0})^{-1}\boldsymbol{B}_{BG} \cdot \begin{bmatrix}\omega_h(t)-1\\ \omega_k(t)-1\end{bmatrix} \\ &= 1 - \left[\frac{1}{x_{hi}}+\frac{1}{x_{ik}}\right]^{-1}\begin{bmatrix}-\frac{1}{x_{hi}} & -\frac{1}{x_{ik}}\end{bmatrix} \cdot \begin{bmatrix}\omega_h(t)-1\\ \omega_k(t)-1\end{bmatrix} \\ &= 1 + \frac{x_{hi}x_{ik}}{x_{hk}}\begin{bmatrix}\frac{1}{x_{hi}} & \frac{1}{x_{ik}}\end{bmatrix}\begin{bmatrix}\omega_h(t)-1\\ \omega_k(t)-1\end{bmatrix} = \frac{x_{ik}}{x_{hk}} \cdot \omega_h(t) + \frac{x_{hi}}{x_{hk}} \cdot \omega_k(t)\end{aligned} \tag{B.22}$$

It is worth noticing that, as a direct consequence of (B.16), the instantaneous frequency $\omega_i(t)$ at a generic point i between the boundaries h and k is a linear interpolation between $\omega_h(t)$ and $\omega_k(t)$ (see lower part of Fig. B.3). Such a linear relation is consistent with the assumption to assume steady-state conditions in the distribution of the frequency along the transmission line. Note also that (B.22) has the same formal structure of a voltage divider of a resistive circuit where the frequencies function as the voltage potential. Hence the chosen name to define (B.16).

The remainder of this section discusses the accuracy of (B.22) through numerical simulations based on the 3-bus system shown in Fig. B.4, which includes two synchronous machines and a load. The impedances of the transmission lines include the step up transformers and transmission lines ($\bar{z} = 0.025 + j0.075$ pu). A standard model for transient stability analysis is firstly considered, where transmission lines are lumped and modelled as constant impedances and generator flux dynamics are neglected. Generators are equal and are modelled as a 6$^{\text{th}}$ order synchronous machine, a IEEE Type DC1 Automatic Voltage Regulator (AVR) and a Turbine Governor (TG) with inclusion of servo and reheater models [37]. The load is modelled as a constant admittance. The disturbance is a three-phase fault that occurs at bus 3 at $t = 1$ s and is cleared after 150 ms by opening one of the two lines connecting buses 1 and 3.

All simulations and plots provided in this section, as well as in the remainder of the document, have been obtained using DOME [38]. The DOME version utilized is based on Python 3.4.1; ATLAS 3.10.1 for dense vector and matrix operations; CVXOPT 1.1.8 for sparse matrix operations; and KLU 1.3.2 for sparse matrix factorization. All simulations were executed on a server mounting 40 CPUs and running a 64-bit Linux OS.

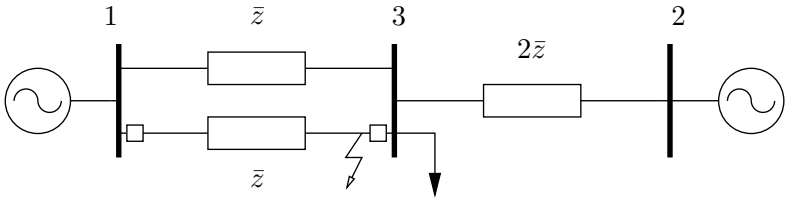

Figure B.4: 3-bus system.

Figure B.5 shows the transient behaviour of synchronous machine rotor speeds, the ω_{COI}, and the estimated frequency at the load bus using the proposed FD approach. Since the inertias of the machines are equal, oscillations are averaged out from the value of ω_{COI} as it can be readily deduced by the COI frequency expression given in Section B.1. On the other hand, the estimated bus frequency $\omega_{\text{Bus }3}$ provided by (B.22) shows oscillations in phase with $\omega_{\text{Syn }1}$, as expected, since the load bus is electrically closer to generator 1 ($x_{13} < x_{32}$). Clearly, the frequency of the COI is also unable to capture the proximity to any machine of the system. ω_{COI} can thus be used only as an indication of the overall *trend* of the system frequency but could be inadequate if utilized as a control signal for devices that regulate the frequency.

The model and the dynamics of the load connected to bus 3 are not included in (B.22) and need not to be known to define $\omega_{\text{Bus }3}$. This is one of the major differences of the proposed approach with respect to [47]. Clearly, load models and dynamics do impact on the transient behaviour of the system, which includes the machines at buses 1 and 2 whose rotor speeds are required to compute $\omega_{\text{Bus }3}$. Load models are thus *implicitly* taken into account in the FD formula.

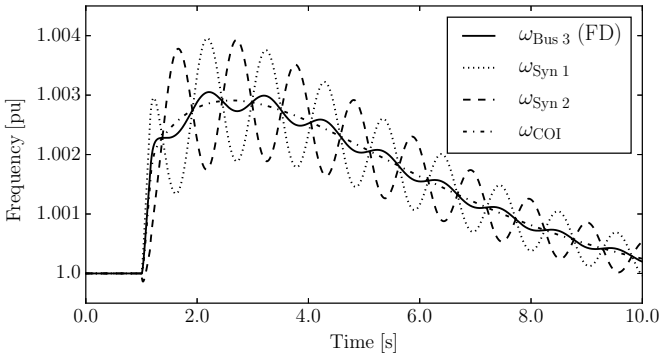

Figure B.5: 3-bus system – Synchronous machine rotor speeds, COI frequency, and frequency at bus 3 estimated based on the proposed FD approach.

The trajectories of the frequency estimation at the load bus for the 3-bus system are now compared using the proposed FD and the conventional WF described in Section B.2. Figure B.6 shows the results obtained with a more detailed model of the system considering 8$^{\text{th}}$ order models of synchronous machines and $dq0$-frame dynamic models of the transmission lines and the load at bus 3. All parameters are the same as in Fig. B.5, which is obtained using standard transient stability models. This more accurate model shows that, during the fault, the frequency drops due to the effect of machine fluxes. After the fault occurrence and clearance, the frequency also shows small high-frequency oscillations which are properly captured by (B.22). These oscillations cause severe numerical issues along the entire simulation in the behaviour of the WF – see also [23] for an in-depth discussion on this matter – as well as a significant delay of the filter to show the over-frequency after the line disconnection.

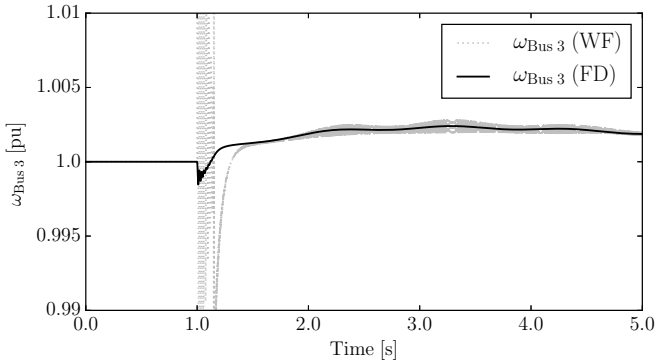

Figure B.6: 3-bus system – Frequency at bus 3 estimated with FD and the conventional WF. The system is simulated using the fully-fledged $dq0$-axis model.

As indicated in Section B.4, one of the main assumptions on which the FD formula is based, is that load currents can be neglected in (B.5). This is a common assumption in most analyses based on the admittance matrix, e.g., short-circuit calculations [4]. Moreover, in standard transient stability analysis, loads are approximated using constant impedances (see, for example, [5]), which, by the way, could be easily included in (B.16).

In the remainder of this section, it is shown that the effect of loads, including nonlinear and dynamic ones is actually negligible for the calculation of the bus frequencies. With this aim, the dynamic response of the 3-bus system of Fig. B.4 is considered again following a short-circuit at bus 3, and the constant admittance load is substituted with a static voltage- and frequency-dependent load (see Fig. B.7) and a 5$^{\text{th}}$-order $dq0$-axis model of an asynchronous motor (see Fig. B.8).

The exponential voltage- and frequency-dependent load is modelled as follows [37, 22]:

$$\begin{cases} p_i = p_0 \left(\dfrac{v_i}{v_0}\right)^{\alpha_p} \omega_i^{\beta_p} \\ q_i = q_0 \left(\dfrac{v_i}{v_0}\right)^{\alpha_q} \omega_i^{\beta_q} \end{cases} \tag{B.23}$$

In the simulations carried out to obtain Fig. B.7, the frequency ω_i is estimated using the WF or the proposed FD formula, depending on the model considered. The parameters p_0, q_0 and v_0 are the initial load active and reactive powers and voltage magnitude at bus i, respectively, determined with the power flow analysis. The parameters α_p, β_p, α_q and β_q resemble those of an aluminium plant and are based on [7]. Finally, the dynamic model of the asynchronous motor is based on [29].

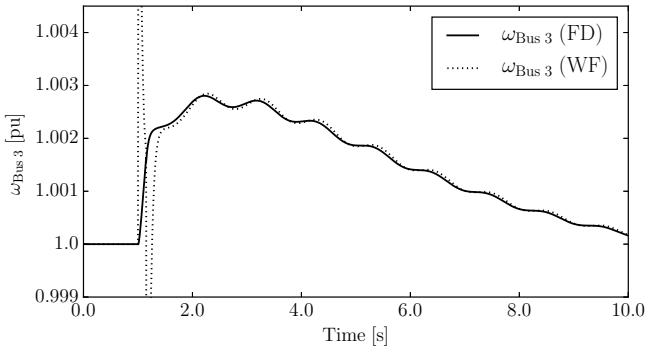

Figure B.7: 3-bus system – Frequency at bus 3 estimated with the FD and the conventional WF. The load is modelled as a frequency-dependent load representing an aluminium plant ($\alpha_p = 1.8$, $\alpha_q = 2.2$, $\beta_p = -0.3$, $\beta_q = 0.6$).

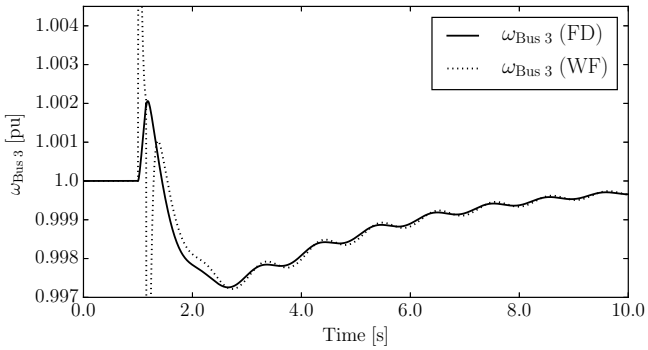

Figure B.8: 3-bus system – Frequency at bus 3 estimated with the FD and the conventional WF. The load is a squirrel cage induction motor with a 5$^{\text{th}}$-order $dq0$-axis model.

B.6 Concluding Remarks

Simulation results confirm that the FD formula (B.16) is accurate as it is able to estimate the frequency at the load bus similarly to the WF but avoiding the numerical issues of the latter. It is interesting to note that the time evaluation of the frequency in the case of the asynchronous motor is consistently different from the static load model. The load model, in fact, does impact on the overall dynamic behaviour of the system and, hence, also on the variations of rotor speeds of synchronous machines. Since the FD is based on such variations, load models are indirectly taken into account in (B.16).

Apart from the simulations included in this section, other nonlinear load models (e.g., induction motors) and several different scenarios have been considered. Moreover, other bigger test networks such as the IEEE 14-bus system and the New England 39-bus, 10-machine system have been considered to test the performance of frequency controlled devices whose input signal is provided by each of the frequency estimators described in this section, and results are provided in the remainder of this document. In every test, results were always consistent and similar to those shown in this section. It can be concluded that the proposed FD formula is accurate and that the approximations discussed in Section B.4, including that related on load models, are reasonable.

C. Validation of the Frequency Divider

In this appendix, the accuracy of the FD formula described in Appendix B is validated. To this aim, the well-known WSCC 9-bus, 3-machine test system is considered. This benchmark network is composed of three synchronous machines, loads and transformers, and six transmission lines. The system also includes primary frequency and voltage regulation, i.e., TGs and AVRs, as well as secondary frequency regulation, i.e., an AGC. The scheme of the WSCC 9-bus system is shown in Fig. C.1 and static and dynamic data can be found in [5].

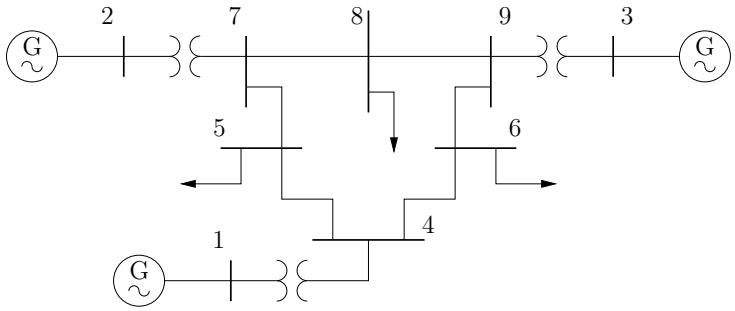

Figure C.1: Scheme of the WSCC 9-bus test system.

The frequency signals estimated through the FD formula are compared to the machine rotor speeds obtained by means of a RTDS using EMT models of the 9-bus test system, and with PMU bus frequency measurements. The contingency is a three-phase fault, located at bus 7. The fault, with a reactance of 10^{-5} p.u. (Ω), is cleared after 70 ms.

The set-up of the RTDS-PMU is depicted in Fig. C.2. The set-up is composed of three stages: real-time power system simulation, synchrophasor measurement system, and the software platform for control centre. The phasor measurement system describes the complete process of phasor measurement acquisition. In this stage, the commercial PMUs accept voltage and current measurements via the analogue output of RTDS and provide phasor measurements synchronized by the GPS signal. Based on the open source software OpenPDC, Phasor data concentrator (PDC) and Super-PDC are implemented to enable aggregation, storage and streaming of the phasor measurement data via an Ethernet network. The final stage is responsible for collecting the synchrophasor measurements, provide a common data storage point and provide a platform for developing the monitoring and control applications.

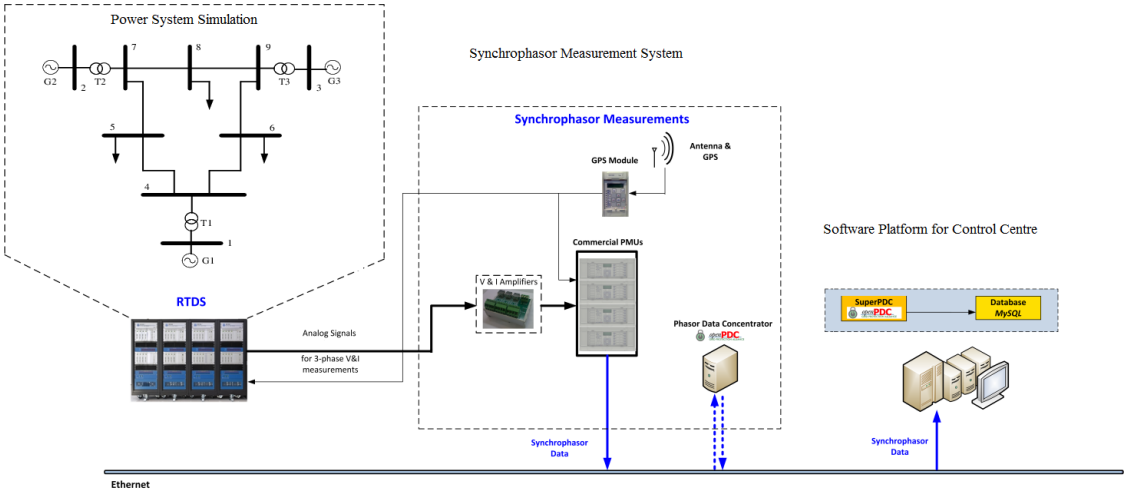

Figure C.2: RTDS-PMU set-up.

The rotor speed of the machines, and the frequencies of buses 1, 2 and 3 measured and estimated by means of the PMUs and the FD formula respectively, are represented in Figs. C.3, C.4 and C.5. It can be seen that the amplitude of the oscillations of the frequencies estimated by means of the FD formula and the PMU measurements are very similar. However, the oscillations of PMU signals show a delay with respect to those of the rotor speed of the machine. Moreover, spikes on the PMU signals are present during the transient, due to the computation of the numerical derivative during a discontinuity of an algebraic variable. On the other hand, the frequency swings of the FD estimations show no spikes, and no delay, and thus they are in phase with the machine rotor speeds. Note that the difference of the oscillation amplitudes between the machine rotor speed and the frequency at the bus of connection is due to the internal impedance of the synchronous machine. The frequency measured and estimated at the remaining system buses are depicted in Figs. C.6– C.10.

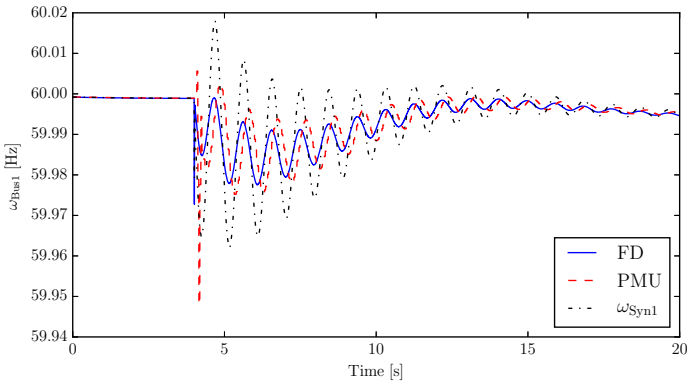

Figure C.3: Sync. machine rotor speed and frequency measured and estimated at bus 1.

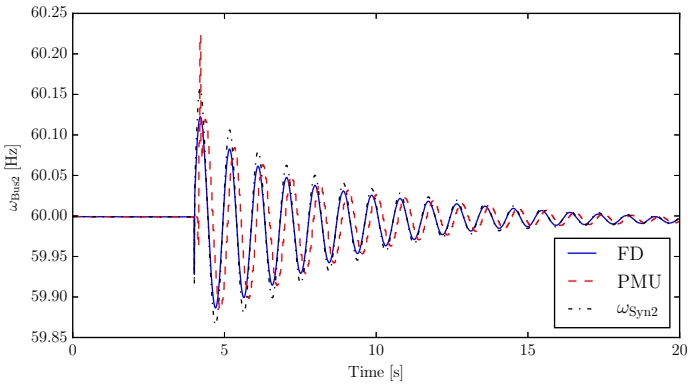

Figure C.4: Sync. machine rotor speed and frequency measured and estimated at bus 2.

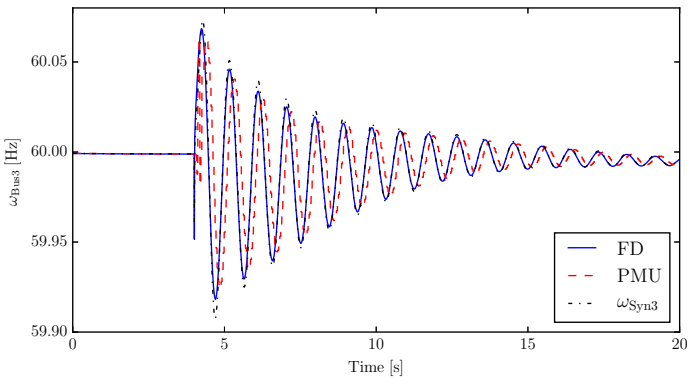

Figure C.5: Sync. machine rotor speed and frequency measured and estimated at bus 3.

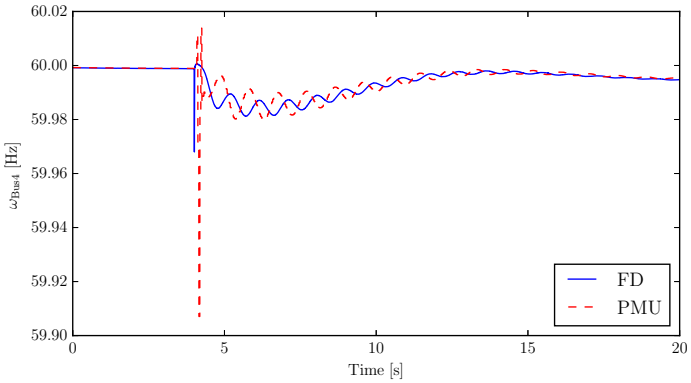

Figure C.6: Frequency measured and estimated at bus 4.

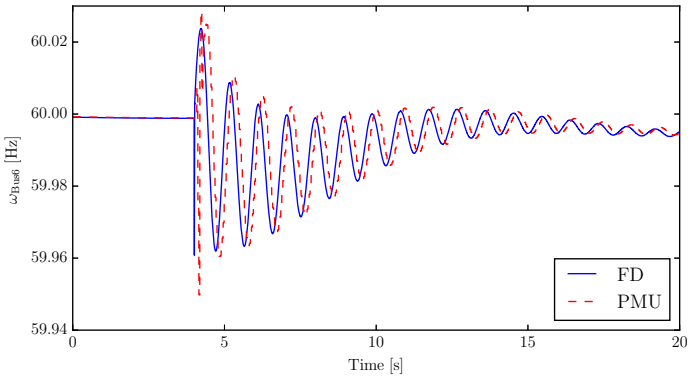

Figure C.7: Frequency measured and estimated at bus 6.

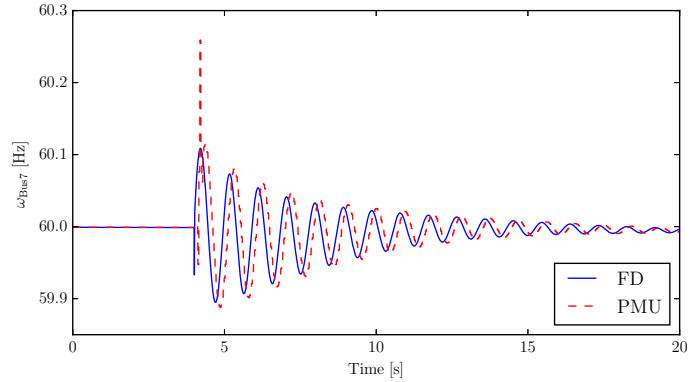

Figure C.8: Frequency measured and estimated at bus 7.

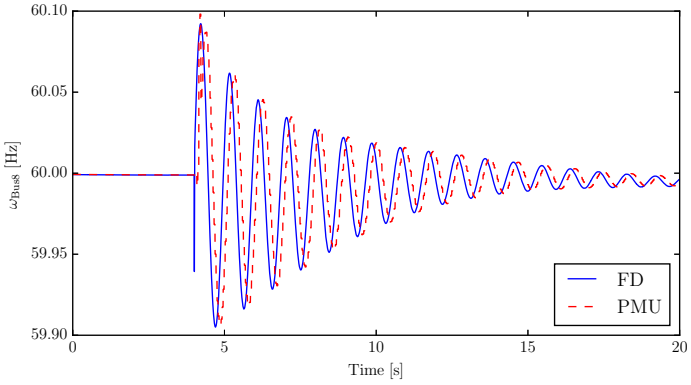

Figure C.9: Frequency measured and estimated at bus 8.

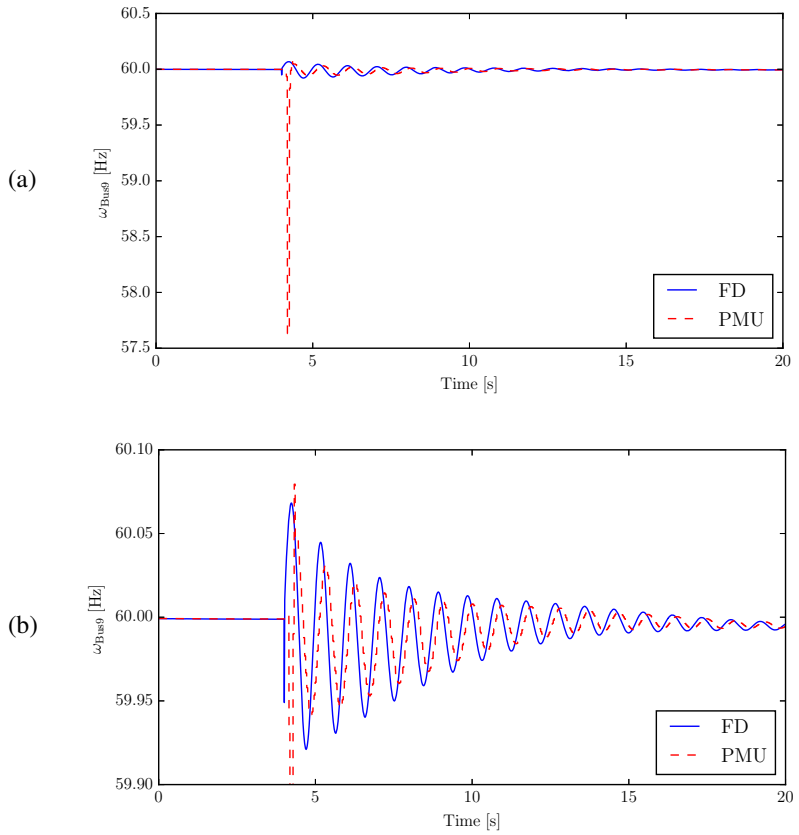

Figure C.10: Frequency measured and estimated at bus 9.

C.1 Concluding Remarks

From the comparison presented above, the accuracy of the proposed FD formula has been demonstrated. The bus frequencies of the WSCC 9-bus test system facing a severe contingency, i.e., a three-phase fault followed by a line outage, have been estimated using the FD formula and compared to those of detailed EMT models as well as of PMU measurements. Results from the comparison show that, from a simulation point of view, the FD formula is suitable to estimate local bus frequency variations, since it provides a signal that is highly accurate, and free of delays and other numerical issues such a spikes during discrete events such as faults and line outages, as opposed to signals provided by PMU devices.

D. Applications to Frequency Control

In this appendix, the effect of the provision of primary frequency control by non-conventional power system devices is studied. With this aim, Wind Energy Conversions Systems (WECSs), Solar Photo-Voltaic Generation (SPVG), Energy Storage Systems (ESSs), and Thermostatically Controlled Loads (TCLs) are analysed in Sections D.1, D.2, D.3, and D.4, respectively. This appendix also provides a comparison of the performance of the frequency controllers of these devices when their input signals are generated by each of the frequency estimation techniques presented in Appendix B.

D.1 Frequency Control of Wind Turbines

In recent years, the rapid growth of the penetration of wind power has led grid operators to face new challenges related to the control and the stability of power systems. Unlike power plants based on synchronous generators, in fact, wind turbines are equipped with limited or null primary regulation capability. In particular, frequency regulation is often not available as wind turbines are operated to produce the maximum power according to wind speed conditions through the maximum power point tracking (MPPT) control. Moreover, the penetration of wind power plants reduces the overall inertia of the system as they are often based on non-synchronous machines and connected to the grid though power electronics devices. This situation is clearly prone to increase frequency and voltage variations following large disturbances and the risk of the occurrence of unstable conditions [72]. To cope with this emerging issue, new rules have been introduced in several grid codes aimed at defining primary and secondary frequency regulation for wind turbines [55].

Several proposals of frequency control strategies for WECS can be found in the literature. In most cases, such controllers measure either the frequency deviation or the RoCoF and then accordingly modify the output of the MPPT device. The devices based on the frequency deviation are basically droop controllers commonly used on synchronous machines. The main difference is that they do not measure the speed of the rotor of the machine but the frequency of the grid at the point of connection of the wind power plant. Due to the limited inertia of wind turbines, such controllers can only provide a transient effect, whereas the long term regulation is obtained through the synchronous machines [35]. The proposal of an additional power signal based on the RoCoF or the frequency deviation to simulate the inertial response of synchronous machines has been extensively explored [16, 43, 55, 44, 33].

The droop and RoCoF controllers work similarly and are typically coupled to the MPPT device of the wind turbine. For this reason, they are described together below.

The droop controller, as the name suggests, is comparable to the primary frequency controllers of synchronous machines, and is also called proportional controller. As shown in Fig. D.1, the droop controller is composed of a washout filter, with time constant T_w, followed by a droop gain. As discussed in [35], non-conventional generators cannot contribute permanently with extra real power production, thus the need for a washout filter, which inhibits steady-state signals from the controller and help preventing the machine from stalling.

Figure D.1 also shows the RoCoF controller. This is composed of a low-pass filter, with time constant T_l, and the time derivative of frequency measurement, followed by an inertial factor (K_l). The low-pass filter is not only needed to reduce noise and numerical errors due to the derivative of a signal, but also to avoid stress of other parts of the WECS, caused by an abrupt signal from the inertial controller.

The resulting frequency control signal is the sum of the output of the droop and inertial controllers, which is then added to the active power reference obtained from MPPT. Each regulating signal is expected to play a different role for different time scales following a contingency. The RoCoF control is more relevant in the first instants after the occurrence of a contingency due to its sensitivity to the rate of change of the frequency, while the frequency deviation is more effective to mitigate the frequency nadir. Hence one can expect that the effects of the two controllers are complementary.

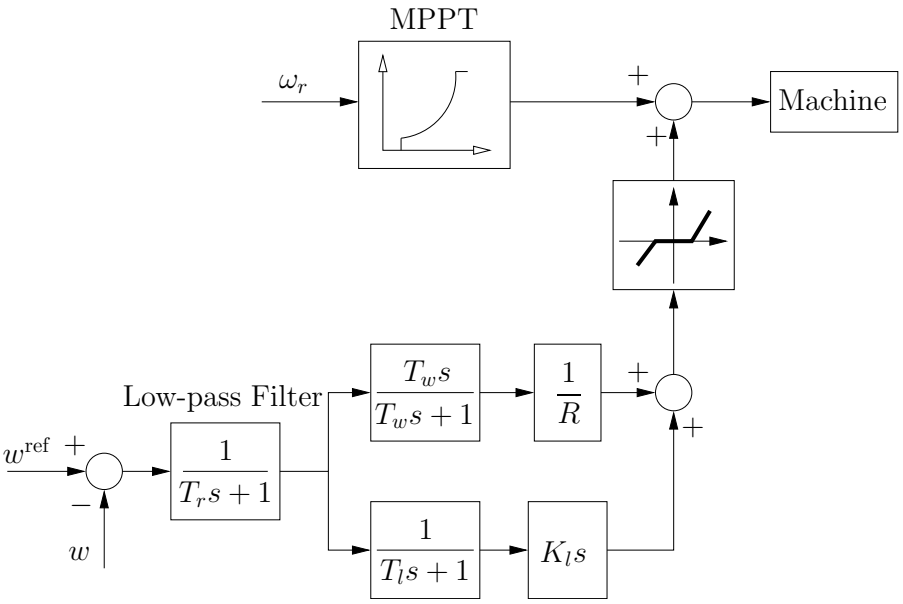

Figure D.1: Scheme of the droop and RoCoF controllers coupled to the MPPT.

D.1.1 WSCC 9-bus Test System

In this section, the performance of the primary frequency control provided by a WECS when its input signal is provided by a PLL or by the frequency estimation approaches based on the COI and the FD formula is compared. The case study is based on the well-known WSCC 9-bus, 3-machine test system, described in Appendix C.

In order to provide a realistic evaluation of the accuracy and performance of the different frequency estimation techniques, noise modeled as Ornstein-Uhlenbeck's process with Gaussian distribution is applied to the magnitudes and angles of all bus voltage phasors of the system. The interested reader can find in [41] a detailed description of the modeling and implementation of stochastic processes applied to bus voltage phasors.

In this scenario, the synchronous machine at bus 3 has been replaced with a wind power plant of the same capacity, composed of 50 variable-speed wind turbines modeled with a 5^{th}-order doubly-fed induction generator (DFIG) model [61]. The stochastic process applied to the wind follows a Weibull distribution [37]. The contingency is the outage of the line connecting buses 5 and 7 at $t = 30$ s. The values of the parameters of the WECS are based on [60], whereas the values of the parameters of the controller depicted in Fig. D.1 are provided in Table D.1.

Table D.1: Values of the parameters of the WECS controller.

Parameter	Value	Unit
T_r	0.5	s
T_w	1000.0	s
T_l	4.0	s
R	0.05	–
K_l	80.0	–

The input signals of the wind plant controller and the subsequent active power outputs are represented in Figs. D.2 and D.3, respectively, for the different frequency estimation approaches. It can be seen that the difference between the signals is relatively small, leading to similar active powers supplied by the wind power plant.

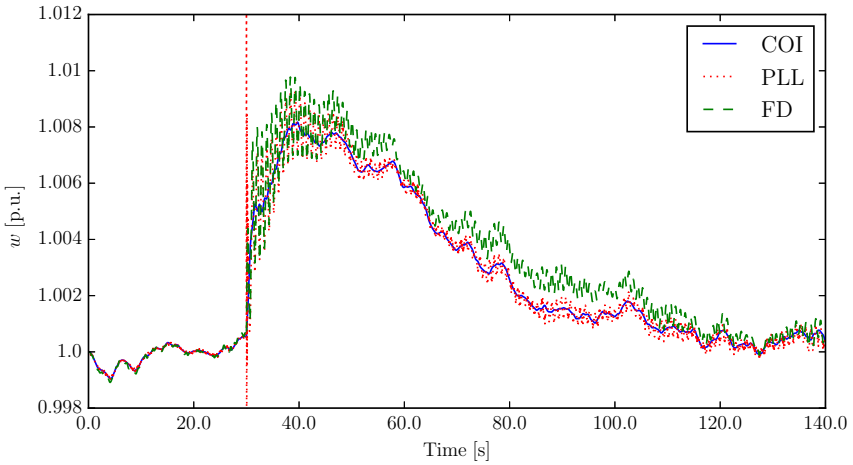

Figure D.2: Input frequency signal of the wind power plant control estimated by different approaches.

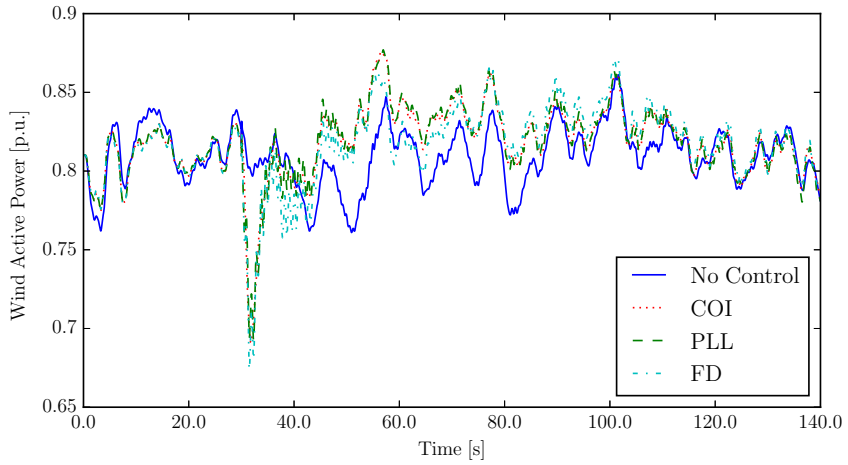

Figure D.3: Active power supplied by the wind power plant.

The response of the frequency of the COI is represented in Fig. D.4 for each of the frequency estimation approaches, and compared with that without the controller of the wind power plant. The inclusion of such a controller reduces the frequency peak caused by the line outage by about 30–40%, being the lowest when the FD formula is used as input signal of the controller. Note that the frequency spikes that can be observed in Fig. D.2 when using the PLL, which vary in the range of $[0.99, 1.02]$ pu, are filtered by the WECS controller.

To study the sensitivity of the three frequency estimation techniques to fast system dynamics, the flux dynamics of the DFIG are now included in the model. Results are shown in Fig. D.5. It can be seen that, while the behaviour of the COI and the FD is similar to the one when no flux dynamics were included, the PLL now shows fast varying, poorly damped oscillations that leads to frequency fluctuations in the range of $[0.99, 1.023]$ pu.

Finally, the effect of the low-pass filter of the WECS frequency control in Fig. D.1 is studied. With this aim, the response of the WECS is studied for the case when the filter time constant is $T_r = 0.5$ s, and for the case when such a filter is disabled (i.e., $T_r = 0$ s). The active power supplied by the WECS during the transient caused by the line outage, and the rotor speed of the synchronous machine at bus 2, $\omega_{\text{Syn }2}$, are depicted in Figs. D.6 and D.7, respectively.

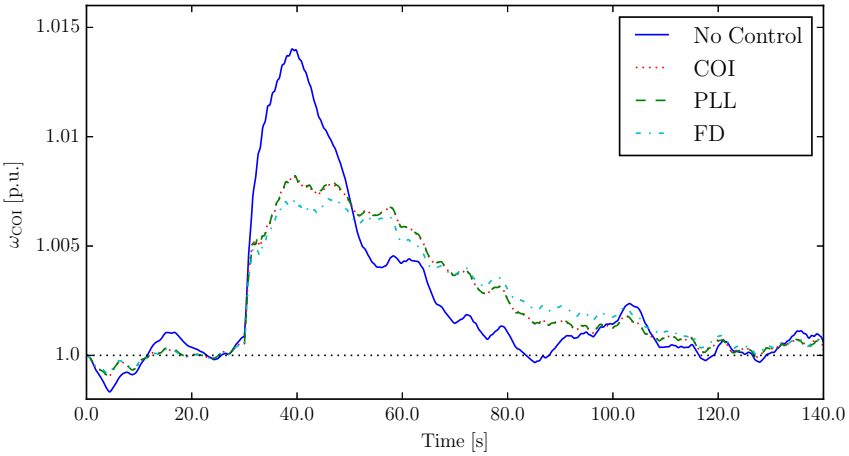

Figure D.4: Frequency of the COI.

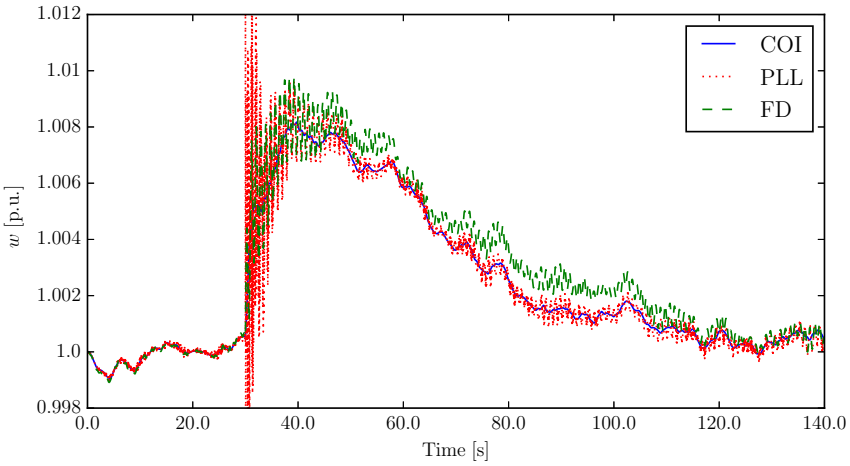

Figure D.5: Input frequency signal of the wind power plant control estimated by different approaches with inclusion of DFIG flux dynamics.

Comparing both figures, it can be seen that the inclusion of the filter highly reduces the oscillations of the active power output of the WECS, thus reducing the stress of the device, for both the FD and the PLL signals, whereas the COI shows little sensitivity to the value of T_r. However, while without the filter the oscillations of $\omega_{\mathrm{Syn}\ 2}$ are damped after about 10 s (FD) and 25 s (PLL), these oscillations last over 30 s when the low-pass filter is included. There is thus a trade-off between reducing the damping of the rotor speeds of the synchronous machines, and the stress of the WECS system. However, if fast dynamics such as the fluxes of the synchronous machines are included, the relevance of the low-pass filter becomes apparent, as shown in Fig. D.8, where the synchronous machines are modelled using the fully fledged, 8$^{\mathrm{th}}$ order model. It can be seen that, if the filter is disabled, the power drops abruptly to about 0.05 p.u. when the PLL signal is used. On the other hand, when the FD is used, the power oscillations are similar to the previous case when 6$^{\mathrm{th}}$ order synchronous machine models were used (Fig. D.6).

These results suggest that fast dynamics can negatively affect the response of controllers based on local frequency measures and that an appropriate filtering should be implemented if PLL devices are to be utilized. On the other hand, filtering should not introduce a delay in the frequency measure to prevent a possible deterioration in the dynamic response.

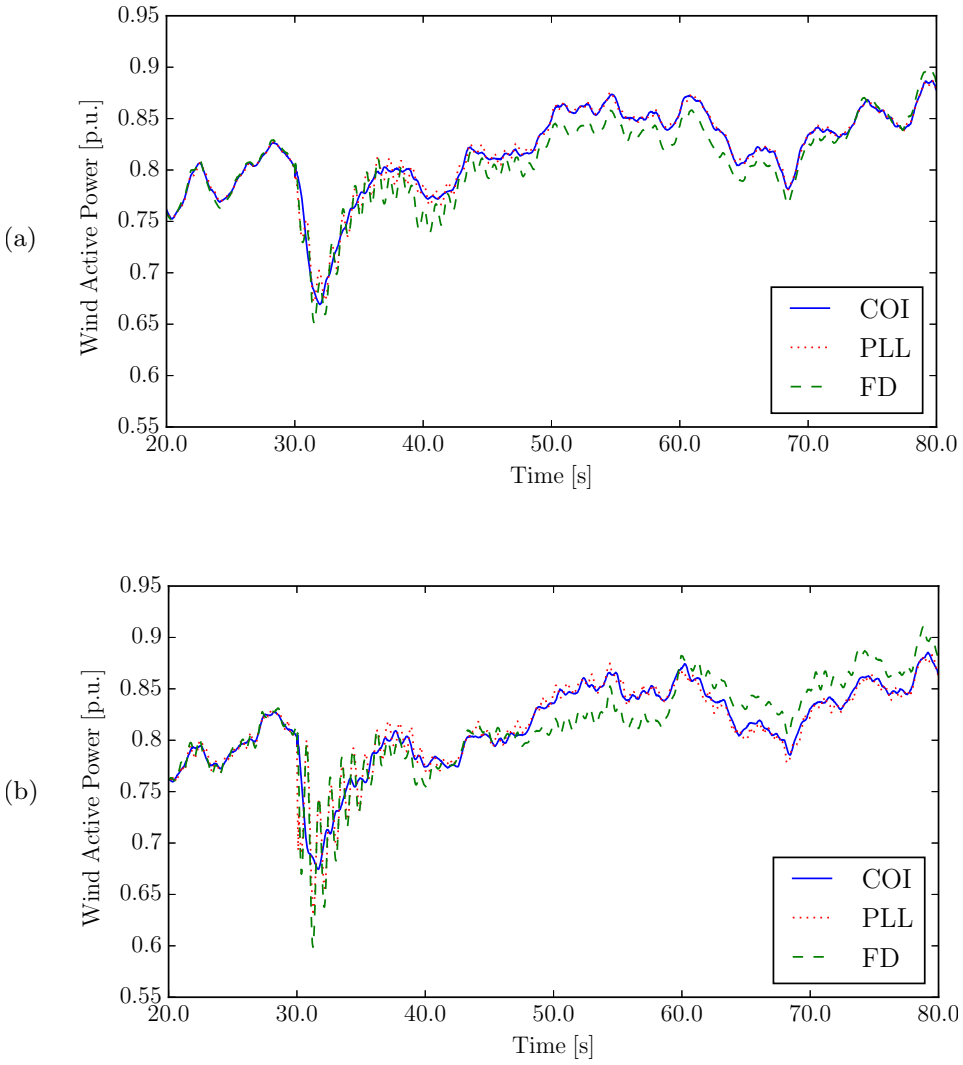

Figure D.6: Active power supplied by the wind power plant. (a) $T_r = 0.5$ s; (b) $T_r = 0$ s.

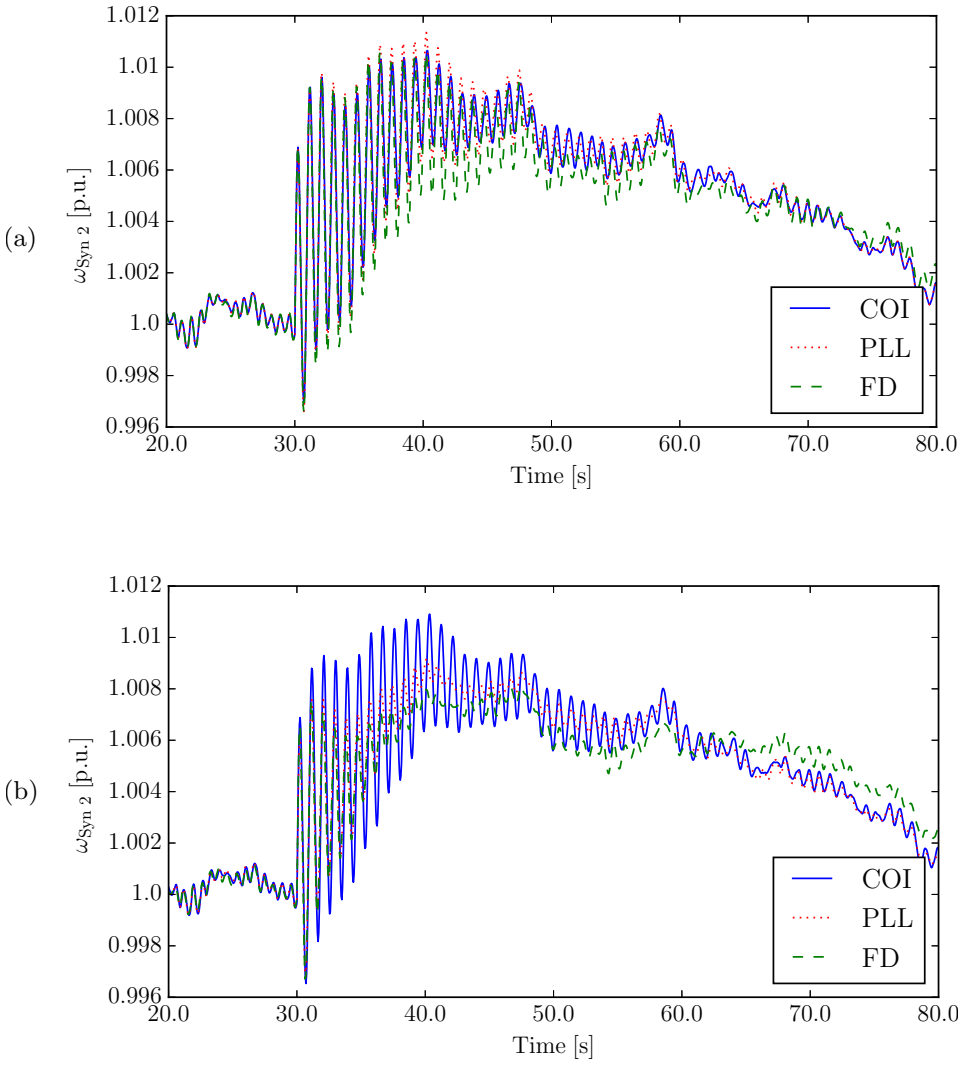

Figure D.7: Rotor speed of the synchronous machine at bus 2. (a) $T_r = 0.5$ s; (b) $T_r = 0$ s.

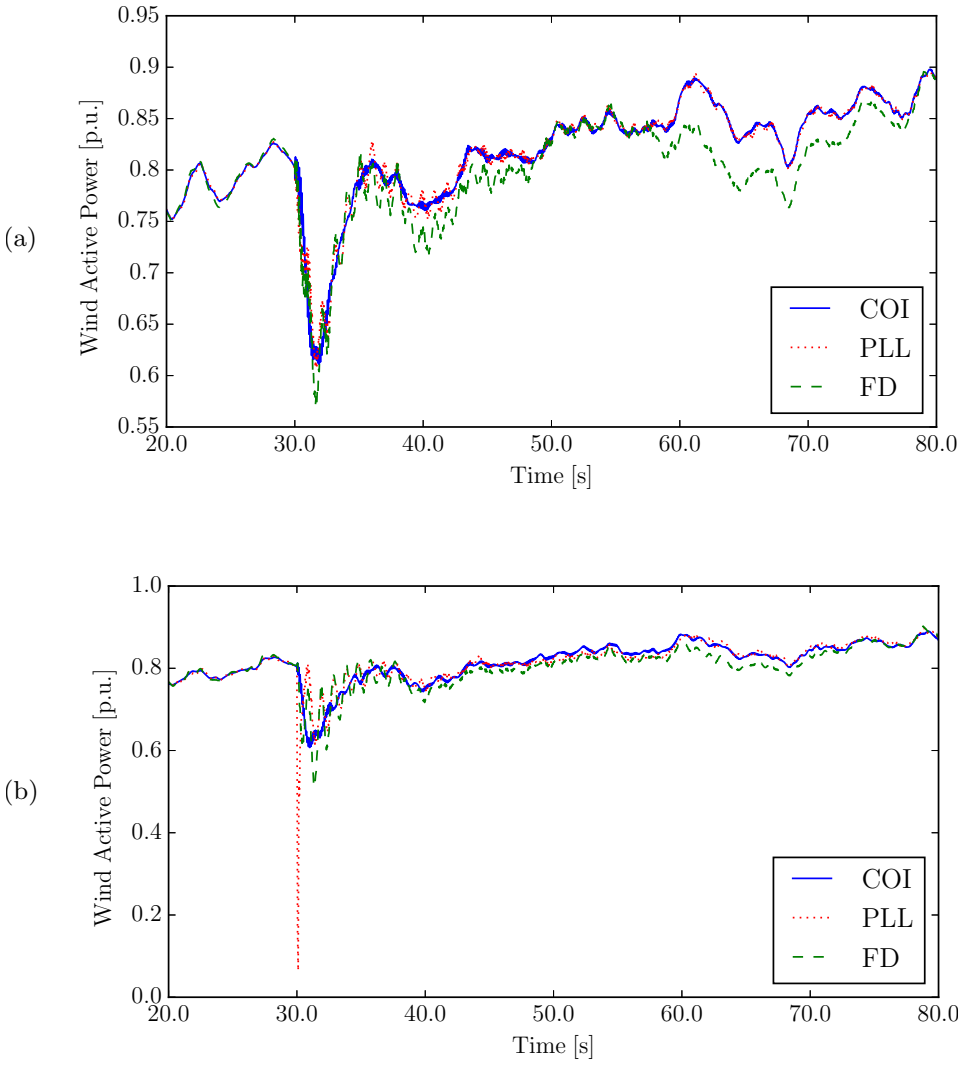

Figure D.8: Active power supplied by the wind power plant. Synchronous machines are modelled using the 8th order model. (a) $T_r = 0.5$ s; (b) $T_r = 0$ s.

D.1.2 Remarks

Based on the simulation results, the following remarks are relevant.

- The FD formula provides the *ideal* value of the local frequency at buses and can thus be utilized as a reference for testing the quality of the frequency estimated by the PLL and other estimation approaches.
- A standard synchronous reference frame model of the PLL works reasonably well compared to the FD formula. Noise and numerical spikes do not deteriorate significantly the quality of the control, provided that WECSs include a proper low-pass filter within their primary frequency controllers. Fast dynamics of fluxes, however, can deteriorate the dynamic response of PLL-based frequency controllers.
- The COI signal is inadequate to simulate the behaviour of WECSs frequency controllers, although its average nature often leads to an overall smoother frequency response. This consideration could be further developed in the future considering coordinated area controllers sharing an average value of the frequency signal rather than utilizing a local one.

D.2 Frequency Control of Solar Photo-Voltaic Generation

Concurrently with WECSs, the penetration of Solar Photo-Voltaic Generation (SPVG) in power systems is experiencing a significant growth in recent years. SPVGs shares with WECSs the fact that they are connected to the grid by means of power electronic converters, and thus, their integration into the power system implies a decrease of the overall inertia of the network, that leads to a poorer frequency response against contingencies. Therefore, to overcome potential system frequency and/or voltage stability issues due to large disturbances, it is important that SPVG provides both frequency and voltage regulation [65].

In this work, the control of the frequency and the voltage at the bus of connection of the SPVG with the grid is performed similarly to [65, 27, 19], and the scheme of the controllers and the converter is depicted in Fig. D.9. Due to the resemblance between the connection of SPVGs and WECSs with the rest of the grid, their controllers also show relevant similarities. With regard to the frequency regulation, a droop control is implemented. The droop control is composed of a droop gain and a low-pass filter, and takes the deviation of the frequency at the bus of connection with respect to a given reference. The output signal is then added to the reference power provided by the MPPT, and processed by a PI regulator, which generates the reference current input signal of the SPVG converter.

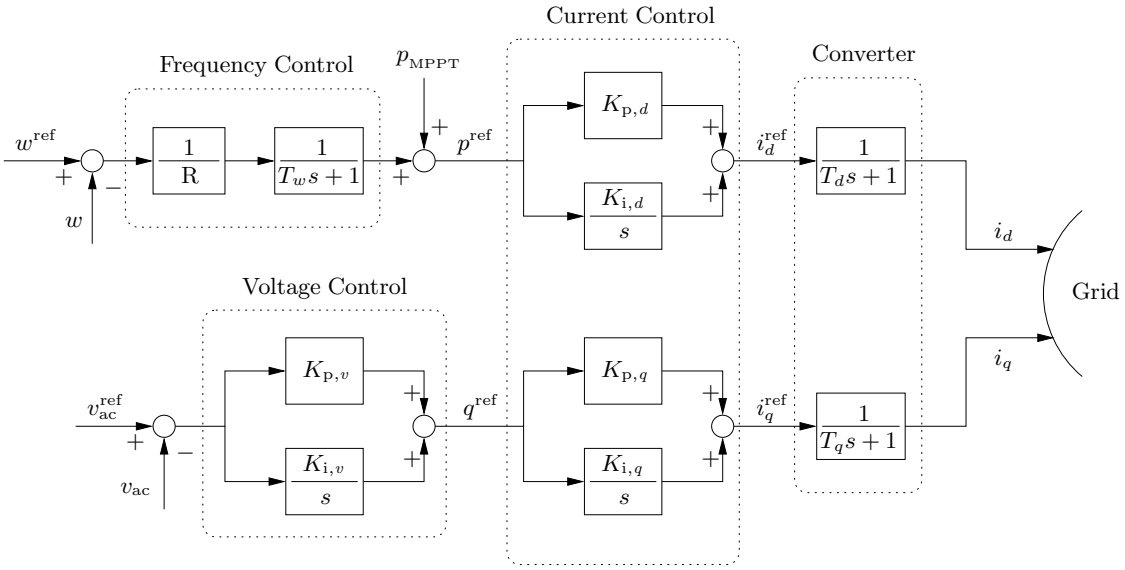

Figure D.9: Scheme of the frequency and voltage control of SPVGs.

D.2.1 WSCC 9-bus Test System

This section studies the capability of SPVGs to provide primary frequency regulation through simulations. With this aim, a similar case study to that presented in Subsection D.1.1 is conducted. The case study is thus based on the WSCC 9-bus, 3-machine test system described in Appendix C, and compares the SPVG primary frequency control for different input signals, i.e., PLL, COI and FD.

Noise modelled as Ornstein-Uhlenbeck's process to bus voltage magnitudes and angles are also applied in this case study [41]. The synchronous machine at bus 3 has been replaced in this case study with a SPVG of the same capacity. Given the short time scales of the simulations, the solar radiation, and consequently, the active power reference provided by the MPPT p_{MPPT}, are assumed to be constant. The contingency is the outage of the line connecting buses 5 and 7 at $t = 30$ s. The values of the parameters of the frequency control loop depicted in Fig. D.9 are provided in Table D.2 [19].

Table D.2: Values of the parameters of the SPVG controller.

Parameter	Value	Unit
T_d	0.015	s
T_w	1.0	s
R	0.05	–
$K_{\mathrm{p},d}$	10.0	–
$K_{\mathrm{i},d}$	5.0	–

Figures D.10 and D.11 show the input signal of the SPVG frequency controller and the SPVG active power output, respectively, for the three frequency estimations, namely COI, PLL and FD. It can be seen that the overall trend of the three signals are very similar, leading to small differences of the SPVG active power output. However, the FD shows relatively high amplitude fluctuations due to the local oscillations of the synchronous machines, that are averaged out from the COI. On the other hand, the PLL shows high sensitivity to the bus voltage noises.

Figure D.12 compares the ω_{COI} of the system without the frequency control of the SPVG, and with the controller for the three frequency estimation signals. The controller reduces the frequency peak by about 70% for the three cases, without significant differences between them. Note that the high frequency oscillations that are present in the PLL and FD signals in Fig. D.10 are filtered out by the low-pass filter of the SPVG frequency control.

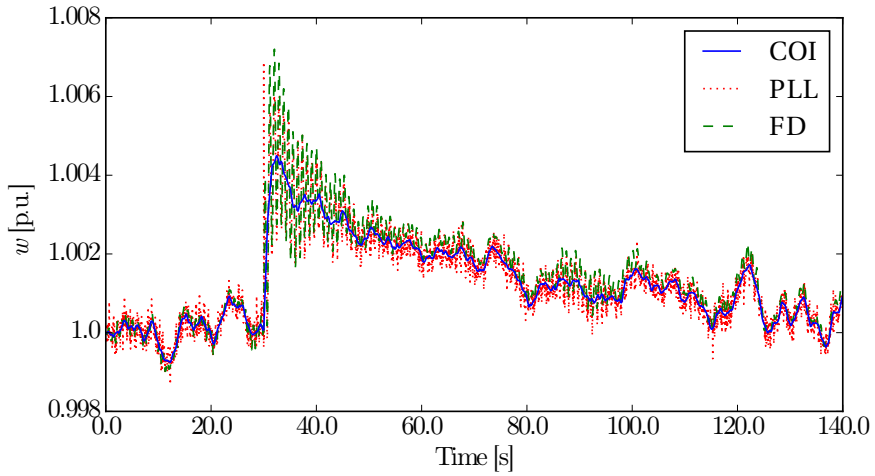

Figure D.10: Input frequency signal of the SPVG control estimated by different approaches.

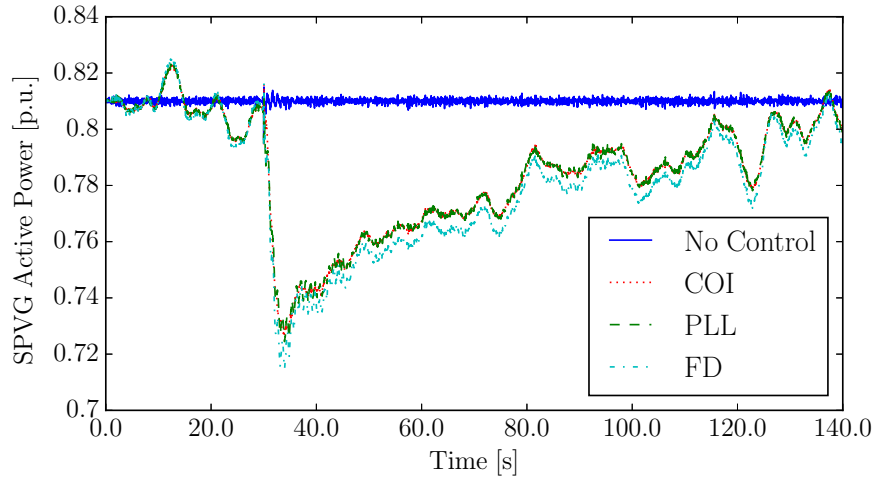

Figure D.11: Active power supplied by the SPVG.

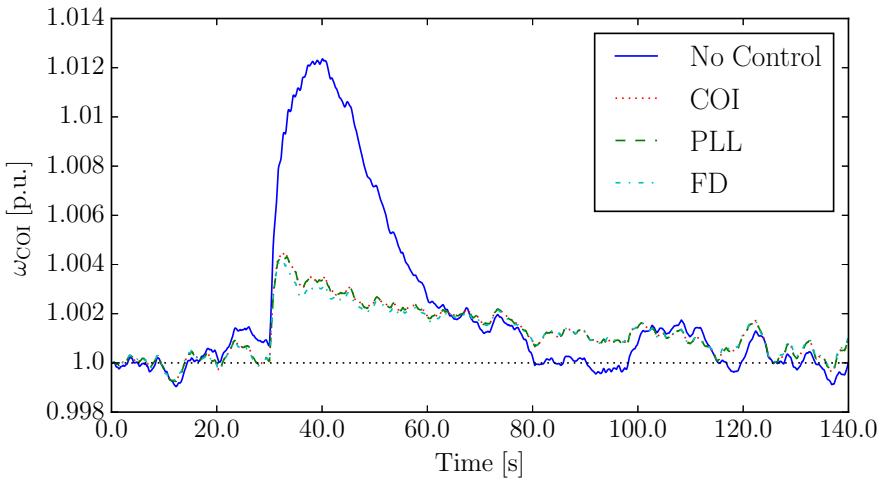

Figure D.12: Frequency of the COI.

D.2.2 Remarks

Remarks on frequency control provided by SPVG are listed below, based on the simulation results.

i. The frequency control provided by SPVGs can considerably improve the response of the system in case of over-frequencies, regardless the frequency estimation technique used as input signal of the controller.

ii. The PLL shows a good accuracy and provides a good performance of the frequency controller, provided that the signal is passed through a low-pass filter, to reduce the inherent sensitivity of the PLL to noises and numerical problems due to discontinuities.

iii. The performance of the SPVG frequency controller is not deteriorated when the COI signal is used as the frequency estimation. This is due to the fact that the average nature of the COI naturally imitates the effect of the low-pass filter in the FD and the PLL signals, leading to similar output signals of the SPVG frequency control, and thus, to similar active power outputs of the SPVG.

D.3 Frequency Control of Energy Storage Systems

Among all currently existing alternatives to improve the performance, reliability and resiliency of power systems with high RES penetration, Energy Storage Systems (ESSs) are one of the most promising [1, 6, 56]. ESSs have the potential to provide a large variety of ancillary services to the system thanks to their capability to supply/absorb active and reactive powers. These services include flattening of the power provided by RESs, active power regulation in transmission lines, local and/or global frequency regulation, RoCoF mitigation, and local voltage regulation. These features of ESSs have led, in recent years, to a huge investment in the research, development, prototyping and installation of a large variety of technologies. Among all ESSs technologies that are currently most promising there are Battery Energy Storage (BES), Compressed Air Energy Storage (CAES), Fuel Cell Energy Storage (FCES), Flywheel Energy Storage (FES), Pumped Hydro Energy Storage (PHES), Super Capacitor Energy Storage (SCES) and Superconducting Magnetic Energy Storage (SMES). Figure D.13 presents a general comparison of the power ratings and the discharge time at rated power of a variety of ESS technologies.

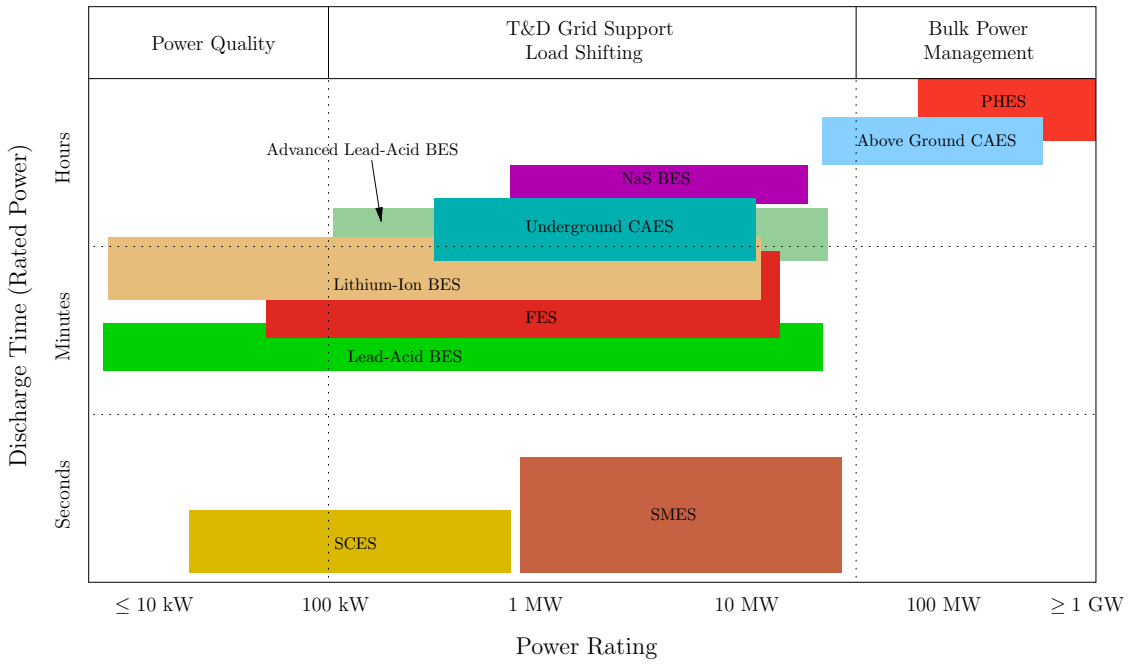

Figure D.13: Comparison of power rates and discharge times of different ESS technologies [2, 53].

A general scheme of a power converter-based ESS connected to a power system is depicted in Fig. D.14). The main objective of ESSs is to regulate a measured quantity of the system w, e.g., the frequency of the bus of connection of the ESS. While the storage device is responsible of the active power support, the Voltage Sourced Converter (VSC) provides reactive power support by regulating the ac voltage at the bus of connection, and it links the storage device with the grid.

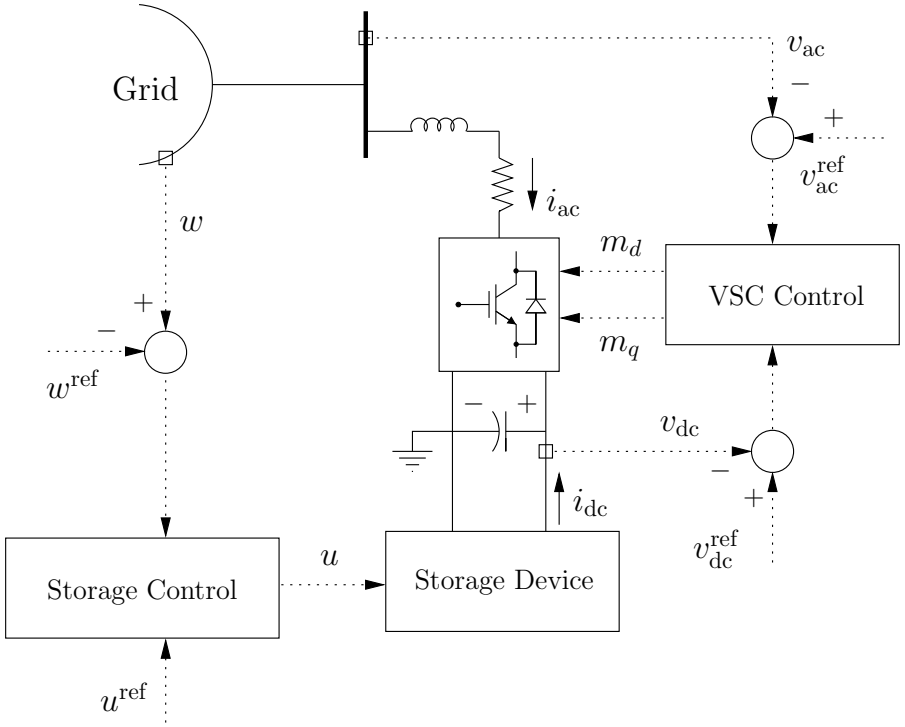

Figure D.14: Scheme of the ESS connected to a grid.

The charge/discharge process of the storage device is regulated by the Storage Control (see Fig. D.15). The input signal of the control is the error between the actual value of w, and a reference value (w^{ref}). If $w = w^{\mathrm{ref}}$, the storage device is inactive and its stored energy is thus kept constant. For $w \neq w^{\mathrm{ref}}$, the storage device injects active power into the ac bus through the VSC (discharge process) or absorbs power from the ac bus (charge process). The typical configuration of this PI-based controller includes a dead-band and low-pass filter blocks that are responsible of reducing the sensitivity of the storage control to small, high-frequency perturbations such as noises. The aim of these blocks is to reduce the number of charge/discharge operations, thus increasing the life of the ESS [40]. The PI regulator is composed of a proportional gain, $K_{\mathrm{p},u}$, and an integrator with gain $K_{\mathrm{i},u}$ and integral deviation coefficient $H_{\mathrm{d},u}$. These parameters are commonly tuned by trial-and-error or pole-placement techniques. The simplicity of the implementation and design, as well as the mass utilization of this controller in industrial applications are its main strengths. Note also that the structure of the PI does not depend on the energy storage technology considered. The scheme shown in Fig. D.15 includes also a block referred to as Storage Input Limiter (SIL) [49]. The purpose of the SIL is to reduce the impact of energy saturations of the storage device on system transients. This block takes the actual value of the energy stored in the device, E, and regulates accordingly the input controlled variable of the storage device, u.

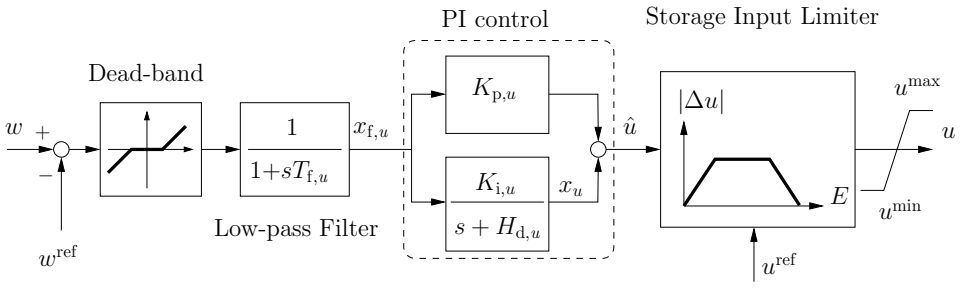

Figure D.15: Storage control scheme.

D.3.1 IEEE 14-Bus Test System

This subsection considers the IEEE 14-bus test system (see Fig. D.16) for the simulations. This benchmark network consists of 2 synchronous machines and 3 synchronous compensators, 2 two-winding and 1 three-winding transformers, 15 transmission lines and 11 loads. The system also includes AVRs, TGs and an AGC. All dynamic data of the IEEE 14-bus system as well as a detailed discussion of its transient behaviour can be found in [28].

Some modifications have been made in this network to study the interaction of the storage device with the rest of the system:

- The capacity of the synchronous generator placed in bus 1 is reduced by 5 times its original value.
- A 30 MW, 70 MVar ESS is connected to bus 4.

Two scenarios have been considered to study the performance of the ESS applying the three control strategies: in Subsection D.3.1.1 the system faces a three-phase fault followed by a line outage, whereas in Subsection D.3.1.2 a wind power plant is included, and stochastic variations of the wind are considered.

D.3.1.1 Three-phase Fault and Line Outage

In this subsection, the contingency is a three-phase fault occurring in bus 5 at $t = 1$ s, and cleared after 70 ms by opening the line that connects buses 5 and 1. Figure D.17 shows the rotor speed of the synchronous machine at bus 2 for the cases without the ESS, and with the ESS regulating the frequency of the COI and of the bus of connection estimated by means of the FD formula and a PLL.

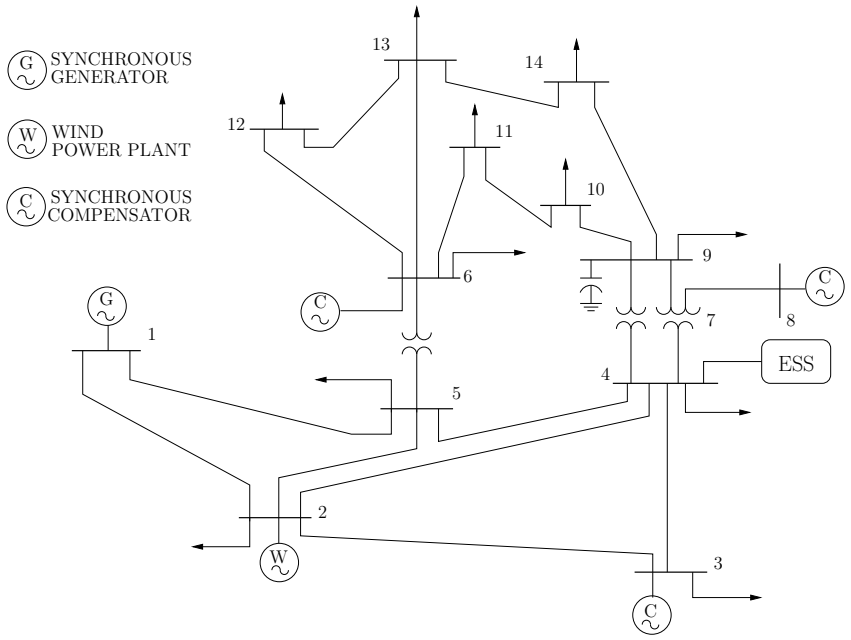

Figure D.16: IEEE 14-bus test system with an ESS device connected to bus 4.

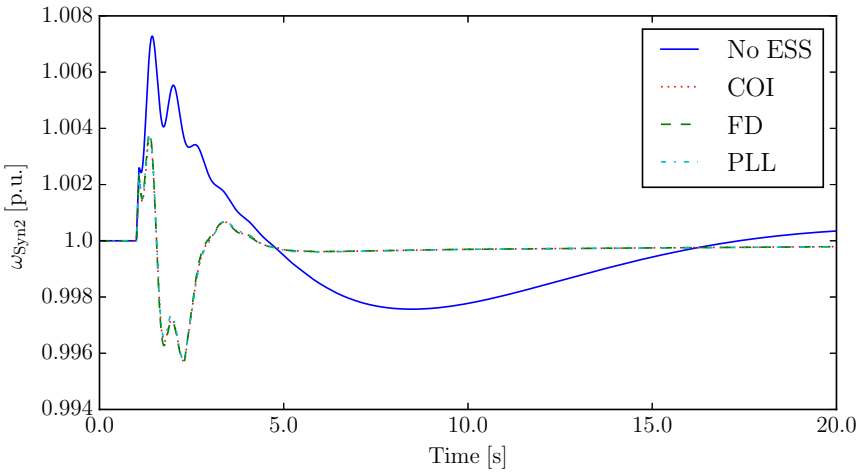

Figure D.17: Rotor speed of the synchronous machine at bus 2 of the IEEE 14-bus test system without and with an ESS regulating a system frequency.

It can be seen that the ESS can reduce the frequency deviation in the first swing by about 50%, and allows the system to reach steady state after about 5 seconds, as opposed to the required $\gtrsim$ 15 seconds without the ESS. On the other hand, a greater frequency nadir is present in the cases with the ESS, due to current saturations of the storage device. Nevertheless, this frequency nadir is about the half of the amplitude of the frequency variation of the first swing without the ESS.

The frequency at bus 4, i.e., the bus of connection of the ESS with the rest of the system, is represented in Fig. D.18.

From Figs. D.17 and D.18, it is worth noticing that the response of the ESS is virtually the same regardless the frequency estimation technique used. However, the signals provided by each technique are considerably different, as shown in Fig. D.19, where the input signal of the ESS control, w, is represented.

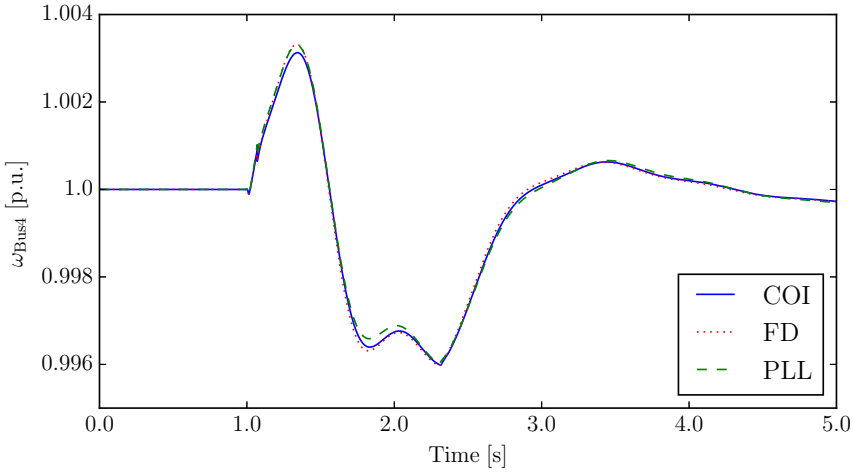

Figure D.18: Frequency at bus 4 when the ESS control input signal is generated by different frequency estimation techniques.

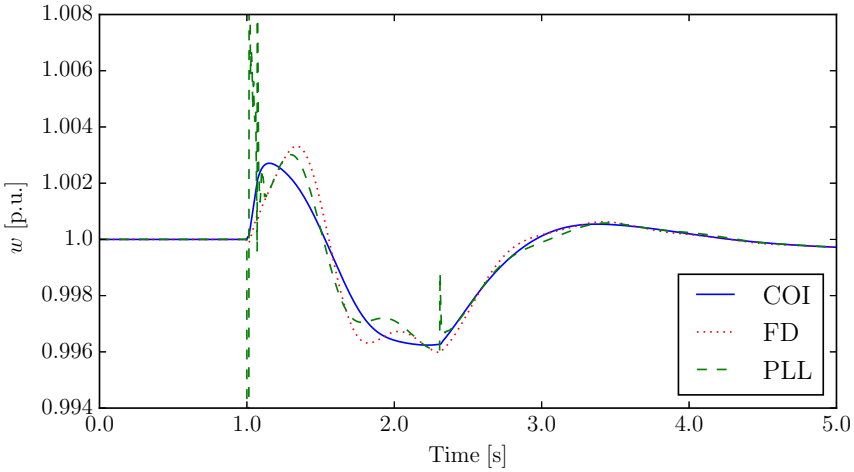

Figure D.19: Input signal of the ESS control generated by each frequency estimation technique.

As expected, the COI filters local frequency oscillations, while the PLL includes spikes in the signal that span from 0.96 to 1.01 p.u. The similarity of the ESS responses despite the differences in the control input signal is due to the presence of the low-pass filter with time constant $T_{\text{f},u}$ (see Fig. D.15). This filter removes to a large extent the amplitude of the PLL spikes, as well as the local frequency oscillations, leading to a similar output signal of the controller, u, and thus, of the active power supplied/absorbed by the ESS, as depicted in Figs. D.20 and D.21, respectively.

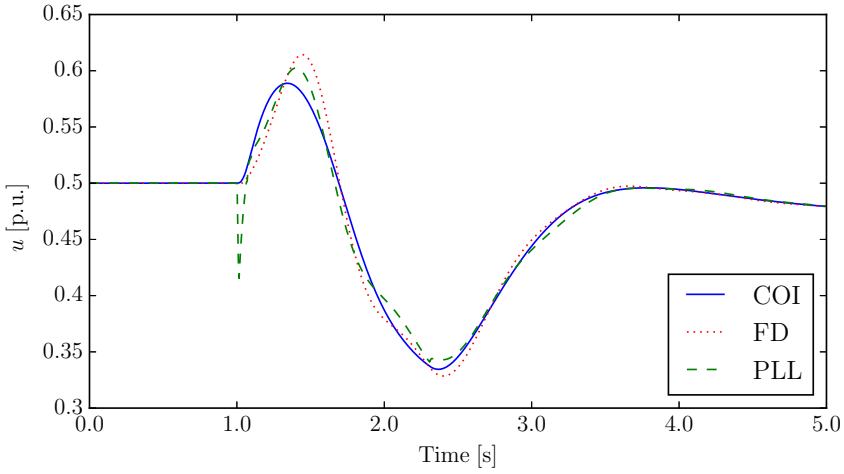

Figure D.20: Output signal of the ESS control for each frequency estimation technique.

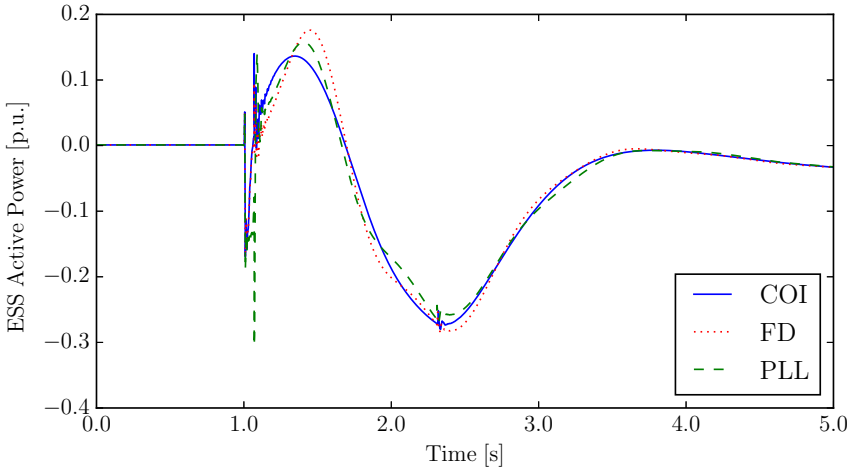

Figure D.21: Active power supplied/absorbed by the ESS for each frequency estimation technique.

D.3.1.2 Stochastic Variations of Wind

In this case study, the synchronous generator placed in bus 2 is substituted by a 60-turbines wind power plant of the same power capacity. A stochastic process that follows a Weibull's distribution is applied to the wind, and its profile is shown in Fig. D.22 [37]. Values of the mean wind speed, scale and shape factors are taken from [12] for the month of August a the height of 65 meters.

The objective of the ESS installed at bus 4 is to regulate the frequency (in this subsection, the only frequency estimation technique considered is the FD formula) and the voltage at the bus of connection with the system, as depicted in Figs. D.23 and D.24, respectively.

It can be seen that the ESS is able to reduce considerably both the frequency and voltage variations due to the wind variations. Moreover, despite the local nature of the ESS controllers, it nevertheless improves the overall system response, as shown in Figs. D.25 and D.26, where the frequency and the voltage at the load bus 14 are depicted, respectively.

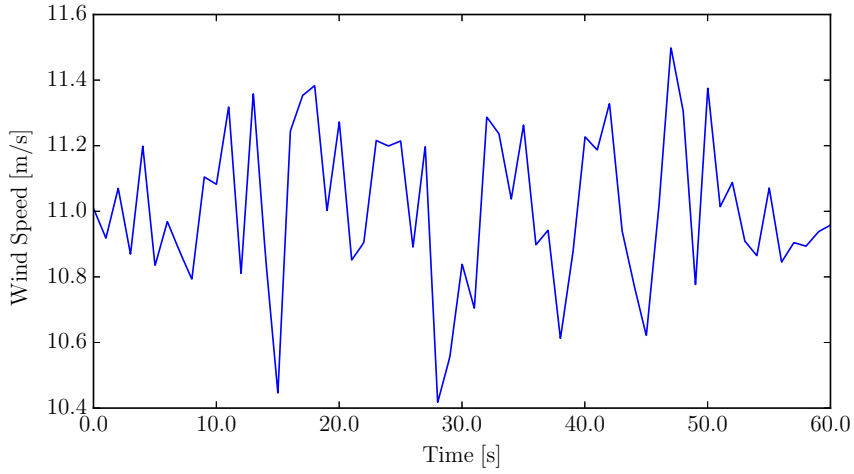

Figure D.22: Wind profile that follows a Weibull distribution.

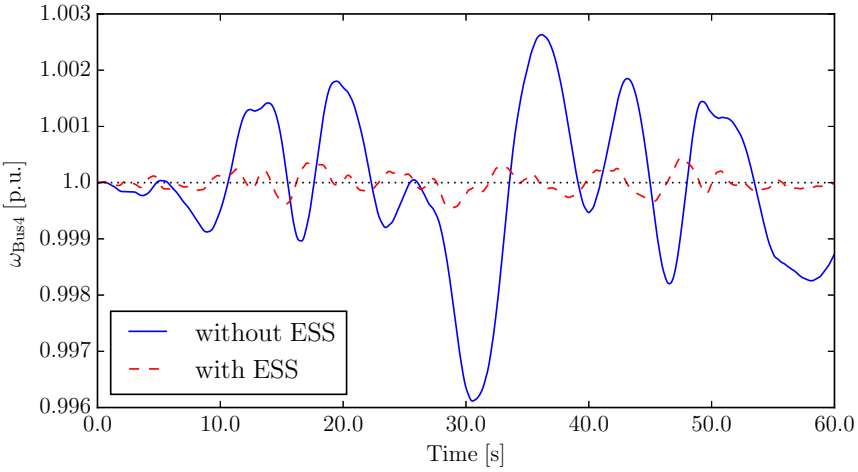

Figure D.23: Response of the IEEE 14-bus test system with stochastic wind perturbations: frequency at bus 4.

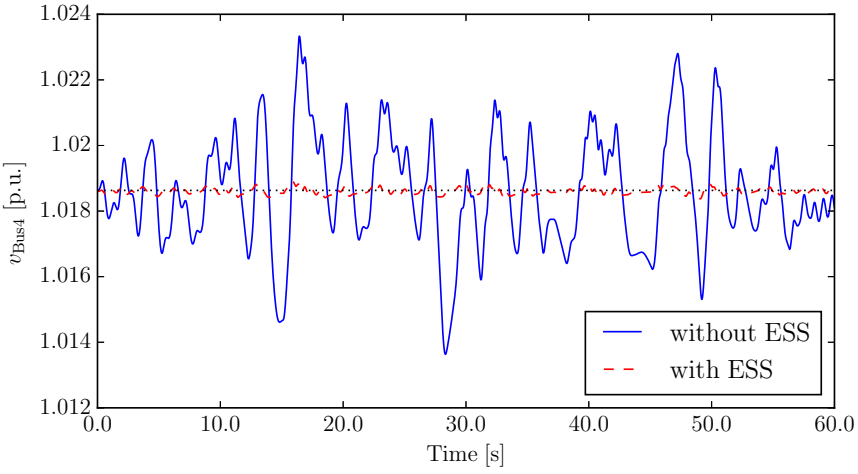

Figure D.24: Response of the IEEE 14-bus test system with stochastic wind perturbations: voltage at bus 4

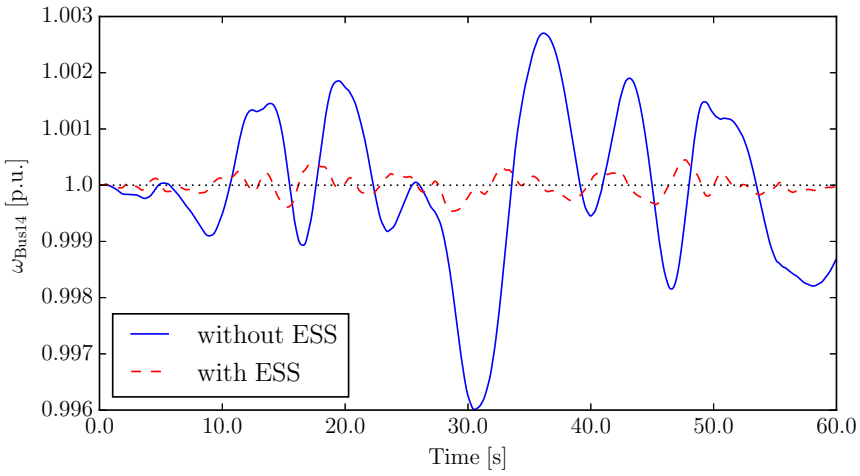

Figure D.25: Response of the IEEE 14-bus test system with stochastic wind perturbations: frequency at bus 14.

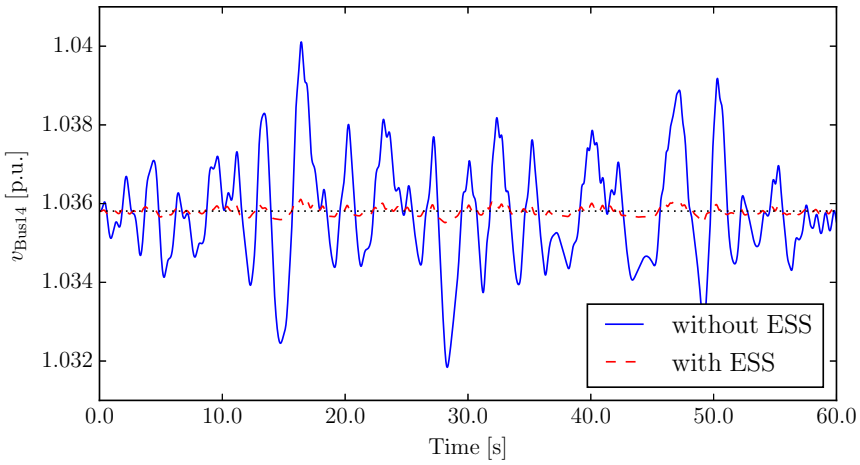

Figure D.26: Response of the IEEE 14-bus test system with stochastic wind perturbations: voltage at bus 14

D.3.2 Remarks

Based on the simulation results presented in this section, the following remarks are relevant.

i. The inclusion of ESSs in the system allows reducing, to a large extent, frequency and voltage variations due to severe contingencies such as faults, and to the stochastic nature of RESs such as wind power plants, thanks to the capability of ESSs to inject/absorb both active and reactive power simultaneously

ii. As for the case with WECSs, the low-pass filter included in the ESS frequency control loop allows reducing the impact of the noise and numerical issues present when the PLL is used to estimate the frequency.

iii. The response of the ESS can be significantly deteriorated if current saturations of the storage device are reached.

iv. Despite the fact that ESSs provide frequency and voltage regulation locally, their effect can be seen system-wide.

D.4 Frequency Control of Loads

This section compares the performance of Thermostatically Controlled Loads (TCLs), which are dynamic loads with temperature control, when their input signal is provided by the COI, WF and FD. These can be air conditioning systems, industrial refrigerators or heating systems [22]. In most cases, the reference temperature is fixed to an assigned value. There are, however, prototypes of TCLs that include a measure of the system frequency and that vary the reference temperature in order to reduce frequency deviations [30, 62, 34]. The control scheme of the TCL is depicted in Fig. D.27. The meaning of the variables are the following: Θ is the load temperature (lumped model); Θ_a is the ambient temperature; g is the equivalent load conductance, v is the load terminal voltage; and P the consumed active power.

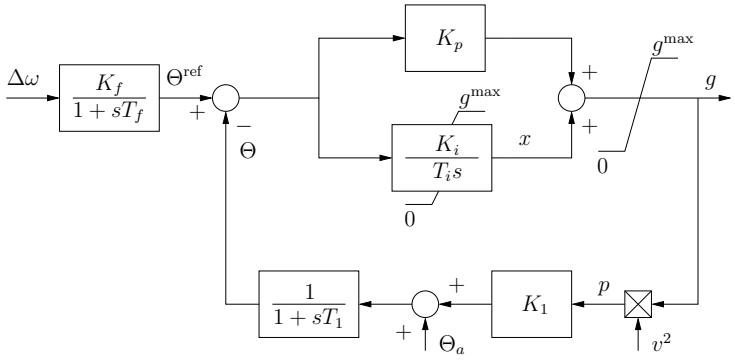

Figure D.27: Thermostatically controlled load with frequency control.

The gain K_1 and the maximum conductance $g^{\max}$ are determined based on the initial values of the voltage, v_0, and the active power, p_0, as follows:

$$K_1 = \frac{\Theta^{\text{ref}} - \Theta_a}{p_0}$$
$$g^{\max} = K_L g_0 \tag{D.1}$$

where $g_0 = \frac{p_0}{v_0^2}$ and K_L is the ceiling conductance output ratio ($K_L < 1$ for cooling systems and $K_L > 1$ for heating systems).

In this study, two benchmark networks are used: the IEEE 14-bus system (Subsection D.4.1), and the New England 39-bus, 10-machine system (Subsection D.4.2).

D.4.1 IEEE 14-Bus Test System

This subsection considers the IEEE 14-bus test system described in Subsection D.3.1 for the simulations. For this scenario, primary and secondary frequency regulation are not included in order to study the effect of the frequency regulation of the TCLs solely. The contingency is the outage of the line connecting buses 2 and 4 in base loading conditions, as well as with 20% of overload. The amount of TCLs in the system is 30% of the total load.

D.4.1.1 Base Loading Conditions

Figure D.28 shows the rotor speed of the synchronous machine at bus 2, the frequency of the bus estimated by the WF and the FD, and the frequency of the COI, for the base case loading conditions and without TCLs. While both WF and FD estimators show a trend similar to the rotor speed of the machine, the signal provided by the FD is more accurate, since it includes oscillations of same period and similar amplitude than those of the rotor speed. On the other hand, the COI "filters" such oscillations, providing only information of the average frequency variation.

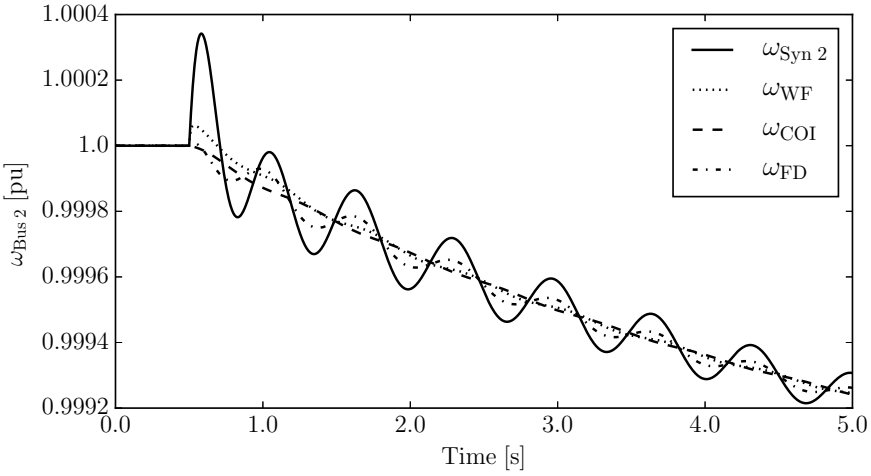

Figure D.28: Frequency of bus 2 when TCLs are not included.

The differences in the estimated frequencies are negligible when including the TCLs, as shown in Fig. D.29. The rotor speed of the machine in bus 2 is depicted for the cases without and with TCLs. In the latter case, the dynamic response of TCLs is compared in three scenarios, corresponding to using as control input signals the frequency estimation provided by the WF, the COI and the FD, respectively.

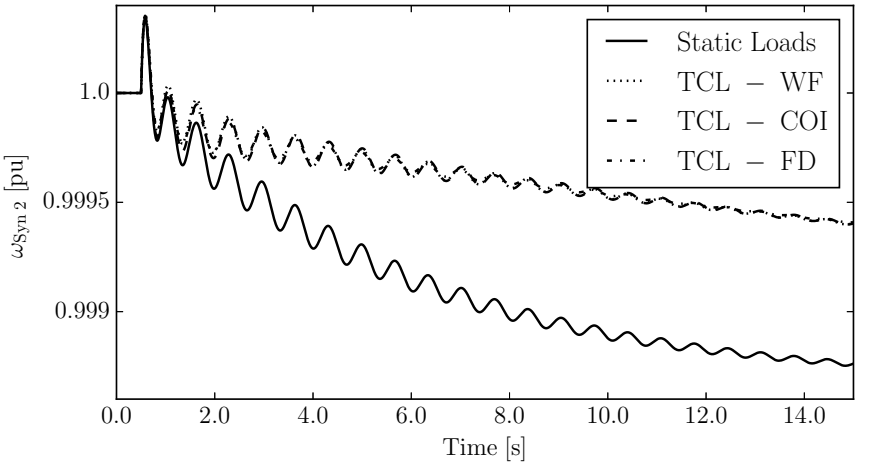

Figure D.29: Rotor speed of the synchronous generator in bus 2 when TCLs are included.

The inclusion of the TCLs reduces the frequency drop by about 50% for the three cases. While in this case the transient response of the system is not affected by the model of the frequency estimation, one cannot conclude that this is always the case. Next subsection proves, in fact, that depending on the loading level the choice of the input signal of the TCLs can provide a considerably different performance of these devices, and therefore, a different behaviour of the whole system.

D.4.1.2 20% Load Increase

Figure D.30 is obtained for a 20% increase of the load with respect to the base case without TCLs and shows the trajectories of the rotor speed of the machine at bus 2 with the signals given by the WF, the COI and the FD.

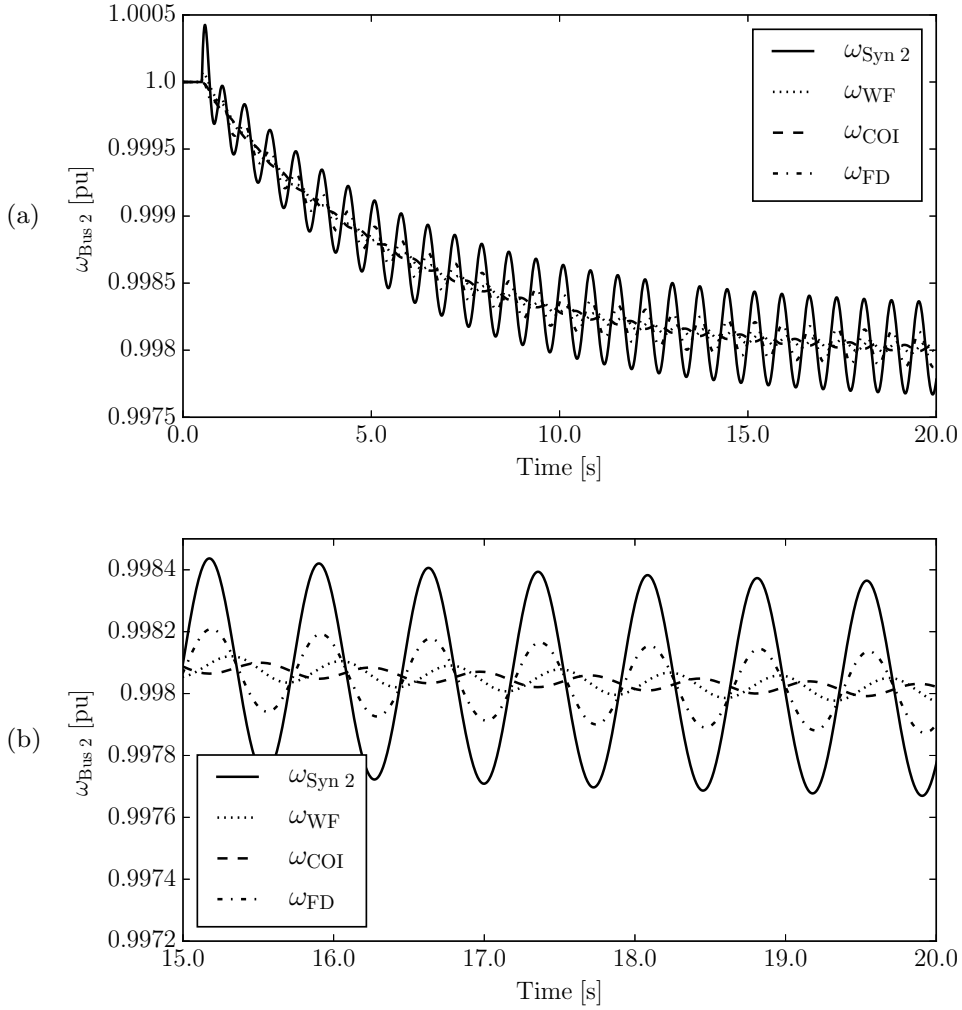

Figure D.30: Frequency of bus 2 with 20% of system overload without TCLs.

Undamped oscillations can be observed due to the presence of a limit cycle in Fig. D.30(a). From Fig. D.30(b), it can be seen that the FD is again the most accurate, while the WF includes a delay in the signal, and the COI contains counter-phase oscillations due to the large size of the synchronous machine at bus 1. Moreover, depending of the chosen frequency estimation technique, considerably different input signals are introduced into the TCL controllers. This is shown in Fig. D.31, where the estimated frequencies at the load bus 14 are compared.

Finally, the rotor speed of the machine at bus 2 is shown in Fig. D.32, which is obtained including TCLs in the system. The frequency drop is again reduced by about 50%. However, while the WF and the COI signals lead to a stationary limit cycle, the usage of the FD indicates that oscillations are actually damped. It is worth noticing that the only difference in the model is the formula to estimate the frequency signal sent to the TCLs. Hence, it is concluded that the choice of the techniques to estimate the frequency can affect considerably the dynamic response of the system, especially if devices controlling the frequency, such as TCLs, are considered. In this case, the WF and the COI are more conservative from the control point of view. This is a consequence of the fact that these models do not capture the variations of local bus frequencies as accurately as the FD.

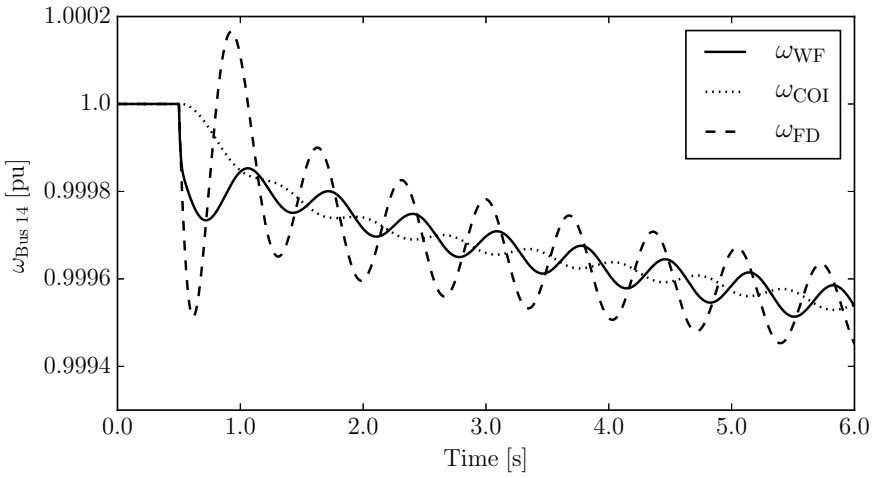

Figure D.31: Estimated frequency at bus 14 using WF, FD and the COI.

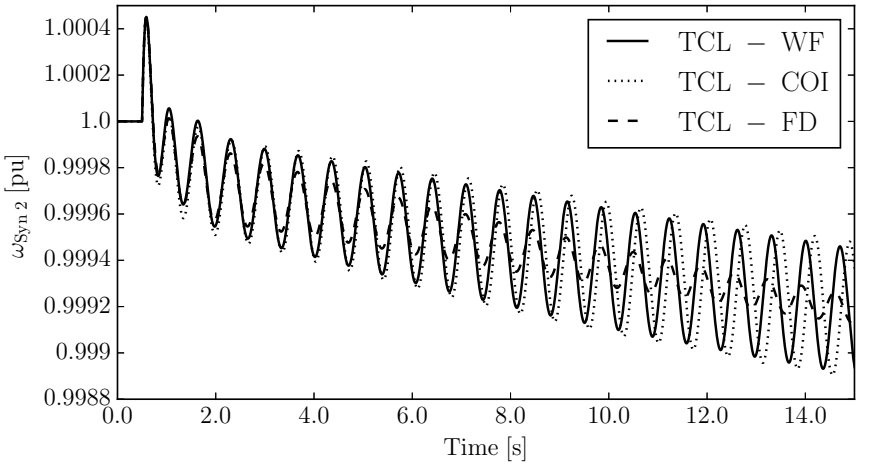

Figure D.32: Rotor speed of the synchronous generator in bus 2 with 20% of system overload and TCLs.

D.4.2 New England 39-Bus, 10-Machine Test System

The single-line diagram of the New England 39-bus, 10-machine test system is depicted in Fig. D.33. This benchmark network contains 19 loads totalling 7,316.5 MW and 1,690.9 MVAr of active and reactive power, respectively (20% load increase with respect to the base case is assumed). The system model also includes generator controllers such as primary voltage regulators, as well as both primary and secondary frequency regulation (TGs and AGC). Dynamic data of the New England 39-bus, 10-machine system can be found in [25]. The contingency is a three-phase fault at bus 21, cleared by the opening of the line connecting buses 16 and 21 after 160 ms. TCLs are the 20% of the total load.

Figure D.34 shows the rotor speed of the machine at bus 31 (Gen 2) without TCLs, and with TCLs considering the three control input signals, namely FD, WF and COI. Three different models of the synchronous machines of the system are compared: the one-axis 3^{rd} order model (Fig. D.34(a)), the Sauer and Pai's 6^{th} order model (Fig. D.34(b)), and the fully-fledged 8^{th} order model (Fig. D.34(c)) [37].

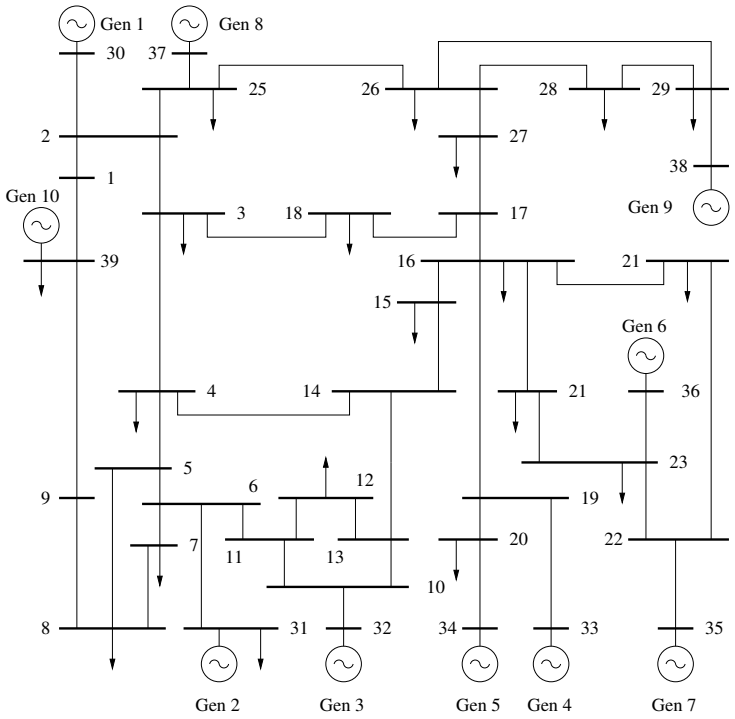

Figure D.33: New England 39-bus, 10-machine system.

Figure D.34(a) shows that including TCLs into the system allows reducing the frequency variations due to the fault. The TCLs reduces the damping of dominant modes. Such modes are slightly better damped if the model includes the FD signal.

Figures D.34(b) and D.34(c) show the response of the system for more detailed and accurate models of the synchronous machines. In these cases, the dynamic interaction of the machine transient and sub-transient dynamics with the TCLs causes poorly damped frequency oscillations. It is interesting to note that, when considering stator flux dynamics and the WF signal (see Fig. D.34(c)) such oscillations become unstable and lead the system to collapse. On the other hand, the TCLs controller coupled to the FD shows that oscillations are properly damped.

D.4.3 Remarks

The following remarks are based on the simulation results presented in this section.

i. The numerical derivative of the bus voltage phase angle of the WF can lead to non-physical oscillations and, possibly to numerical instabilities.

ii. The average rotor speed provided by the COI filters local frequency variations. This fact may cause poorly-damped frequency oscillations, especially if coupled to devices with a slow response, such as TCLs.

iii. Controllers using signals obtained with the FD are less prone to introduce numerically-driven undamped oscillations.

From the results above, it is clear that a proper modelling of the control signals can make a significant difference in the transient stability analysis of a power system with inclusion of frequency controllers other than primary frequency regulators of synchronous machines. The definition of a criterion to estimate the fidelity of such power system models is thus an interesting and urgent research topic.

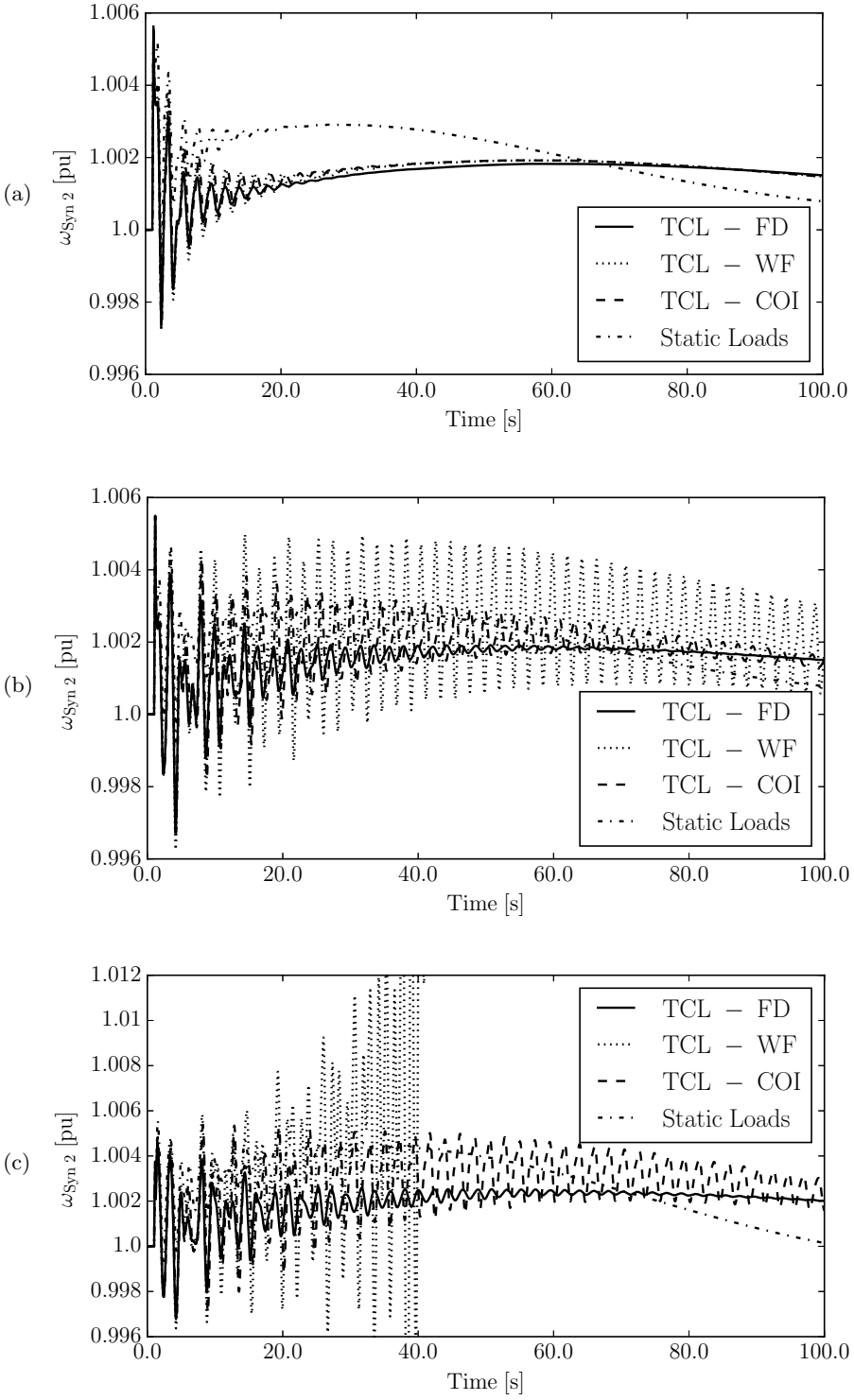

Figure D.34: Rotor speed of the synchronous generator in bus 31 (Gen 2). (a) 3^{rd} order synchronous machine model; (b) 6^{th} order synchronous machine model; (c) 8^{th} order synchronous machine model.

E. Improving the Frequency Divider Formula: Reduced D Matrix

While the FD formula (B.16) offers a wide range of benefits from the point of view of the simulation of power systems, as properly discussed in the previous appendices, it nevertheless shows a significant limitation from the practical implementation point of view. As indicated in Section B.4, the matrix $\mathbf{D}$, in fact, is generally fully dense, i.e., each bus frequency element in $\boldsymbol{\omega}_B$ depends on the rotor speeds of *all* synchronous machines. While this statement is mathematically correct, it is to be expected that not all rotor speeds weight in the same way when calculating the frequency at a given bus. Moreover, the knowledge of all machine rotor speeds is very unlikely in practice, since TSOs and/or ISOs usually do not have access to such information, but rather, they measure the frequency at a number of chosen pilot buses by means of, e.g., PMUs.

One thus needs a criterion to define which measures are most relevant for the calculation of bus frequencies. This can be attained by exploiting a property of matrix $\mathbf{D}$, as follows. In transmission systems, for which one can safely assume that the transmission line ratio R/X is nearly homogeneous, the summation σ_{D} of all the elements in every row of $\mathbf{D}$ is close to 1 [13]:

$$\sigma_{\mathrm{D},i} = \sum_{j=1}^{n_G} D_{i,j} \approx 1, \quad \forall i = 1, \ldots, n_B \tag{E.1}$$

where n_G and n_B are the number of synchronous machines and of system buses, respectively. Each element $D_{i,j}$ thus represents the contribution – or normalized weight – of the machine rotor speed $\omega_{G,j}$ to the frequency of bus $\omega_{B,i}$. Hence, without any further calculation and given a threshold, the matrix $\mathbf{D}$ itself contains the information on the subset of synchronous machines that contribute the most to the frequency of a given system bus.

Two approaches to reduce the density of matrix $\mathbf{D}$ based on (E.1) are proposed in this appendix:

- **Approach 1 (AP1):** In this approach, each row i of $\mathbf{D}$ is sorted in descending order. Then, the first m_i elements of each row of the sorted matrix $\tilde{\mathbf{D}}$ are summed such that $\sum_{h=1}^{m_i} \tilde{D}_{i,h} < \alpha_{\mathrm{D}} \sigma_{\mathrm{D},i}$, where $\alpha_{\mathrm{D}} \in [0, 1]$ is a given threshold. Finally, the reduced matrix $\mathbf{D}_{\mathrm{r}}$ is obtained by setting to zero all elements $\tilde{D}_{i,h}$ with $h = m_i + 1, \ldots, n_B$, and rearranging $\tilde{D}_{i,h}$ according to their original positions before the sorting, i.e., $D_{i,j}$. Therefore:

$$\mathbf{D}_{\mathrm{r}} = \begin{cases} \mathbf{0}\,, & \text{if } \alpha_{\mathrm{D}} = 0\,, \\ \mathbf{D}\,, & \text{if } \alpha_{\mathrm{D}} = 1\,, \\ \mathbf{D}_{\mathrm{r}}\,, & \text{otherwise.} \end{cases} \tag{E.2}$$

- **Approach 2 (AP2):** The reduced matrix $\mathbf{D}_{\mathrm{r}}$ is obtained by neglecting all the elements $D_{i,j}$ that are below a given threshold $\beta_{\mathrm{D}} \in [0, 1]$ (generally, $\beta_{\mathrm{D}} \ll 1$). While this approach is considerably simpler and computationally more efficient than the previous one, it lacks the capability to control the desired accuracy of the FD formula that is provided by AP1. In fact, if the contributions of the synchronous machines to the frequency at a given bus i are similar, there is the risk of neglecting all of them if β_{D} is too low, thus row i of $\mathbf{D}_{\mathrm{r}}$ is null. On the other hand, if β_{D} is too high, all contributions are taken into account, and thus row i of $\mathbf{D}_{\mathrm{r}}$ is dense. Therefore, a careful tuning of β_{D} is required.

The contributions of this study will be the following:

- A thorough description and comparison of the two proposed approaches to reduce the density of the FD matrix, based on large, real-world systems, namely, the all-island Irish and the ENTSO-E transmission systems.
- A comprehensive discussion of the implications of this study from the practical implementation point of view.

Some preliminary results of the AP1, based on a case study that considers the dynamic model of the all-island Irish transmission system facing a three-phase fault are presented below. The system includes 1,479 buses, 1,851 transmission lines and transformers, 245 loads, 22 conventional synchronous power plants modeled with 6th order synchronous machine models with AVRs and turbine governors, 6 PSSs and 176 wind power plants, of which 34 are equipped with constant-speed (CSWT) and 142 with doubly-fed induction generators (DFIG). The topology and the steady-state data of the system are based on the actual real-world systems provided by the Irish TSO, EirGrid. However, all dynamic data are guessed based on the knowledge of the technology of power plants.

Figure E.1 shows the density d_{D} of matrix $\mathbf{D}_{\mathrm{r}}$, i.e., the percentage of non-zero elements, for a range of values of α_{D} with increments of 0.01. It can be seen that the curve shows a saturation at $\alpha_{\mathrm{D}} \approx 0.7$, from which d_{D} rapidly increases with α_{D}.

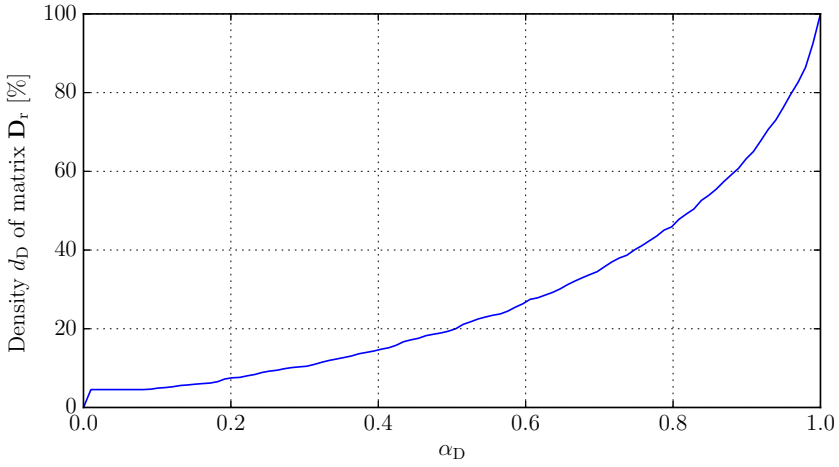

Figure E.1: Density of matrix $\mathbf{D}_r$ of the Irish transmission system. $\boldsymbol{\alpha_{\mathrm{D}}} \in [\mathbf{0}, \mathbf{1}]$.

Figures E.2 and E.3 show the frequency estimated at a bus where a wind power plant is installed, for different values of α_{D}, and the absolute error ϵ_{ω} with respect to the ideal case (i.e., $\alpha_{\mathrm{D}} = 1$). Figure E.2 also shows the density d_{D} of the reduced frequency divider matrix $\mathbf{D}_r$, while Fig. E.3 also includes the error of between the ideal case and the frequency of the COI, ω_{COI}, as a limit case for the desired accuracy of the reduced FD matrix.

While the density of matrix $\mathbf{D}$ can be reduced considerably with the AP1, it nevertheless captures the local frequency oscillations with a high level of accuracy. This proves the intuition that, in real-world transmission systems, only a very reduced number of synchronous machines are required to estimate the frequency of a certain bus of the network. Moreover, it is to be expected that, the larger the system under study is, the higher will be the density reduction that can be achieved.

A comprehensive comparison of the two approaches AP1 and AP2 in terms of accuracy, density reduction and computational efficiency, considering the Irish system, as well as other large, real-world networks such as the Romanian system or the ENTSO-E, will be provided. Results of this study will be also relevant to determine the recommendations for policies and network codes.

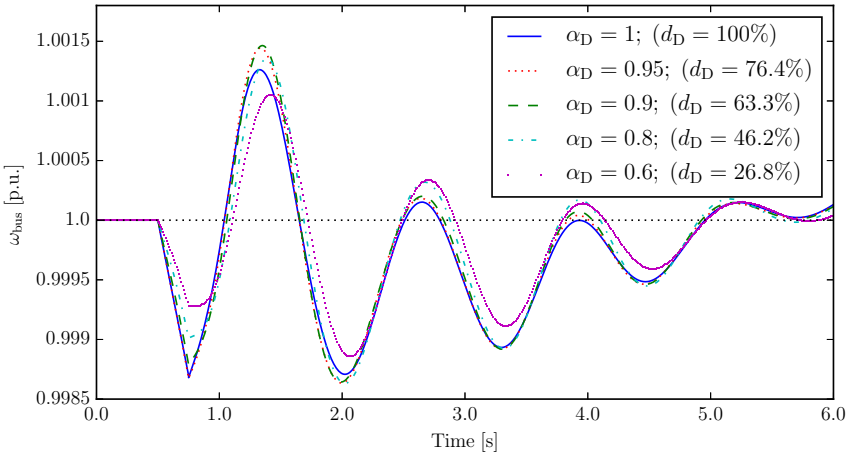

Figure E.2: Frequency estimated at a non-synchronous generation bus of the Irish transmission system facing a three-phase fault.

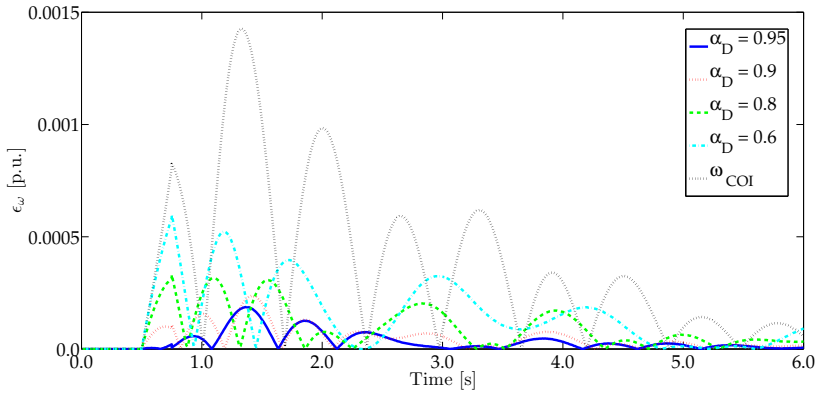

Figure E.3: Error of the frequency estimated at a non-synchronous generation bus of the Irish transmission system facing a three-phase fault.